8

Dielectric and emissive properties of terrestrial surfaces

The purpose of this chapter is to consider the basic characteristics (the intensity and spectral dependencies) of the radiation field of physical substances most widespread on the surface and in the atmosphere of the Earth. The frequency properties of the characteristics of dielectrics are considered from the viewpoint of the phenomenological approach to studying the relaxation mechanisms (the Debye model and models with a multiplicity of relaxation times). The basic statements of dielectric spectroscopy theory and practice are presented. The main attention in the chapter is given to studying the dielectric and emissive properties of salt (seawater) and freshwater and to the relation of these properties to the physicochemical structure of these substances by determining the frequency dispersion of electromagnetic properties of dielectrics. The dielectric and emissive properties of natural objects, containing freshwater and aqueous electrolytic solutions at different phase states, are considered. These states include: freshwater ice, sea ice, glacial ice, moist fertile soil, salinas. The chapter presents a rich set of experimental findings on emissive characteristics and dielectric properties of substances distributed both on the Earth and on terrestrial planets.

8.1 FREQUENCY DISPERSION OF THE ELECTROMAGNETIC PROPERTIES OF DIELECTRICS

Virtually all known natural substances and physical objects on our planet belong (when considering their electromagnetic properties) to the class of dielectrics. This class includes all atmospheric (non-ionized) gases, virtually all liquids (including fresh and ocean water), solid bodies (soil, grounds, rocks), vegetation, artificial (manufactured) materials and buildings, and also the objects of animate nature. The basic mechanisms of interaction of such physical systems with the electromagnetic field are reduced to redistribution of the electronic density of internal

electric charges in a medium and to polarization features arising in the distribution of charges (see section 1.6).

8.1.1 Dispersive properties

The polarization of a dielectric when an electric field is applied takes place, not instantaneously, but over a certain time called the relaxation time. The temporary character of the relaxation process is rigidly bound to the physicochemical properties and structure of the substance and is clearly exhibited in studying frequency characteristics of electromagnetic properties – the so-called dispersive properties. The range of frequencies in which the expressed changes of dielectric properties of substances mostly take place is called the dispersion region. Investigation of the dispersive properties of substances can provide very important information on the structure of physical objects and on their physicochemical composition. Investigations can be carried out both directly, by laboratory study of the dielectric properties of substances, and remotely, by studying the spectral properties of thermal radiation. The microwave band of electromagnetic waves represents just that range of frequencies where dispersive phenomena become essential for the overwhelming majority of earth covers, and, on the other hand, where macroscopic description by means of classic Maxwellian electrodynamics is possible (see section 1.6). Thus, the electrical polarization of a dielectric can be described within the framework of Maxwellian electrodynamics, taking into account the principal circumstance that the unambiguous time-dependence of values of the electrical and magnetic induction fields with the instantaneous values of electric and magnetic fields is violated. In other words, the physical system will possess a certain inertia when the external electrical field is applied, or some kind of memory when the external field is removed and the system tends to the equilibrium state. Since in remote sensing tasks fairly weak values of electric fields are applied, the relationship between the induction and electrical field remains linear.

Under the physical limitations indicated the most general form of relation between the induction and electrical field at all previous time instants can be written in the form of the following integral relationship (Landau and Lifshitz, 1957):

$$\mathbf{D}(t) = \varepsilon_\infty \mathbf{E}(t) + \int_0^\infty f(\tau)\mathbf{E}(t-\tau)\,\mathrm{d}\tau, \tag{8.1}$$

where $f(\tau)$ is the function of time which characterizes the process of relaxation of the electrical polarization at the application or removal of the external electrical field and depends on the physical and physicochemical properties of the medium, ε_∞ is the dielectric permittivity of a medium at high frequencies, i.e. at frequencies lying outside the active relaxation region of the given relaxation mechanism.

Transferring to a set of monochromatic components (by using the Fourier expansion), in which the time-dependence is given by multiplier $\exp(-\mathrm{j}\omega t)$, we obtain the relation between **D** and **E** (in the SI system) as follows:

$$\mathbf{D} = \varepsilon_{0V}\mathbf{E} + \mathbf{P} = \varepsilon(\omega)\varepsilon_{0V}\mathbf{E}, \tag{8.2}$$

where ε_{0V} is the permittivity constant of vacuum* (see section 1.6), **P** is the polarization vector, and $\dot{\varepsilon}(\omega)$ is the relative complex permittivity unambiguously bound with the process of establishing the balance in a dielectric and defined as:

$$\dot{\varepsilon}(\omega) = \varepsilon_\infty + \int_0^\infty f(\tau) \exp(\mathrm{j}\omega\tau)\, \mathrm{d}\tau. \tag{8.3}$$

The frequency-dependence of $\dot{\varepsilon}(\omega)$ is said to be the law of its dispersion, or its dispersive properties.

Function $\dot{\varepsilon}(\omega)$ is complex, generally speaking. From the definition of (8.3) it directly follows, that

$$\dot{\varepsilon}(-\omega) = \dot{\varepsilon}^*(\omega). \tag{8.4}$$

Separating in this relation the real and imaginary parts, we obtain

$$\varepsilon_1(-\omega) = \varepsilon_1(\omega); \varepsilon_2(-\omega) = -\varepsilon_2(\omega). \tag{8.5}$$

Thus, $\varepsilon_1(\omega)$ is an even, and $\varepsilon_2(\omega)$ an odd function of frequency. For low frequencies (as compared to the active relaxation zone) the function $\varepsilon(\omega)$ can be expanded in a series in powers of ω. The expansion of the even function $\varepsilon_1(\omega)$ contains the terms of even powers only, and the expansion of the odd function $\varepsilon_2(\omega)$ the terms of odd powers. In the limit $\omega \to 0$ function $\dot{\varepsilon}(\omega)$ in dielectrics tends, certainly, to the relative permittivity, which is usually designated as ε_0 (this designation should not be confused with the permittivity of vacuum (see section 1.6)). Therefore, in dielectrics the expansion of $\dot{\varepsilon}(\omega)$ begins with the constant term ε_0; the expansion of $\varepsilon_2(\omega)$, however, begins, generally speaking, with a term proportional to ω. This is especially clearly seen in the analysis of the Maxwell equations for dielectrics in the presence of noticeable direct current conductivity (perfect conductors). Using equations (1.1a) and (1.3), we obtain the following limiting expression for $\varepsilon(\omega)$ for low frequencies (Landau and Lifshitz, 1957):

$$\dot{\varepsilon}(\omega) = \mathrm{j}\frac{\sigma}{\omega\varepsilon_{0V}}. \tag{8.6}$$

Thus, in dielectrics with a noticeable direct current conductivity the expansion of function $\varepsilon(\omega)$ begins with the imaginary term proportional to $1/\omega$, which is expressed in terms of conventional direct current conductivity. As the frequency further increases, the value of this term sharply decreases, and the relaxation mechanisms come into effect. They are manifested as specific (and sometimes rather complicated) frequency dependencies, including electromagnetic energy dissipation. Thus, for dielectrics with internal relaxation mechanisms of external energy transformation and in the presence of finite direct current conductivity in them the complete expression for the complex dielectric constant $\dot{\varepsilon}_\sigma(\omega)$ can be written as:

$$\dot{\varepsilon}_\sigma(\omega) = \dot{\varepsilon}_\mathrm{R}(\omega) + \mathrm{j}\frac{\sigma}{\omega\varepsilon_{0\mathrm{V}}}, \tag{8.7}$$

where $\dot{\varepsilon}_\mathrm{R}(\omega)$ is the relaxation part of the permittivity.

* This quantity is redesignated in this chapter (with respect to section 1.6) to avoid confusion into designations.

Such dielectrics are called 'poor' conductors of electricity in physics (Landau and Lifshitz, 1957).

In practical applications this form of dielectric constant is written using the numerical expression for the permittivity constant of vacuum (see section 1.6 and Appendix A, Table A.4) in a somewhat different, but, certainly, fully equivalent form

$$\dot{\varepsilon}_\sigma(\lambda) = \dot{\varepsilon}_R(\lambda) + 60\sigma\lambda, \tag{8.8}$$

where the wavelength is taken in metres, and the dimension of electrical conductivity in $(\Omega m)^{-1}$ (see Appendix A, Table A.2).

In practical applications no distinction is usually made between these two parts of the expressions presented above, putting the term caused by the direct current conductivity directly into the expression for an imaginary part of the dielectric constant caused by a pure relaxation mechanism. In studying liquid electrolytes, the relaxation part of a dielectric constant $\dot{\varepsilon}_{\mathrm{R}}(\omega)$ is called the 'adjusted' part, which means the value of $\dot{\varepsilon}(\omega)$ with subtraction of the correction for the 'through' (ionic in solutions) component of conductivity. Hereafter we shall use, for simplicity, the full expression for a dielectric constant, not using the subscript in (8.7) or (8.8).

The presence of full dielectric losses, as follows from (8.2), results in the appearance of a phase shift between instantaneous values of the induction and electric field vectors. Physically, this is equivalent to the appearance of the effects of time delay of polarization in a medium with respect to the external field. The spectral (wavelength) dependence of the tangent of the angle of losses can be written in this case as

$$\operatorname{tg}\delta(\lambda) = \frac{\varepsilon_2(\lambda) + 60\sigma\lambda}{\varepsilon_1(\lambda)}. \tag{8.9}$$

In the optical and IR wavelength bands the frequency properties of relaxation mechanisms of dielectrics are often presented and studied in the form of spectral (frequency or wavelength) dependencies of real and imaginary parts of the complex index of refraction. The transition to a complex dielectric constant can be accomplished according to well-known rules (see section 1.6, equations (1.26)–(1.28)).

In the limit $\omega \to \infty$ function $\dot{\varepsilon}(\omega)$ tends to unity. This is already clear from simple physical considerations: if the field changes rapidly enough, the polarization processes, resulting in establishing induction **D** differing from **E**, have no time to occur at all. So, it becomes possible to find (Landau and Lifshitz, 1957) the limiting form of function $\dot{\varepsilon}(\omega)$ at high frequencies, which is valid for any body – metal or dielectric – indifferently. That is to say, the frequency of a field must be high as compared to the frequencies of motion of all (or, at least, of the majority of) electrons in atoms of the given substance. If this condition is met, we can, in calculating the polarization of the substance, consider the electrons to be free, neglecting their interaction among themselves and with the nuclei of atoms (the so-called electronic polarization). Actually, the field of applicability of such an approach begins from the far ultraviolet (UV) band for the lightest elements, or from X-ray frequencies for heavier elements.

The majority of substances which are of interest for remote sensing activity (such as water vapour, water, ice and soil) possess a lot of relaxation mechanisms whose active zones (the dispersion regions) stretch from virtually zero frequencies (tens and hundreds of hertz) up to the optical and UV bands. Because of the drastic distinction in the values of frequencies, relaxation mechanisms in natural substances are usually analysed completely independently for various frequency bands of electromagnetic radiation. Therefore, to avoid confusion, one should have in mind that quantity ε_∞ in one relaxation mechanism can serve as ε_0 in another (the next on the frequency axis) mechanism. Moreover, cases of 'superposition' of various mechanisms are possible. It is just such a situation we shall soon encounter in studying relaxation mechanisms in water.

8.1.2 The Kronig–Kramers relations

Since function $\dot{\varepsilon}(\omega)$ was determined in a fairly general form (8.2), it has turned out that some quite general and important properties of this function can be established by considering ω as a complex variable ($\omega = \omega' + \mathrm{j}\omega''$). Since function $f(\tau)$ in (8.3) is, by its physical sense, finite for all values of its argument, it follows from the definition of (8.3) that in the whole upper half plane of $\dot{\varepsilon}(\omega)$ there exists an unambiguous function which does not turn to infinity anywhere. In other words, it does not have any singular points. One should pay attention to the fact that the conclusion on the absence of singular points in the $\dot{\varepsilon}(\omega)$ function in the upper half plane is, from the physical point of view, a consequence of the causality principle. This principle consists in the fact that the integration in (8.3) is carried out only over the time preceding the given instant t, as a result of which the range of integration in formula (8.3) extends from 0 to ∞ (but not from $-\infty$ to $+\infty$). The use of well-known theorems from the theory of complex variable functions makes it possible to obtain the important relations between the imaginary and real parts of function $\dot{\varepsilon}(\omega)$. If we are dealing with a pure dielectric, the aforementioned relations state (Landau and Lifshitz, 1957), that:

$$\varepsilon_1(\omega) - 1 = \frac{1}{\pi} \int_{-\infty}^{\infty} \frac{\varepsilon_2(x)}{x - \omega} \, \mathrm{d}x, \tag{8.10}$$

$$\varepsilon_2(\omega) = -\frac{1}{\pi} \int_{-\infty}^{\infty} \frac{\varepsilon_1(x) - 1}{x - \omega} \, \mathrm{d}x, \tag{8.11}$$

where the crossed sign of integral implies that the integral is understood in the sense of its major value. Relations (8.10)–(8.11) are called the Kronig–Kramers relations. Remember that the only essential property of the $\dot{\varepsilon}(\omega)$ function used in deriving these formulas is the absence of singular points in the upper half-plane. Therefore, we can say that the Kronig–Kramers formulas are a direct consequence of the physical causality principle.

Making use of odd function $\dot{\varepsilon}(\omega)$, formula (8.10) can be reduced to the form

$$\varepsilon_1(\omega) - 1 = \frac{2}{\pi}\int_0^\infty \frac{x\varepsilon_2(x)}{x^2 - \omega^2}\,\mathrm{d}x. \tag{8.12}$$

If the conductor is considered, then at point $\omega = 0$ function $\dot{\varepsilon}(\omega)$ has a pole, near which $\dot{\varepsilon}(\omega) = \mathrm{j}(\sigma/\omega\varepsilon_{0\mathrm{V}})$ (see (8.6)). This results in the appearance of the additional term in formula (8.12):

$$\varepsilon_2(x) = -\frac{1}{\pi}\int_{-\infty}^\infty \frac{\varepsilon_1(x)}{x - \omega}\,\mathrm{d}x + \frac{\sigma}{\omega\varepsilon_{0\mathrm{V}}}. \tag{8.13}$$

The principal physical significance of the Kronig–Kramers relations consists in the fact that they stipulate the strict and unambiguous analytical dependence between frequency properties of real and imaginary parts of the dielectric constant (or the complex index of refraction). The frequency dielectric properties of natural media cannot change in an arbitrary (not mutually interrelated) manner. They allow researchers to reconstruct the frequency characteristic of one of the parts of a dielectric constant if the other one is measured (or obtained empirically) well enough. For example, the measured frequency-dependence of dielectric losses in a medium unambiguously determines the frequency characteristic of the dielectric permittivity (and vice versa). The strict and unambiguous relationship (8.12) enables us to find the frequency characteristic of the dielectric permittivity, even from the approximately measured experimental function $\varepsilon_2(\omega)$. The considered relations are often also used for correlating the measurements of the frequency characteristic of dielectric parameters in the case of these measurements being carried out with serious errors (for whatever technical reason). The techniques of application of the Kronig–Kramers relations are diverse and many-faceted.

Since, as we have already noted, in the natural media we encounter, in a series of cases, the superposition of various relaxation mechanisms (see section 8.2), the direct use of the Kronig–Kramers relations for particular applications within limited frequency bands requires a thorough and detailed approach and analysis. In addition, for poor dielectrics there exist frequency bands where function $\dot{\varepsilon}(\omega)$ loses its physical sense in connection with the effects of spatial inhomogeneity of the field. In such cases the use of specific formal procedures is necessary.

8.2 PHYSICAL MECHANISMS OF THE POLARIZATION OF DIELECTRICS

The mechanisms of polarization of dielectrics are diverse and depend on the structure of the substance and on the character of the physicochemical bonds. For example, in ionic crystals (NaCl and others) the polarization is a result of shifting the ions relative to each other (ionic polarization) and of the deformation of electronic shells of individual ions (electronic polarization). In crystals with a covalent bond (the diamond, for instance) the polarization is mainly caused by displacement of electrons giving rise to chemical bonds. In so-called polar dielectrics the molecules

(or the radical groups) represent electric dipoles, which are chaotically oriented in space in the absence of the external electrical field and acquire a predominant orientation in the presence of the external field. Such an 'orientational' polarization is typical for many liquids (such as freshwater) and gases. A similar polarization mechanism is related to a 'jump' of individual ions from one equilibrium position into another under the electrical field effect. Such a mechanism is observed most frequently in electrolytes (salt water and seawater) and in substances with a hydrogen bond, for example in ice, where the hydrogen ions have several equilibrium positions.

In the electronic polarization mechanism the maximum of losses (the dispersion region) falls in the optical frequencies ($\approx 10^{15}$ Hz) and in the near-IR band. In the polarization caused by displacement of ions, the maximum of dielectric losses shifts to the IR band (10^{12} to 10^{13} Hz). The lower frequencies (in the radio-frequency band) correspond to the maximum of losses at orientational polarization of individual molecules (freshwater, water vapour) or of clusters of molecules (salt water).

In low-molecular organic compounds each molecule has a single dipole and its rotational dynamics is weakly associated with adjacent dipoles. Polar polymeric compounds consist of a great number of dipoles of polar links bound by chemical bonds. Their rotational dynamics depend on each other. The maxima of dielectric losses for such media lie within a wide range of frequencies (10^4 to 10^8 Hz). The forces of intermolecular dipole–dipole interaction between molecules and side groups of adjacent links preclude the turning of links (around simple bonds). As a result, the links undergo only rotational oscillatory motions, rather than full rotation. However, in the absence of freedom of rotation there are some sections in a polymeric chain, called segments, which are capable of changing their form independently of each other. The smaller the segment, the greater the flexibility of molecules and the higher the polymer's capability to be oriented in the electrical field. Depending on the temperature range, the dipole-group and dipole-segmental polarizations are revealed in polar polymers, the dipole-group polarization being typical for polymers.

In some cases it becomes possible to obtain very rigid chemical bonds in polymers. Owing to the low mobility of the basic polymeric chain and limited capability of motion of individual groups and links, the dipole-group polarization is insignificant, and in the glassy state the dielectric permittivity of polymers is at a minimum. And also at a minimum are the dielectric losses and losses for pure conductivity. Such polymers are widely used in technological applications as polymeric and composite insulating materials (rubbers, plastics, glasses). A similar situation arises in some widely used building materials (such as asphalt, cement, concrete and some modern synthetic materials).

In electrically inhomogeneous media the intersurface polarization can take place, which is caused by the motion of free carriers of charges, which are accumulated near the interface boundaries of regions with heightened specific resistance (intercrystalline sheets, microcracks, fluctuations of physicochemical composition, etc.). The maxima of dielectric losses for such media lie within a wide range of

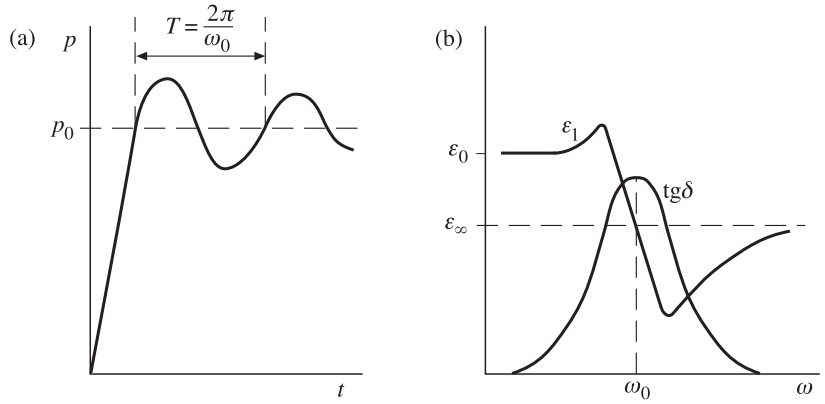

Figure 8.1. Schematic presentation of the effect on polarization properties in the case of the resonance mechanism. (a) Polarization variation in time in cases where the external electric field is switched on. (b) Frequency characteristics of $\varepsilon_1(\omega)$ and $\mathrm{tg}\delta(\omega)$.

frequencies (10^3 to 10^9 Hz). Bright natural examples of such media are various modifications of seawater and freshwater ice, wet soil with bound water electrolytes inside the soil, as well as the water–ice system and snow cover at the phase transition instant.

The frequency character of $\varepsilon_1(\omega)$ and $\mathrm{tg}\delta(\omega)$ dependencies in the dispersion region is determined by the polarization mechanism. In the case of ionic and electronic polarization on applying the external field **E** the variation in time t has a character of attenuating oscillations (Figure 8.1(a)). Accordingly, the frequency dependencies of $\varepsilon_1(\omega)$ and $\mathrm{tg}\delta(\omega)$ are called resonance dependencies (Figure 8.1(b)). This is due to the fact that, since the polarization of a dielectric is mainly caused by small displacements of electrons and ions, the dielectric can be considered as a set of harmonic oscillators which experience forced oscillations with attenuation in the alternating field. This type of polarization is sometimes called the deformation polarizability of dielectrics.

In orientational (dipolar) polarization the latter one has a relaxation character (Figure 8.2(a)), and then the frequency dependencies of $\varepsilon_1(\omega)$ and $\mathrm{tg}\delta(\omega)$ are called relaxation dependencies (or Debye-type relaxations) (Figure 8.2(b)). The times of polarization establishment or disappearance depend in this case on the intensity of the thermal motion of atoms, molecules (or ions), i.e. on the physicochemical structure of the substance and on the physical temperature. In orientational polarization the characteristic relaxation time is determined by the time of orientation of individual molecules in the direction of the external field **E**. It depends on the value of dipole moments of molecules, on the viscosity of a medium, on the dipole–dipole interaction energy and on the other physicochemical parameters. At room temperature the characteristic time varies within very wide limits, from 10^{-3} to 10^{-10} s, for gases and fluids, this time being, as a rule, lower than for solid bodies. In solid dielectrics the dipole polarization is often caused by weakly bound ions, which can have several equilibrium positions. Under the effect of an external field and thermal

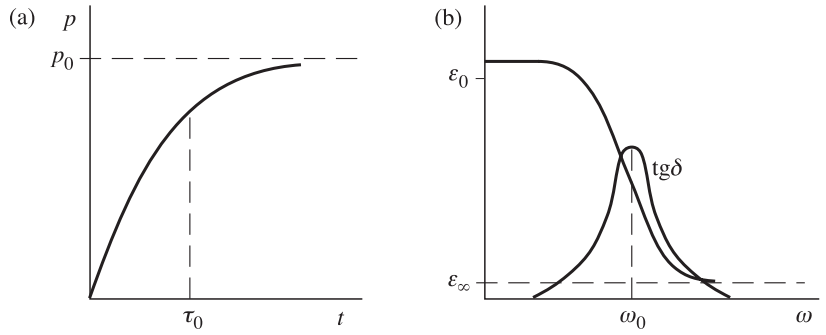

Figure 8.2. Schematic presentation of the effect on polarization properties in the case of the relaxation mechanism. (a) Polarization variation in time in cases where the electric field is switched on. (b) Frequency characteristics of $\varepsilon_1(\omega)$ and $\mathrm{tg}\delta(\omega)$.

motion the ions can transfer from one equilibrium position to another, while overcoming potential barriers. In this case the characteristic times vary within a wide range, occupying large time domains.

In electrically inhomogeneous media an intersurface polarization is observed that is caused by the motion of free carriers of charge accumulating near the boundaries of regions with sharply distinguished electrical properties. In these media processes of a complicated percolation type take place, as well as the processes of propagation of the charge-density wave state (Pinteric *et al.*, 2001; Bordonskii and Filipova, 2002). These effects are related to the multi-scale structural features and to the hierarchic, fractal-type structure of current-conducting admixtures (Park, 2001). The issues of finding the characteristic time domains in such systems are fairly complicated and ambiguous. Studies in this direction are being efficiently developed now.

In real dielectrics several polarization mechanisms with different characteristic times can often take place simultaneously, which results in a more complicated character of frequency dependencies of $\varepsilon_1(\omega)$ and $\mathrm{tg}\delta(\omega)$. In this case in some frequency bands the mechanisms of pure Debye type and of resonance type can merge with relaxation systems that have a wide spectrum of dielectric relaxation times. For these reasons the separation and fixation of various mechanisms from the real experimental data represents a complicated experimental problem.

As an important example, we shall consider the frequency features of the complex index of refraction for liquid water in a very wide wavelength band – from 10^{-4} to 10^{+4} cm, i.e. ranging over eight orders of magnitude (see Figure 8.3). The analysis of an imaginary part of the index of refraction indicates that some kind of basic pattern (designated as KDC in Figure 8.3) of the frequency-dependence of $\chi(\lambda)$ is the characteristic form of the pure Debye-type relaxation mechanism. It has a maximum at a wavelength of about 1 cm and then the characteristic drops in the direction of increasing values of wavelengths as λ^{-1} and in the directin of decreasing values of wavelengths as λ^{+1}. The total band of frequencies included in this mechanism are called the Debye absorption band. The index of refraction (its real

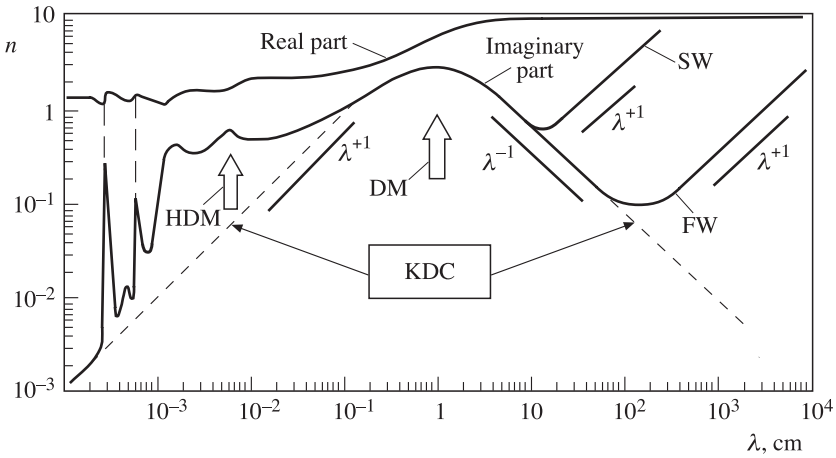

Figure 8.3. The semi-quantitative presentation of a complex index of refraction for liquid water. The temperature is 25°C. KDC is the key Debye contribution. DM is the maximum of the Debye absorption band. HDM is the maximum of the hyper-Debye absorption band. FW is freshwater. SW is salt (sea) water. Graphs are by E. Sharkov using data from work by Ray (1972); Afsar and Hasted, 1977; Sharkov (1983, 1984); Liebe *et al.* (1991).

part) is characterized by the rapid drop (decrease) of its value at the absorption maximum frequency (Figure 8.2(b)). Beginning with the wavelengths of about 1 mm another relaxation mechanism comes into effect. It is called the hyper-Debye-type mechanism, though it is, in general, very close to the pure Debye-type mechanism with an absorption maximum near 0.06 mm. This circumstance sharply distorts the characteristic Debye-type drop in absorption in the direction of short wavelengths (Figure 8.3). The next (in the direction of shorter wavelengths) absorption maximum, also of the Debye type, falls in the wavelength of about 0.02 mm. The next two absorption bands with maxima at wavelengths of 6×10^{-4} and 3×10^{-4} cm are already determined by resonance types of polarization, which have a typical frequency form both in absorption and in the real index of refraction (Figure 8.1(b)).

As far as salt water (electrolyte) is concerned, for a long time (more than 50 years) there had existed a naive knowledge about the pure Debye-type relaxation mechanism in the polarization properties of electrolytes, in which only one known component, caused by ionic conductivity, was taken into account (see equations (8.7)–(8.8)). Strictly speaking, this knowledge is reflected in Figure 8.3 in the frequency dependencies of the imaginary part of the index of refraction at long wavelengths for fresh water (with low conductivity) and for salt water (with high conductivity). However, the critical insight into the problem, undertaken by E. Sharkov (1984), has demonstrated the complete groundlessness of this point of view. The relaxation mechanism of electrolytes was found to significantly differ from the Debye-type, both in the type of absorption band, and in a sharp (and rather surprising) dependence of electrostatic permittivity on the salt concentration of a solution. We shall analyse this problem in more detail in section 8.

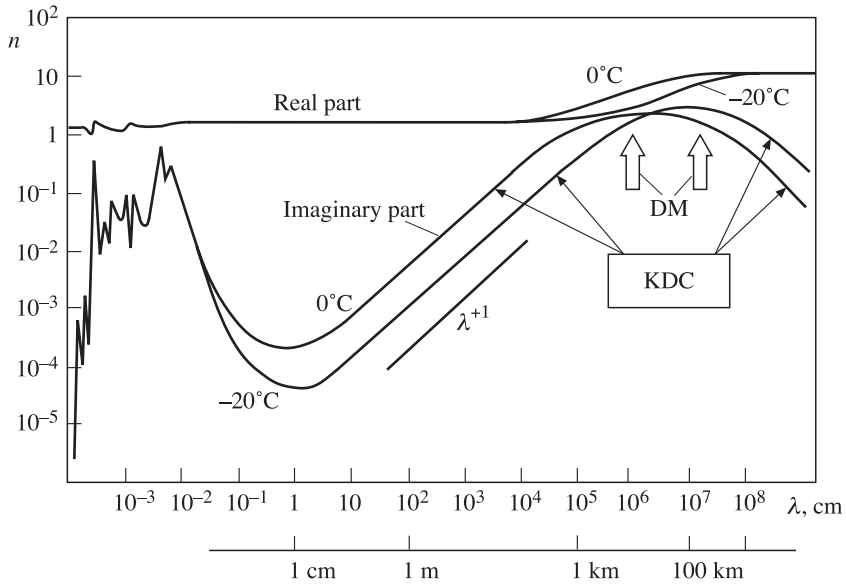

Figure 8.4. The semi-quantitative presentation of a complex index of reflection for ice samples. The temperature range is 0–20°C. Graphs are by E. Sharkov using an interpolation between microwave data and infrared data (Ray, 1972; Fujita *et al.*, 2000; Matsuoka *et al.*, 1996). See notation in Figure 8.3.

The phase transition of liquid water into the solid state is characterized by a basic change of its polarization properties. The frequency characteristics of the complex index of refraction for water in a solid state (ice) are presented in Figure 8.4 within a very wide wavelength band – from 10^{-4} to 10^{+9} cm (or thirteen orders of magnitude (!)). A key feature of the polarization properties of ice is the fantastic 'jump' in the numerical value of relaxation wavelength from 1 cm to 10–100 km (depending on the temperature), i.e. 6–7 orders of magnitude. Such a grand reconstruction in the polarization mode of the most widespread substance on our planet (water) nonplussed researchers for a long period of time. It was believed that for the solid phase of water (freshwater ice) the pure Debye relaxation model remained valid with changing the value of the time relaxation constant only.

Modern investigations have shown that for the microwave band (1–100 GHz) the real part of the relative dielectric permittivity of freshwater ice (for homogeneous samples) still remained a fairly definite and stable quantity that is almost independent of frequency $\varepsilon_1(\omega) = 3.15$ (Matzler, 2000; Fujita *et al.*, 2000). It was found that the imaginary part can be presented in this band as an articulation of two branches – the high-frequency tail of the Debye dispersion and the low-frequency tail of lattice vibration in the far-infrared region. In this connection, it emerges that the imaginary part depends critically on weak mineralization (which is always present in natural freshwaters), on the presence of organic substance and admixtures of gas bubble type, and to the thermodynamic temperature. But, in general, modern

authors adhere to the Debye relaxation spectrum $\varepsilon_2(\omega) \sim \omega^{-1}$ (Bordonskii, 1990; Fujita *et al.*, 2000; Bordonskii *et al.*, 2002). In the low-frequency (kilohertz and hertz) band the chief effect is the structural (possibly, of Debye-type) polarization of fractal and percolation type, as well as the presence of mineral admixtures (the chemical purity of a sample). Here we are dealing, apparently, with a complicated, complex mode of polarization. The researchers began to fix their attention on this wavelength band in connection with two issues: (1) studying the depth distribution of moisture in soils and grounds (Stoffregen *et al.*, 2002); and (2) the attempts of active electromagnetic sensing the surface covers of Mars with the purpose of detecting subsurface water, water-ice and rock–ice–water mixtures in them (Grimm, 2002).

The solid phase, formed from seawater, turned out to be so complicated (in the electrodynamic sense) and diverse that it is difficult now to compose a generalized picture of dielectric properties. This is because of the fact that they were found to be strongly dependent on the mineral composition of seawater in a particular area, on the temperature and on the meteorological history of the solid phase formation. This results, in its turn, in the formation of a variety of types of sea-ice with sharply distinctive dielectric properties. The strong spatial-temporal variability of sea-ice fields and their hierarchic structure highly complicate the pattern-recognition procedures in remote microwave observations (Bespalova *et al.*, 1976b; Comiso and Kwok, 1996; Belchansky and Alpatsky, 2000; Comiso, 2000).

Because glacial ice (in the Antarctic, Greenland, mountain glaciers) is formed via the morphological ice formation from precipitated snow, rather than from a liquid phase, then, obviously, the internal geometrical structure in three-dimensional mesoscales has a strong effect on the dielectric and emissive properties of the glacial ice fields. This has been clearly exhibited even in the first radiothermal investigations of the Antarctic ice cover – the so-called 'Antarctica puzzle' (Basharinov *et al.*, 1971; Gurvich *et al.*, 1973; Gloersen *et al.*, 1974). In glacial ice samples, taken for laboratory investigation, the dielectric properties (in 'micro-scales') were found to be close to those of freshwater ice, but with strong temperature effects and dielectric anisotropy (Matsuoka *et al.*, 1996, 1997). However, the overall pattern (in the wide wavelength band) of glacial ice's dielectric properties has not been developed yet.

The judgements have already repeatedly been stated that, in spite of having identical names, all these substances – freshwater ice, sea-ice and glacial ice, as well as freshwater and seawater – are significantly different in the electrodynamic sense, if they are qualified by class of dielectric and, accordingly, by emissive characteristics.

8.3 RELAXATION POLARIZATION MODELS

Many substances on our planet belong to the class of polar dielectrics whose overall polarization is made up from deformational and orientational polarizations. In this case, however, the prevailing type of polarization in these substances is

the orientational one. Therefore, below we shall consider in more detail the basic types of models of orientational (relaxation) polarization and, first of all, the Debye-type models (with a single relaxation time), as well as relaxation models with a wide spectrum of relaxation times (the concept of a multiplicity of relaxation times).

8.3.1 The Debye model

The formulas for the description of frequency dependencies of the simplest-type relaxation polarization and the simplest hydrodynamic model of such a relaxation were established by P. Debye (Debye, 1929). The processing methodology, developed in this work, was widely disseminated afterwards in processing the experimental results obtained from studying a vast class of dielectrics, as well as systems of a different physical nature. This circumstance is physically associated with the fact that here is considered the simplest and, as it turned out later, a completely fundamental model, where the polarization dependence $f(\tau)$ (see equations (8.1) and (8.3)) is exponential:

$$f(\tau) = \text{const} \exp(-\tau/\tau_0) = \frac{\varepsilon_0 - \varepsilon_\infty}{\tau_0} \exp(-\tau/\tau_0), \tag{8.14}$$

where τ_0 is some characteristic quantity having the dimension of time and indicating that during the time τ_0 the polarization will change (increase and decrease) e times.

The substitution of (8.14) into (8.3) and appropriate integration results in the expression:

$$\dot{\varepsilon}(\omega) - \varepsilon_\infty = \frac{\varepsilon_0 - \varepsilon_\infty}{1 + \mathrm{j}\omega\tau_0}. \tag{8.15}$$

Separating the real and imaginary parts of the complex dielectric permittivity, we obtain the well-known Debye formulas:

$$\varepsilon_1(\omega) = \varepsilon_\infty + \frac{\varepsilon_0 - \varepsilon_\infty}{1 + \omega^2\tau_0^2}, \tag{8.16}$$

$$\varepsilon_2(\omega) = (\varepsilon_0 - \varepsilon_\infty)\frac{\omega\tau_0}{1 + \omega^2\tau_0^2}. \tag{8.17}$$

These formulas have been widely used in various areas of natural science (not only in dielectric relaxation theory), since the exponential system's response to the external (stepwise) effect is characteristic of a very wide class of physical systems – radio-engineering and radiophysical systems for instance (see Chapters 2 and 3).

The spectral behaviour of quantities $\varepsilon_1(\omega)$ and $\varepsilon_2(\omega)$ as a function of $\lg(\omega t)$ is presented in Figure 8.5 in the dimensionless form. As the figure shows, in the low-frequency $\lg(\omega t) < -3$ and high-frequency $\lg(\omega t) > 3$ ranges no variation of the complex permittivity with $\lg(\omega t)$ is observed. For intermediate values $-3 \leq \lg(\omega t) \leq 3$ the appearance of dispersion $\varepsilon(\omega)$ is typical. From Figure 8.5 it directly follows that the relaxation maximum frequency is related to the relaxation time as follows: $f_S = (2\pi\tau)^{-1}$. In some cases the notion of the relaxation maximum

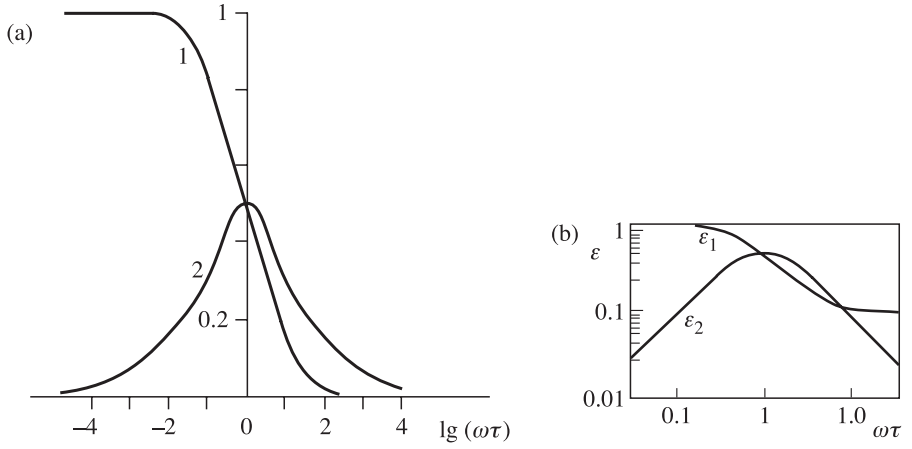

Figure 8.5. Frequency properties of $\varepsilon_1(\omega)$ and $\varepsilon_2(\omega)$ for Debye type dielectric media: (a) in semi-logarithmic coordinates in normalized dimensionless form, 1, $(\varepsilon_1(\omega) - \varepsilon_\infty)/(\varepsilon_0 - \varepsilon_\infty)$, 2, $\varepsilon_2(\omega)/(\varepsilon_0 - \varepsilon_\infty)$; (b) in bi-logarithmic coordinates for single Debye relaxation between $\varepsilon_0 = 1$ and $\varepsilon_\infty = 0.1$.

wavelength is used, whose value is equal to $\lambda_S = c(2\pi\tau)^{-1}$. The analysis of an imaginary part of the index of refraction of real media (water) indicates that in exactly this part of the frequency band the Debye mechanism forms some kind of pattern (designated as KDC in Figure 8.3) of the frequency dependence $\varepsilon_2(\lambda)$ (Figure 8.5(b)). This pattern represents the characteristic form of the pure Debye-type relaxation mechanism, which has a maximum at the wavelength λ_S and then the characteristic drops in the direction of long wavelengths as λ^{-1} and in the direction of shorter wavelengths as λ^{+1} (Figure 8.5(b)). This frequency peculiarity is quite typical for the pure Debye-type mechanism only, and we shall use it in analysing the experimental data and in revealing the Debye type of relaxation.

It follows from the equation, that for $\omega = 0$, $\varepsilon_1 = \varepsilon_0$, where ε_0 is (as we have already noted) the static dielectric constant. At very low frequencies the dipoles have time enough to synchronously follow the variation of the external electric field, and the polarization reveals itself completely. The value of the factor of losses $\varepsilon_2(\omega)$ is insignificant in this case. At very high frequencies the dipoles have no time to be oriented; they can be considered as motionless, and the orientational polarization is absent in this case. Therefore, for $\omega \to \infty$ $\varepsilon_2 = 0$ as well. Note that the frequency tending to infinity is certainly a purely formal procedure. Really, here we deal with the region lying outside the sphere of influence of the given relaxation mechanism. However, as we have already shown for the example of the dielectric properties of water, the merging of effects of various mechanisms is possible in some frequency bands (see Figure 8.3 and section 8.2). The prominent dispersion of quantity $\varepsilon(\omega)$ is characteristic for the intermediate range of frequencies.

The relaxation time τ was introduced for the first time as a parameter into the relaxation Debye theory (Debye, 1929). The substance response to the effect of the

external electromagnetic field, varying in time according to the harmonic law, is described by the phenomenological equation (8.3). The response function depends on the character of thermal motion of polar molecules. It is the dynamics of molecules which is usually associated with the relaxation time. The given parameter characterizes, in the general case, the process of spontaneous transition of a nonequilibrium macroscopic system into the state of thermodynamic equilibrium. The relaxation time depends on the temperature and on the intermolecular interaction potential. This quantity is determined directly from the experiment and corresponds, in the general case, to the frequency at which the maximum of dielectric losses is achieved. The reverse relaxation time $1/\tau_0$ characterizes the rate of dipoles' polarization establishment during the field action time. The use of the 'relaxation' term is most justified in describing the dynamics of molecular processes as the rate of equilibrium state establishment after removing the external effect. Exactly such a sense is given to the relaxation parameter that appeared in equations (8.15)–(8.17) in the Debye relaxation theory.

The simplest of existing ideas on the character of relaxation processes in polar liquids are based either on the hydrodynamic (and phenomenological) Debye model (Debye, 1929), or on the Frenkel model (Frenkel, 1975). In the Debye model the process of molecules reorientation in the liquid phase is considered to be the result of rotational diffusion of a solid sphere in the continuous viscous medium. According to Frenkel, on the other hand, the reorientation of molecules in the liquid phase is accomplished by jumps, by overcoming some potential barrier. Both models, in spite of their great difference, result in the simplest type of relaxation process, which can be characterized by a single relaxation time τ_0. In other words, the spectrum $G(\tau)$ of relaxation times (if it does really exist) can be presented in the form of delta-function $G(\tau) = \delta(\tau - \tau_0)$.

It was shown in some papers that a single relaxation time will always be observed in a liquid, if the following conditions are satisfied:

(1) the orienting interactions between molecules are absent;
(2) the molecules' reorientation process (when applying or removing the external electric field) takes place as the rotation with friction or as the transition over the potential barrier; and
(3) all dipoles are at equivalent positions.

If these conditions are met, the dielectric characteristics of a polar liquid as a function of the external field frequency will correspond to the Debye model (with a single relaxation time).

The following relation can easily be obtained from the Debye formulas (8.16) and (8.17):

$$\left[\varepsilon_1(\omega) - \frac{\varepsilon_0 - \varepsilon_\infty}{2}\right]^2 + \varepsilon_2^2 = \left(\frac{\varepsilon_0 - \varepsilon_\infty}{2}\right)^2. \tag{8.18}$$

Expression (8.18) represents the equation of a circle with radius $(\varepsilon_0 - \varepsilon_\infty)/2$.

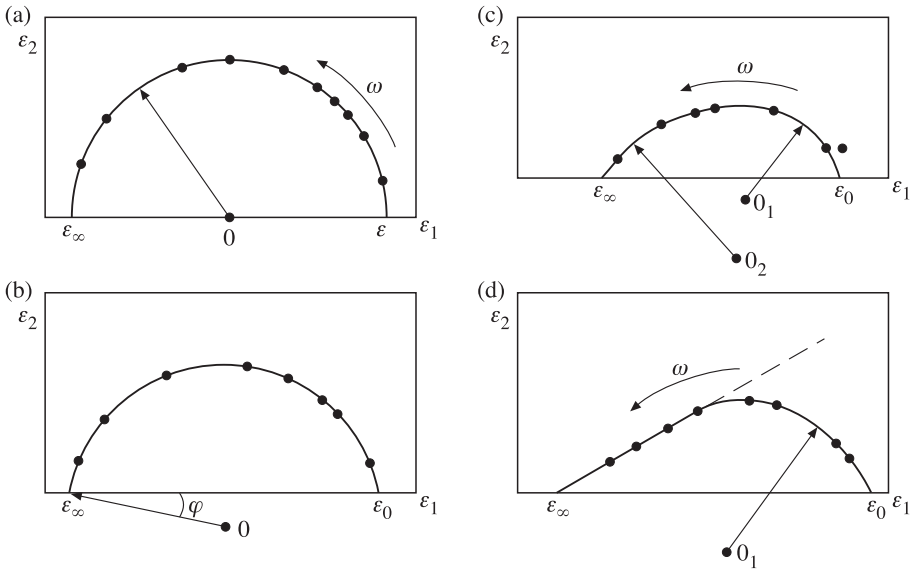

Figure 8.6. Relationship of the imaginary part of complex permittivity as a function of the real part (Cole–Cole diagram) for dielectric medium with various polarization mechanisms. (a) Debye model, (b) Cole–Cole model, (c) Davidson–Cole model, (d) Havriliak–Negami model. Experimental data are marked by black dots. The arrow points to an increase in frequency.

Therefore, for performing the diagram technique on the experimental data correspondence to the Debye model it is necessary to plot the values of ε_1 along the abscissa axis and the values of ε_2, found at various frequencies, at $T = \text{const}$, along the ordinate axis. And if the Debye formulas are valid, we shall obtain a full semicircle, whose centre lies on the abscissa axis at point $(\varepsilon_0 - \varepsilon_\infty)/2$ (Figure 8.6(a)). The position of the experimental data in the Cartesian coordinate system $\varepsilon_1 - \varepsilon_2$ was called the Cole–Cole diagrams. The deviations in the experimental data position from a semicircle will testify to the obvious deviation of relaxation properties of a dielectric from the Debye model. Such a kind of presentation is used not only in analysing the relaxation properties of dielectrics, but in studying the other physical systems with the relaxation mechanism close to the Debye one.

The relaxation time value can be estimated by formulas which directly follow from the Debye relations (8.16)–(8.17):

$$\tau_0 = \frac{1}{\omega} \frac{\varepsilon_2(\omega)}{\varepsilon_1(\omega) - \varepsilon_\infty}, \tag{8.19}$$

where the real and imaginary parts of the dielectric permittivity are taken from the experimental data at the working (given) frequency of measurements.

The diagram technique is very convenient for estimating the values of ε_0 and ε_∞, based on using strictly linear interpolation in the following relations being a

consequence of the Debye formulas:

$$\varepsilon_1(\lambda, t) = \varepsilon_0(t) - \lambda_S(t)\frac{\varepsilon_2(\lambda, t)}{\lambda}, \tag{8.20}$$

$$\varepsilon_1(\lambda, t) = \varepsilon_\infty(t) + \lambda\frac{\varepsilon_2(\lambda, t)}{\lambda_S(t)}. \tag{8.21}$$

The symmetry in the Debye formulas makes it possible to form one more series of graphical techniques for experimental data processing; they are summarized in the book by Akhadov (1977).

The deviations in using the Cole–Cole diagram and linear approximations are so noticeable and impressive that they can serve as clear evidence of the deviation of a dielectric's polarization properties from the Debye model. Some indicative examples of using these approaches in analysing the dielectric properties of fresh and salt water are presented in papers by Sharkov (1983, 1984, 1996c) and Liebe *et al.* (1991) (see also sections 8.4 and 8.5 below).

8.3.2 Models of multiplicity of relaxation times

The Debye model successfully describes the frequency dispersion of the complex dielectric permittivity for some dielectrics (such as freshwater or alcohols). However, many cases are known (and of importance for us is to mention, first of all, solutions of salts: electrolytes and seawater), where the Debye formulas do not describe the experimental frequency dependencies in principle. However, the success of the Debye model was so great, that the further development of non-Debye relaxation mechanisms has advanced mainly by way of using the concept of a multiplicity of Debye relaxation times for non-Debye-type dielectrics. Certainly, such an approach is only one of those possible; however, it dominates now in dielectric relaxation theory. Its essence is as follows.

In liquids and solid substances (of polymer type), consisting of composite clusters of molecules or of polyatomic molecules, a variety of dielectric Debye relaxation times is observed where each dipole has its own polarization establishment time. In other words, there exists some particular distribution of dielectric relaxation times around its most probable value. The character of the distribution and its parameters will be just those important physical characteristics that determine the structure of the substance. And it can be supposed that for polar high-molecular systems (including organic compounds) the existence of a variety of dielectric relaxation times should be observed all the more.

Thus, if the number of relaxation times is fairly high, their distribution can be presented as a continuous set of times. And in this case we can use the methodology of introducing the distribution density $F(\tau)$ (or, as is sometimes said, the 'spectrum') of Debye-type relaxation times in the field of their existence (see Chapter 2). In the general case the complex dielectric permittivity is written as

$$\frac{\dot{\varepsilon}(\omega) - \varepsilon_\infty}{\varepsilon_0 - \varepsilon_\infty} = \int_0^\infty \frac{F(\tau)\,\mathrm{d}\tau}{1 + \mathrm{j}\omega\tau}, \tag{8.22}$$

where $F(\tau)\,\mathrm{d}\tau$ is the fraction of the Debye relaxation processes with the relaxation time falling in the range of $\tau + \mathrm{d}\tau$. If we suppose the existence of a single relaxation time in a system (or, in other words, $F(\tau) = \delta(\tau - \tau_0)$), then expression (8.22) automatically transfers into the Debye relationship (8.15). As usual, natural normalization is introduced for function $F(\tau)$, namely,

$$\int_0^\infty F(\tau)\,\mathrm{d}\tau = 1. \tag{8.23}$$

Separating the real and imaginary parts of expression (8.22), we obtain:

$$\frac{\varepsilon_1(\omega) - \varepsilon_\infty}{\varepsilon_0 - \varepsilon_\infty} = \int_0^\infty \frac{F(\tau)\,\mathrm{d}\tau}{1 + \omega^2\tau^2}, \tag{8.24}$$

$$\frac{\varepsilon_2(\omega)}{\varepsilon_0 - \varepsilon_\infty} = \int_0^\infty \frac{\omega\tau F(\tau)\,\mathrm{d}\tau}{1 + \omega^2\tau^2}. \tag{8.25}$$

In view of the fact that the relaxation spectra, as experiments have shown, overlap considerable spans of time, the distributions of dielectric relaxation times are considered in the logarithmic coordinates. That is, with the replacement of variables $s = \ln(\tau_0/\tau)$ the new function $Z(s)$ of relaxation times distribution is introduced, which follows from the normalization condition:

$$\int_0^\infty F(\tau)\,\mathrm{d}\tau = \int_{-\infty}^\infty Z(s)\,\mathrm{d}s = 1. \tag{8.26}$$

Then expressions (8.24) and (8.25) will take the form, respectively,

$$\frac{\varepsilon_1(\omega) - \varepsilon_\infty}{\varepsilon_0 - \varepsilon_\infty} = \int_{-\infty}^\infty \frac{Z(s)\,\mathrm{d}s}{1 + \exp\,[2(x - s)]}, \tag{8.27}$$

$$\frac{\varepsilon_2(\omega)}{\varepsilon_0 - \varepsilon_\infty} = \int_{-\infty}^\infty \frac{\exp\,(x - s)Z(s)\,\mathrm{d}s}{1 + \exp\,[2(x - s)]}, \tag{8.28}$$

where $x = \ln\,(\omega\tau_0)$.

Thus, the procedure of the experimental data analysis is reduced to searching for function $Z(s)$, since it is just an instantaneous frequency characteristic of molecular mobility in a studied object and is determined by physicochemical properties of the latter.

Strictly speaking, finding a true distribution function $Z(s)$ is reduced to the solution of so-called reverse problems of the dielectric spectrometry (Usmanov, 1996), namely, to the relations:

$$\int_{-\infty}^\infty \frac{Z(s)\,\mathrm{d}s}{1 + \exp\,[2(x - s)]} = U(x), \tag{8.29}$$

$$\int_{-\infty}^\infty \frac{\exp\,(x - s)Z(s)\,\mathrm{d}s}{1 + \exp\,[2(x - s)]} = V(x), \tag{8.30}$$

where $U(x)$ and $V(x)$ designate quantities $(\varepsilon - \varepsilon_0)/(\varepsilon_0 - \varepsilon_\infty)$ and $\varepsilon_2/(\varepsilon_0 - \varepsilon_\infty)$,

which were obtained experimentally with some measurement errors. The latter, in their turn, represent an additive type of noise having a fluctuation character, with the normal distribution law (see Chapter 2).

Indeed, the solution of integral equations (8.29) and (8.30) results in the well-known reverse problem of restoring $Z(s)$ from the approximate values of $U(x)$ and $V(x)$, which is just an indicator of incorrectly stated problem (Tichonov and Arsenin, 1979). The sought distribution function $Z(s)$ is determined by solving the first-order Fredholm equation of convolution type. Really, the integral equations (8.29) and (8.30) can easily be rewritten in the form of the first-order Fredholm equation of convolution type. For example, equation (8.30) can be written as

$$\int_{-\infty}^{\infty} K(x-s)Z(s)\,\mathrm{d}s = V(x), \tag{8.31}$$

where

$$K(x-s) = \frac{\exp(x-s)}{1+\exp[2(x-s)]} = \frac{1}{2}\mathrm{ch}(x-s) \tag{8.32}$$

($\mathrm{ch}(x-s)$ is the hyperbolic cosine) is called the core of the integral equation. For solution of the integral equations of convolution type some rather complicated techniques of statistical regularization are applied, including Tichonov's method of regularization (Tichonov and Arsenin, 1979), which require serious mathematical training and appropriate computer means (Usmanov, 1996).

Historically, however, the first graphical constructions applied in polarization investigations of dielectrics were those of the Cole–Cole diagram type. Such approaches were called the 'traditional' methods, applying the 'matching' empirical functions of distribution of dielectric relaxation times, offered by Cole and Cole (1941), Davidson and Cole (1950), Havriliak and Negami (1967) as well as the series of other functions. Such a graphical 'traditional' approach was found to be, nevertheless, in many cases a rapid and rather reliable method for studying the dielectrics. And for these reasons such an experimental technique is actively applied now (we shall demonstrate this below in the analysis of dielectric properties of freshwater and electrolytes). It should be emphasized that similar graphical approaches are used not only in studying dielectrics, but also in studying physical systems of a quite different nature which possess relaxation properties at the same time.

Now we consider briefly the technique of graphical determination of limiting values of dielectric permittivity for a given (single) relaxation mechanism. The values of parameters ε_0 and ε_∞ in the case of applying any of considered empirical distribution functions $Z(s)$ are determined similarly. If $\omega\tau \to \infty$, then in all cases $\varepsilon_1(\omega) \to \varepsilon_\infty$ and $\varepsilon_2(\omega) \to 0$; therefore, $\varepsilon(\omega) \to \varepsilon_\infty$. When $\omega\tau \to 0$, $\varepsilon_1(\omega) \to \varepsilon_0$ and $\varepsilon_2(\omega) \to 0$; then $\varepsilon(\omega) \to \varepsilon_0$. For these reasons the dielectric parameters ε_0 and ε_∞ can be found as the points of intersection of experimental dependencies $\varepsilon_2 = f(\varepsilon_1)$ with the axis of real numbers at high and low frequencies for any polarization mechanism. In the given context we mean, certainly, the frequency bands in which the given (single) relaxation mechanism is actively manifested. The most probable

dielectric relaxation time τ_0 (under the action of any mechanism) is determined from the condition of maximum of the frequency dependence of the factor of losses:

$$2\pi f_0 \tau_0 = 1, \tag{8.33}$$

where f_0 is the frequency of a maximum of the factor of losses. As a rule, in the region of active manifestation of polarization properties the experimental dependence $\varepsilon_2 = f(\omega)$ has a prominent extremum (see examples in Figures 8.3 and 8.4), and f_0 is determined fairly reliably for the given mechanism. If, however, the interrelation between various mechanisms is complicated, the problem of determination of the frequency of a maximum of losses and limiting values of dielectric permittivity represents a fairly complicated problem (Sharkov, 1983, 1984, 1996c; Liebe *et al.*, 1991). In this case it is necessary to use *a priori* data about possible relaxation mechanisms.

8.3.3 The Cole–Cole model

As we have noted above, many experimental results are known where the Debye formulas do not describe the frequency behaviour of dielectric properties of a dielectric. In this case the experimental curve $\varepsilon_2 = f(\varepsilon_1)$ is not a full arc of semicircle with the centre lying on the abscissa axis. It represents either a non-full arc segment of a circle, or 'bevelled arcs', composed as though of two semicircles with spaced centres and with various values of radii. More complicated constructions are also possible, such as the line segment transferring into the arc segment of a circle. It is important to note that each of these geometrical constructions corresponds to some particular feature of the relaxation mechanism.

If the experimental curve $\varepsilon_2 = f(\varepsilon_1)$ represents an arc of a semicircle with the centre lying below the abscissa axis (Figure 8.6(b)), then in this case, as the special investigations have shown (Cole and Cole, 1941), the dielectric permittivity can be described by the following empirical equation called the Cole–Cole equation:

$$\frac{\dot{\varepsilon}(\omega) - \varepsilon_\infty}{\varepsilon_0 - \varepsilon_\infty} = [1 + (\mathrm{j}\omega\tau_0)^{1-\alpha}]^{-1}, \tag{8.34}$$

where τ_0 is some average (or effective) value of the relaxation time of the dielectric polarization process, and α is some parameter describing the character of distribution of relaxation times. All these considerations are valid, of course, provided that the concept of multiplicity of relaxation times is accepted.

As the solution of integral equations (8.29)–(8.30) has shown, the Cole–Cole equation corresponds to the symmetrical distribution of relaxation times, which is close to the Gaussian distribution and is determined by the function:

$$Z(s) = \frac{1}{2\pi} \frac{\sin(\pi\alpha)}{\mathrm{ch}\,[(1-\alpha)s] + \cos(\pi\alpha)}. \tag{8.35}$$

Investigation of the molecular mobility of dipoles of some polar substances has shown that the use of a purely normal (Gaussian) distribution of relaxation times is expedient. However, the direct use of the techniques of reverse spectrometry

problems (8.29)–(8.30) is rather cumbersome in this case, which requires the development of a series of approximate methods (Usmanov, 1996).

8.3.4 The Davidson–Cole model

Suppose the molecular structure of a dielectric is such that the distribution of relaxation times has a sharply asymmetric form. So, for example, the dielectric does not have any relaxators with a relaxation time lower than the specified one. In this case the aforementioned circumstance is clearly exhibited on the graphical presentation $\varepsilon_2 = f(\varepsilon_1)$ as well – it becomes sharply asymmetric also. If the function of distribution of relaxation times $Z(s)$ is written in a sharply asymmetric form:

$$Z(s) = \begin{cases} \dfrac{\sin(\beta\pi)}{\pi}(1 - \exp(-s)^{-\beta} & \tau > \tau_0 \\ 0 & \tau \le \tau_0 \end{cases}, \tag{8.36}$$

then, as Davidson and Cole (1950) have shown, the complex dielectric permittivity can be presented by the following semi-empirical Davidson–Cole equation:

$$\frac{\dot{\varepsilon}(\omega) - \varepsilon_\infty}{\varepsilon_0 - \varepsilon_\infty} = (1 - \mathrm{j}\omega\tau_0)^{-\beta}. \tag{8.37}$$

In the graphical form of the Cole–Cole diagram this model represents a 'bevelled arc' composed as though of two non-full arcs with spaced centres and with various values of radii (Figure 8.6(c)). Special graphical techniques were developed for the determination of distribution parameters (Akhadov, 1977; Usmanov, 1996).

8.3.5 The Havriliak–Negami model

Two various empirical expressions for the function of distribution of relaxation times, used earlier for description of the 'arc segment' (8.34) and 'bevelled arc' (8.37), can be generalized in the form of the Havriliak–Negami distribution (Havriliak and Negami, 1967):

$$\frac{\dot{\varepsilon}(\omega) - \varepsilon_\infty}{\varepsilon_0 - \varepsilon_\infty} = [1 + (\mathrm{j}\omega\tau_0)^{1-\alpha}]^{-\beta}. \tag{8.38}$$

If we assume that in equation (8.38) $\beta = 1$, we shall obtain the expression for the Cole–Cole distribution function in the form of (8.34). For $\alpha = 0$ we obtain the expression for the Davidson–Cole distribution function in the form of (8.37), and at simultaneous equalities $\alpha = 0$ and $\beta = 1$ formula (8.38) represents the Debye function (8.15). Figure 8.6(d) represents the asymmetric arc function $\varepsilon_2 = f(\varepsilon_1)$, which corresponds to the Havriliak–Negami distribution function. As seen from the figure, this theoretical curve $\varepsilon_2 = f(\varepsilon_1)$ is linear in the high-frequency band and represents an arc segment in the low-frequency band. To check the possibility of quantitative description of the experimental data of dielectric measurements by the empirical Havriliak–Negami distribution function (8.38), it is necessary to determine graphically the values of five dispersion parameters $(\varepsilon_0, \varepsilon_\infty, \alpha, \beta, \tau_0)$.

Parameter ε_0 is obtained by extrapolation up to intersection of dielectric permittivity $\varepsilon_1(\omega)$ with the abscissa axis in the low-frequency band, and parameter ε_∞ is found by linear extrapolation of experimental data points $\varepsilon_2 = f(\varepsilon_1)$ up to intersection with the same axis in the high-frequency band (Figure 8.6(d)). The other parameters are determined by the special graphical procedure (Usmanov, 1996).

Detailed dielectric investigations of complex polar dielectrics (of natural and artificial origin) have indicated that in many natural substances there takes place the superposition of both relaxation dipole processes and the phenomena of resonance character, and this occurs in rather complicated combinations (the simplest versions are demonstrated in Figures 8.3 and 8.4). For analysing such complicated dipole-cluster dielectric processes, researchers have used, along with the models listed above, some more complicated empirical functions of distribution of relaxation times and, accordingly, more complicated graphical data processing techniques.

As a whole, we note that the recognition of various polarization mechanisms from the experimental data represents a quite specific problem, and its detailed discussion is beyond the scope of this book. The appropriate useful information can be drawn up from the original sources and the specialized literature (Cole and Cole, 1941; Davidson and Cole, 1950; Havriliak and Negami, 1967; Akhadov, 1977; Usmanov, 1996).

8.4 DIELECTRIC PROPERTIES OF FRESHWATER

The development and manufacturing of high-sensitivity microwave remote sensing and scatterometric onboard systems in recent years (see Chapter 14) makes it possible to investigate fine features of radiobrightness fields (of the order of 0.5–0.1 K and lower) and backscattering fields (0.5 dB) of the Earth surfaces. This circumstance necessitates, in its turn, the development and formation of a high-precision relaxation model of the dielectric characteristics of liquid water, since in the majority of problems of remote sensing the terrestrial surfaces and dispersive atmospheric formations the relaxation model represents a fundamental basis for theoretical and practical calculations (see Chapters 7, 11 and 12). Using known microwave remote sensing and radiolocation relations, it can easily be shown (Sharkov, 1983) that the relative dielectric constant variations of $\pm 5\%$ may cause radiobrightness contrasts of $\pm(1.5–2)$ K (in the centimetre and millimetre bands) and scattering cross-section variations of $\pm(0.05–0.15)$ dB (for grazing angles in the millimetre and centimetre bands). Therefore, the problem of developing such a numerical relaxation model should be stated now. Such a model would allow us to describe the experimental results to an accuracy not worse than $\pm 1\%$ in a wide range of temperatures and wavelengths (from 1 km to the submillimetre band). In spite of the fact that the indicated problem was first formulated rather long ago (Sharkov, 1983), recent investigations (Lipton *et al.*, 1999) have shown, that its final solution should not be expected soon. This is, first of all, due to the situation in

studying the structural properties of liquid (fresh) water and the physicochemical properties of supercooled water.

8.4.1 The structure of water

The structure of liquid water is the subject of intensive investigations and discussions at present (see, for example, Sinyukov, 1976; Horne, 1969). The polar nature of a water molecule and its ability to generate strong intermolecular hydrogen bonds result in associating water molecules into the multi-molecular complex containing a multitude of molecules. Liquid water represents a mixture of such sets, or 'clusters', with more or less 'free', or monomeric, water molecules. As the temperature grows, the clusters are 'melted', and, since their specific volume is greater than that of non-associated water, the hydrostatic pressure results in the destruction of structured sections existing in a liquid.

Our ideas on the shape of a water molecule are mainly based on studying its gaseous state. However, there is no reason to believe that in water, or in any fluid, the structure of a molecule is quite different.

According to modern notions, the electron cloud of a water molecule has the shape of truncated four-bladed propeller, which can be placed in an irregular cube. In this case the oxygen atom is at the centre, and the two hydrogen atoms are at opposite corners of one of the cube's faces (Figures 8.7(a) and (b)). The H–O–H angle constitutes $104^\circ\ 31'$. Two of the eight electrons of an oxygen atom are situated near its nucleon, another two electrons are associated with hydrogen atoms, and two non-separated pairs of electrons form the branches, which extend up to opposite corners of that cube's face which is opposite to the face occupied by the hydrogen atoms. These branches of an electron cloud are of special interest for us, because, being the areas of concentration of negative charges, they attract positively charged hydrogen atoms of adjacent molecules and provide the bond between water molecules (the so-called hydrogen bond) (Figure 8.7(c)). The O–H distance for a water molecule in the gaseous phase equals 0.9568 A and slightly increases in the solid (ice) phase, reaching 0.99 A.

Although the problem of the precise distribution of a molecule charge has yet to be finally solved, it is in any case of importance that the charge distribution causes a large electrical dipole moment of a water molecule and a strong hydrogen bond between the molecules. These quantum-mechanical characteristics are of principal importance, because, if the water molecules did not have negatively charged electron cloud branches and dipole moments, they would not be able to interact between each other, and no liquid water would exist on the Earth's surface. The World Ocean would be gaseous and, accordingly, no evolved biological life would exist on the Earth.

Water vapour does not have any structure. It consists of monomeric water molecules, rarely encountered dimers of water. The first models of liquid water structure are subdivided into two types: some theories consider the water structure as a homogeneous continuum; in other models the existence of a mixture of various structures is supposed. But in both cases the structure of a solid state (ice) is used as a

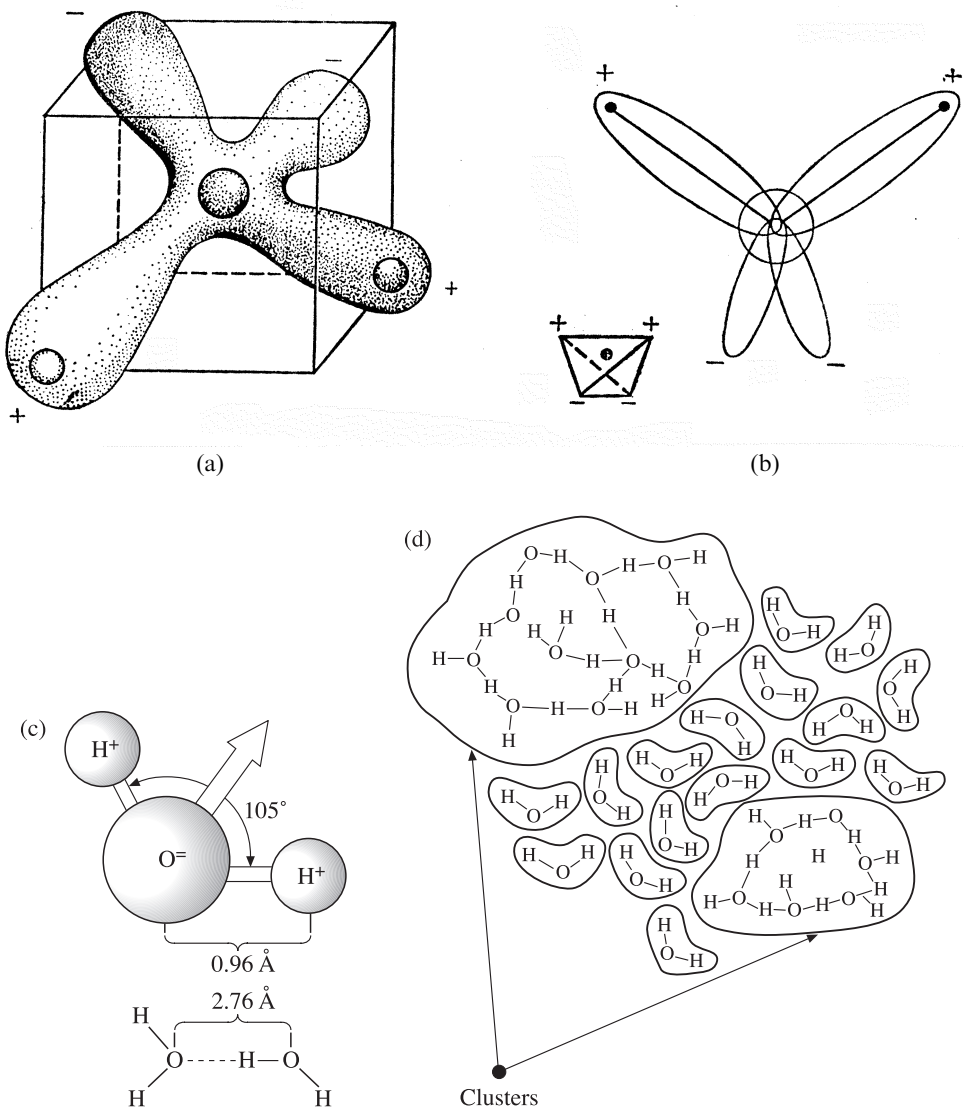

Figure 8.7. Electronic and structural peculiarities of the water molecule. (a) Electronic 'clouds' of water molecule. (b) Molecular orbitals of water molecule. (c) Schematic presentation of structural properties of water molecule and hydrogen bond. The direction of the dipole moment is marked by a white arrow. (d) The structure of liquid water in the Frank–Wen model of 'flickered' clusters (Horne, 1969).

starting point. Further development has led to the cluster Frank–Wen model. Its essence consists in the fact that liquid water is supposed to represent a conglomerate of 'flickered' clusters composed of molecules associated by hydrogen bonds and 'floating' in a more or less 'free' water (Figure 8.7(d)). The theory does not

postulate the existence of remainders of a crystal lattice of ice and does not explain in detail either exactly how the water molecules are combined in clusters or whether the quasi-crystalline structure exists inside the clusters at all. Of principal significance here is the idea of the 'flickering' nature of clusters, which are constantly forming and dissolving. Outside the clustered zones the hydrogen bonds are broken up, and the water behaves as a 'monomeric non-bonded water' (Horne, 1969).

In the case of both quasi-crystalline and cluster models the presence of monomeric water molecules in parcel of water is postulated and, accordingly, there should exist a certain contribution of monomers to the relaxation properties. Such ideas are very close to the original hydrodynamic Debye model (Debye, 1929), namely, the idea of a solitary dipole in a viscous homogeneous medium. This model leads to the well-known Debye relaxation mechanism (with a single relaxation time) (section 8.3). It can easily be seen here that the presence of both quasi-crystalline structures and flickering clusters should generate a variety of relaxators with various relaxation times and, thereby, it should sharply transform the purely Debye model of liquid water into one of versions of models with a multiplicity of relaxation times. However surprising this idea may seem, the study of dielectric relaxation (see below) indicates that in fresh water (unlike in electrolytes, e.g. salt water) there exists only one type of rotating particle (relaxator), which is presumably supposed to be a dipole-monomer with a single relaxation time.

Another complicated problem in this area is the structure of highly supercooled (well below freezing point) water, whose presence is experimentally recorded in convective cloudy systems (Rosenfeld and Woodley, 2000). The question is: does the supercooled water keep the structure of so-called 'warm' water (with temperature higher than 0°C), or is it significantly rearranged (Angell, 1982)? No unambiguous answer to this question has yet been given.

However, in spite of certain successes in studying the physicochemical properties of liquid water, no-one has managed to develop a strictly quantum (without phenomenological enclosures in the form of structural models) theory of the electrodynamic properties of liquid water that allows one to obtain design values of the dielectric parameters of water to a high degree of accuracy ($\sim$1%). Researchers have for a long time been forced to follow the path of developing and modernizing semi-empirical dependencies of appropriate parameters in the Debye (D) relaxation model (equation (8.15)) or in the Cole–Cole (C-C) model (equation (8.34)), as new and new experimental data have appeared (Saxton, 1952; Hasted, 1961, 1972; Ray, 1972; Rozenberg, 1972; Mason *et al.*, 1974; Mitnik, 1978; Kaatze and Giese, 1980;Zaghloul and Buckmaster, 1985; Sharkov, 1983, 1996c; Liebe *et al.*, 1991).

Whereas all these models are fairly close in respect of the qualitative character of frequency dependencies of dielectric properties of water, they are quite contradictory in their detail. This concerns, first of all, the values of the distribution parameter α (i.e. the definition of the type of model, in essence) and of the 'optical constant', and the dependencies of these parameters on temperature. So, in the generalized paper by Mason *et al.* (1974) the proposed two versions of relaxation models for liquid fresh water – the D model and the C-C model – were compared with the experimental data available in 1974. This comparison has not shown any essential advantages in using

the C-C model as compared to the Debye model. Both models, in general (for some particular applications), to a low but satisfactory degree of accuracy (of 4–7%), are supported by the experimental data on the complex permittivity (CP) in the metre, decimetre and centimetre bands. Further advance into the millimetre and submillimetre bands is characterized, however, by sharp distinctions between the initial experimental data, reaching 25% or more, even within the narrow temperature range of 19–22°C (Sharkov, 1983). Data for a wider temperature range are absent. This situation was also noticed later by Liebe *et al.* (1991). It can easily be seen (Sharkov, 1983) that, in re-calculating for emissive characteristics (Chapter 7), the uncertainty in values of radiobrightness temperature for the water surface reaches 15–20 K. And such an accuracy is already inadmissible when studying a variety of modern remote sensing tasks (see Chapters 7 and 12).

Sharkov (1983) has shown that the main physical reason for discrepancy between empirical models (in parameter ε_∞, first of all) is the illegitimate use of experimental data obtained in the millimetre and submillimetre bands (i.e. outside the sphere of influence of the purely Debye absorption band) for forming the simplest emipirical models, for example, the D model. However, the question of determining the high-frequency boundary of the Debye absorption band could not be considered in detail because of the absence of experimental data within a wide temperature range at that time. Liebe *et al.* (1991) have since shown that in this range the formation of the double Debye model with a double relaxation time value was possible. In other words, the question can be raised here about using the Davidson–Cole model (equation (8.34)) in this wavelength band. Strictly speaking, exactly this possibility is demonstrated by the qualitative pattern of frequency characteristics of the dielectric properties of water presented in Figure 8.3.

The purpose of this section is: (1) to compare, to a high degree of accuracy ($\sim$1%), the parameters of existing empirical design models both among themselves and with the D model parameters obtained by Sharkov (1983, 1996c) and Liebe *et al.* (1991) from CP experimental data processing in 1975–1991; and (2) to form the high-precision numerical relaxation model of the dielectric properties of liquid water and to consider the possibilities of its being applied to the solution of remote sensing tasks.

In so doing, special attention is given to determining the type of relaxation model that would adequately describe the dielectric parameters of liquid water in the millimetre band, as well as for supercooled water (in the temperature range from 0° to −40°C).

8.4.2 The experimental data processing technique

The values for the parameters of model D were obtained by Sharkov (1983, 1996c) by means of the diagram technique, which is based on constructing the linear approximation dependencies from the experimental data presented in the rectangular coordinate system (8.20)–(8.21). It follows from these relations that the sought values of the $\varepsilon_0(t)$ and $\varepsilon_\infty(t)$ parameters are determined at the point of intersection of linear approximations of data points on the ordinate axis. And the $\lambda_S(t)$ values are

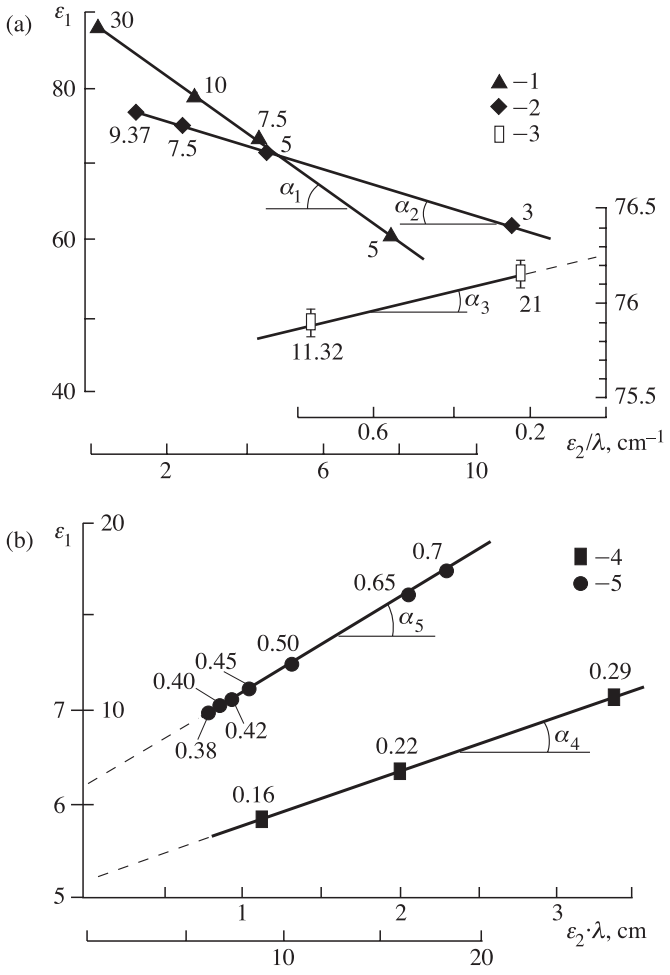

Figure 8.8. Experimental diagrams for $\varepsilon_1(\lambda)$ as function $\varepsilon_2(\lambda)/\lambda$ (a) and for $\varepsilon_1(\lambda)$ as function $\varepsilon_2(\lambda)\cdot\lambda$: (1) evidence of work (Kaatze and Giese, 1980) at $t = -4.1^\circ$C; (2) evidence of work (Burdette *et al.*, 1980) at $t = 23^\circ$C; (3) evidence of work (Ho and Hall, 1973) at $t = 30^\circ$C; (4) evidence of work (Blue, 1980) at $t = 20^\circ$C; and (5) evidence of work (Demyanov *et al.*, 1974). The solid lines show linear interpolations for equations (8.20) and (8.21). Experimental points are marked with wavelengths (in centimetres), at which they are obtained. Values for tangents of angles α_1, α_2, α_3, and cotangents of angles α_4, α_5 are given in corresponding columns in Table 8.1.

determined, accordingly, from the gradient of slope (the tangent or cotangent of the angle of slope, respectively) of the indicated dependencies. Examples of such constructions are presented in Figure 8.8(a) for centimetre and decimetre bands, and in Figure 8.8(b) for the millimetre band. The experimental data processing results are presented in Table 8.1 and in Figures 8.9–8.11. The discussion of the values of the

Table 8.1. Parameters of the D relaxation model for freshwater from experimental evidence

No. (1)	t, °C (2)	ε_0 (3)	ε_∞ (4)	λ_S, cm (5)	λ, cm (6)	Reference (7)
1	−4.1	89.1 ± 0.3		3.76 ± 0.1	2.3; 3.0; 3.4; 4.1; 5; 7.5; 10; 16.7; 30	Kaatze and Giese, 1980
2	0	87.8 ± 0.2		3.30 ± 0.05	3.9; 4.57; 5.66	Pottel and Lossen, 1967
3	0		5.9 ± 0.1	3.28 ± 0.05	0.82; 1.72; 1.18; 1.98	Pottel and Lossen, 1967
4	5	88.0 ± 0.5	5.0 ± 0.3	2.95 ± 0.03	3.19; 2.14	Lyaschenko *et al.*, 1976
5	20		5.2 ± 0.05	1.76 ± 0.05	0.163; 0.22; 0.29	Blue, 1980
6	20		5.9 ± 0.1	1.68 ± 0.05	0.38; 0.4; 0.42; 0.45; 0.5; 0.65; 0.70; 0.818	Demyanov *et al.*, 1974
7	23	79.0 ± 0.3		1.60 ± 0.03	3; 5; 7.5; 9.4; 14.3	Burdette *et al.*, 1980
8	25	78.2 ± 0.1		1.61 ± 0.02	5.66; 11.49	Pottel and Lossen, 1967
9	25	76.5 ± 0.5	5.0 ± 0.3	1.44 ± 0.02	3.19; 2.14	Lyaschenko *et al.*, 1976
10	25	78.9 ± 0.3	5.2 ± 0.3	1.60 ± 0.05	0.88; 1.55; 3.12	Van Loon and Finsy, 1957
11	30	76.27 ± 0.08			11.32; 20.98	Ho and Hall, 1973
12	35	75.2 ± 0.3		1.27 ± 0.05	0.82; 1.12; 1.72; 2.41; 3.9	Pottel and Lossen, 1967
13	50	70.9 ± 0.4		0.92 ± 0.03	0.82; 1.12; 1.72; 2.41; 3.9	Pottel and Lossen, 1967
14	50	69.5 ± 0.5	5.0 ± 0.3	0.77 ± 0.02	3.19; 2.14	Lyaschenko *et al.*, 1976
15	60	66.8 ± 0.1			17.24; 52.00	Pottel and Lossen, 1967
16	60	65 ± 1			0.84; 0.63; 3.15	Asheko *et al.*, 1989
17	80	60 ± 1			0.63; 0.84; 3.15	Asheko *et al.*, 1989

Note. Original experimental evidence for processing performed by Sharkov (1983) was carried over from literature references. λ are operating wavelengths. Errors indicated on parameters are determined from graphical processing.

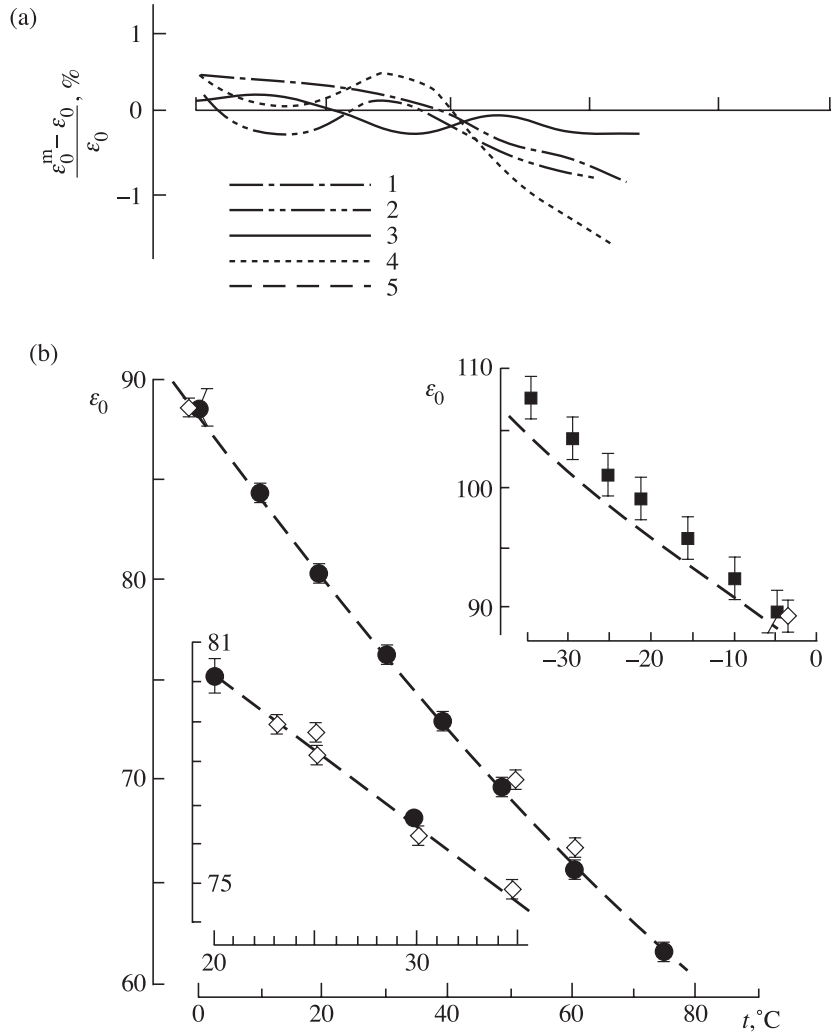

Figure 8.9. Temperature-dependence of static constant of liquid water. (a) Values ε_0 of models I–IV relative to model VI ε_0 (Mason *et al.*, 1974). (1 is model I; 2 is model II; 3 is model III; and 4 is model IV). (b) Absolute values of $\varepsilon_0(t)$. Dots present data of model IV with 90% confidence intervals. Squares present experimental evidence of work (Hasted and Shahidi, 1976). Diamonds present results obtained by Sharkov (1983) with processing experimental evidence available in literature (numerical values are given in Table 8.1). (5) Data of model VII, interpolating with equation (8.44).

parameters of model D thus obtained is given below. The efficiency of the considered technique (Sharkov, 1983, 1996c) is demonstrated by the inset in Figure 8.8. It can be seen here that the construction (8.20) enables us to obtain the value of parameter $\varepsilon_0(t)$ (with regard to errors of both geometrical constructions and experiment

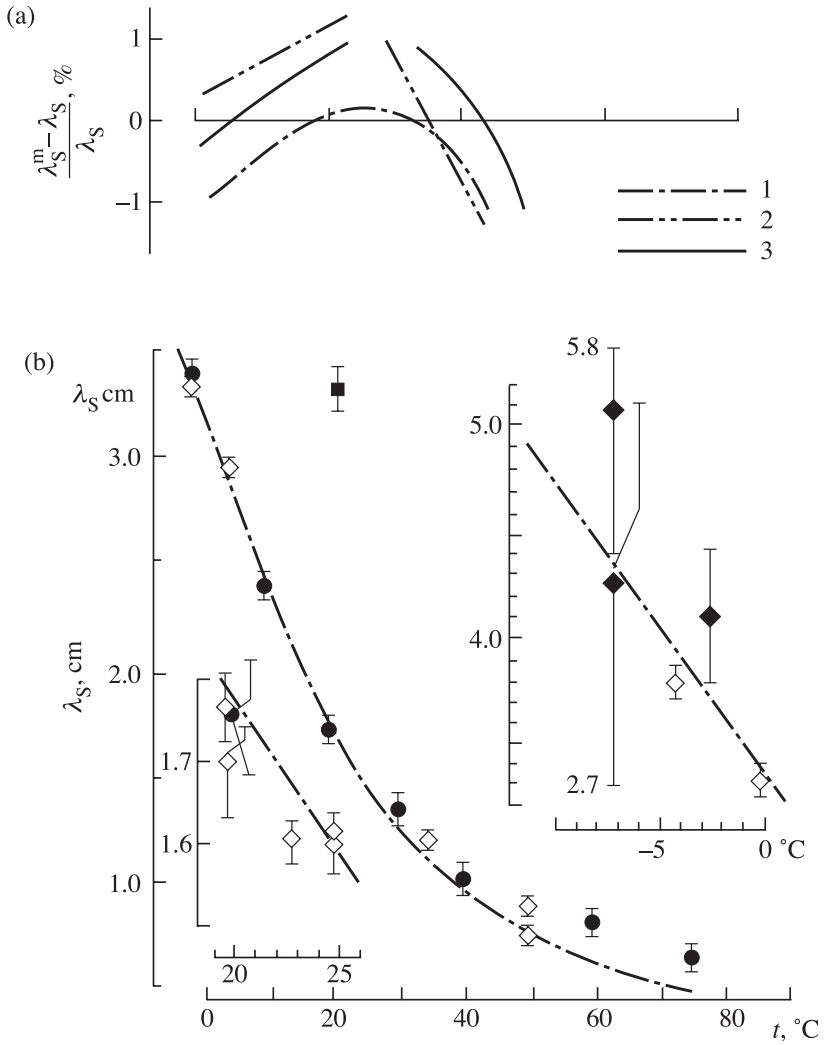

Figure 8.10. Temperature-dependence of relaxation wavelength. (a) Values λ_S of models I–III relative to model VI λ_S (Mason *et al.*, 1974) (1 is model I; 2 is model II; 3 is model III). (b) Absolute values of $\lambda_S(t)$. Solid dots present data of model VI with 90% confidence intervals. Solid diamonds present result obtained by Sharkov (1983) with processing remote sensing data of Akvilonova and Kutuza (1978). Open diamonds present results obtained by Sharkov (1983) with processing laboratory evidence on dielectric properties of liquid water (numerical values are given in Table 8.1).

(Ho and Hall, 1973)) to a record accuracy – better than 0.1%, in fact, $\varepsilon_0 = 76.27 \pm 0.08$ $(t = 30^\circ\,\mathrm{C})$. This result is virtually inaccessible using the other graphical techniques, in particular, in constructing the standard C-C diagram (using equation (8.18) and Figure 8.6(a)).

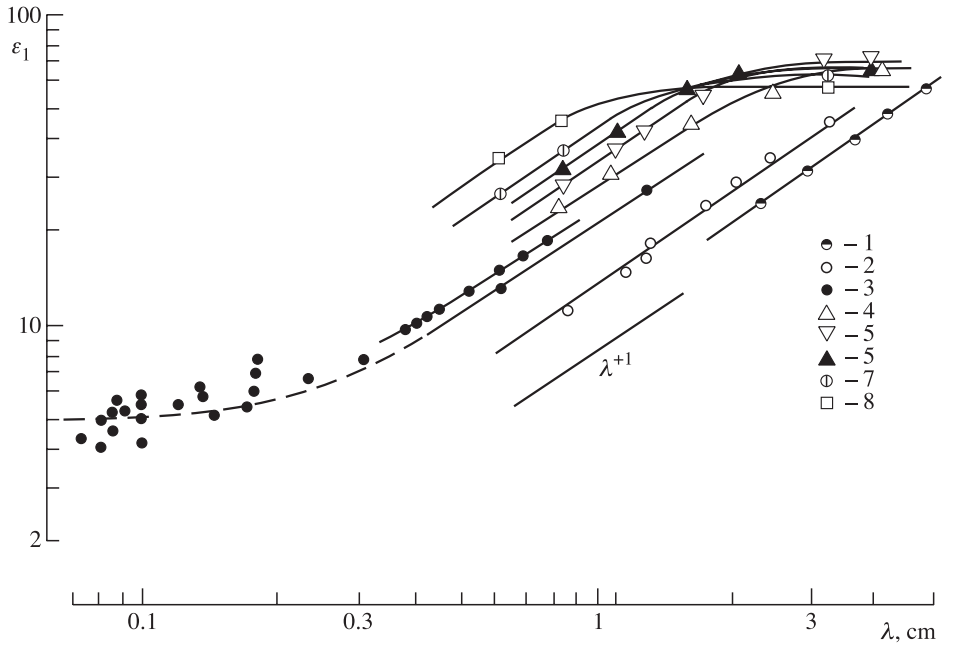

Figure 8.11. Frequency dependence of the real part for the complex permittivity at temperatures from −4.1°C to 80°C. 1 is at temperature −4.1°C (Kaatze and Giese, 1980). 2 is at temperature 0°C (Hasted, 1972; Pottel and Lossen, 1967). 3 is at temperature 19–21°C (Blue, 1980; Demyanov *et al.*, 1974; Apletalin *et al.*, 1970; Meriakri *et al.*, 1980; Volkov *et al.*, 1980). 4, 5, 6 are at temperature 25°C, 35°C and 50°C (Pottel and Lossen, 1967). 7 and 8 are at temperatures 60°C and 80°C (Asheko *et al.*, 1989).

8.4.3 Empirical models

Consider the values of parameters $\varepsilon_0(t)$, $\varepsilon_\infty(t)$ and $\lambda_S(t)$ for some relaxation models used now in practical calculations (in all formulas the temperature is expressed in Celsius degrees and $\lambda_S(t)$ in centimetres).

The Saxton–Hasted–Stogryn model, formed from the data obtained by Saxton (1952), Hasted (1961) and Stogryn (1971) and called here model I conventionally, is as follows:

$$\begin{aligned} \varepsilon_0(t) &= 87.74 - 0.4008t + 9.398 \times 10^{-4}t^2 + 1.4 \times 10^{-6}t^3, \\ \lambda_S(t) &= 3.0[1.11 - 3.82 \times 10^{-2}t + 6.938 \times 10^{-4}t^2 - 5.096 \times 10^{-6}t^3], \\ \varepsilon_\infty(t) &= 4.9 \pm 0.98, \\ \alpha &= 0. \end{aligned} \tag{8.39}$$

The working range of temperatures, over which, in this author's opinion, this approximation model is valid, is as follows: $0 \leq t \leq 40$°C.

The Ray model (Ray, 1972), called here model II conventionally, is as follows:

$$\begin{aligned}
\varepsilon_0(t) &= 78.54[1.0 - 4.579 \times 10^{-3}(t - 25.0) + 1.19 \\
&\quad \times 10^{-5}(t - 25.0)^2 - 2.8 \times 10^{-8}(t - 25.0)], \\
\lambda_S(t) &= 3.383 \times 10^{-4} \exp\left\{\frac{2513.18}{t + 273}\right\}, \\
\varepsilon_\infty(t) &= 5.27 + 2.164 \times 10^{-2} t - 1.313 \times 10^{-3} t^2, \\
\alpha(t) &= 6.0926 \times 10^{-2} - \frac{16.81}{t + 293}.
\end{aligned} \tag{8.40}$$

The working range of temperatures, over which, in this author's opinion, this approximation model is valid, is as follows: $-20^\circ\text{C} \leq t \leq 50^\circ\text{C}$.

The Rozenberg model (Rozenberg, 1972), called here model III conventionally, is as follows:

$$\begin{aligned}
\varepsilon_0(t) &= 88.2 - 0.4088t + 0.000\,81t^2, \\
\lambda_S(t) &= 1.466 \exp\{-0.0634t\} + 1.36 \times 10^{-4} t^2 - 2.729 \times 10^{-2} t + 1.873, \\
\varepsilon_\infty(t) &= 5.5, \\
\alpha &= 0.
\end{aligned} \tag{8.41}$$

The working range of temperatures, over which, in this author's opinion, this approximation model is valid, is as follows: $-40^\circ\text{C} \leq t \leq 75^\circ\text{C}$.

The other designed empirical models are to some extent a consequence of the abovementioned models, but with some changes in the temperature dependencies of parameters. For example, the models used by Rabinovich and Melentev (1970) (called here model IV conventionally), differ from model I in the $\varepsilon_\infty(t)$ dependence, in accordance with the data of Hasted and ElSabeh (1953), namely,

$$\varepsilon_\infty(t) = 5.0 + 0.0225t \tag{8.42}$$

and model V, in a paper by Klein and Swift (1977), in the $\varepsilon_\infty(t)$ dependencies, namely,

$$\varepsilon_0(t) = 88.045 - 0.4147t + 6.295 \times 10^{-4} t^2 + 1.075 \times 10^{-5} t^3. \tag{8.43}$$

Note that the authors, as a rule, have not studied in detail the validity of approximation models in the indicated temperature ranges.

Statistical processing of the experimental data obtained before 1974 has allowed Mason *et al.* (1974) to formulate the model VI, which was presented in the original paper in the form of tables of mean values and 90% confidence intervals ($0 < t < 75^\circ\text{C}$) and reproduced in Figures 8.9, 8.10 and 8.12. This model, having been most justified experimentally for the year 1979, consists of two versions: the purely Debye model and the C-C model, the distinctions between these versions in their mean $\varepsilon_\infty(t)$ values not exceeding 0.05% and in their $\lambda_S(t)$ values, 1.5%. The confidence intervals are for $\varepsilon_\infty(t)$ less than 0.5%, and for $\lambda_S(t)$ about 3.5%. In other

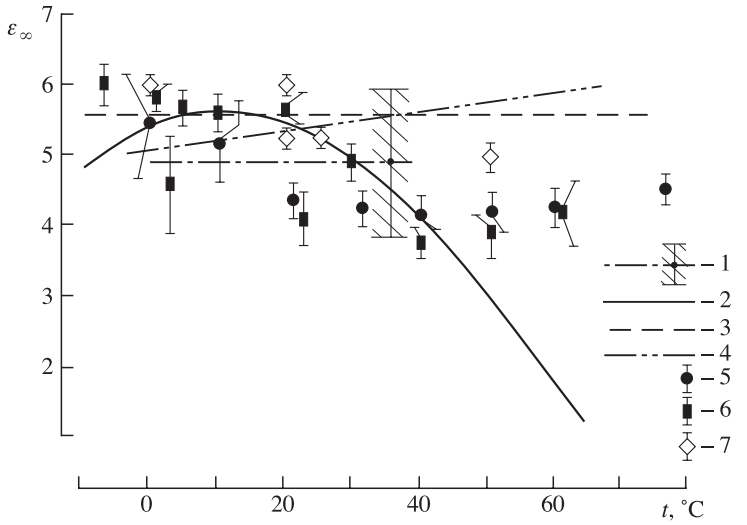

Figure 8.12. Temperature-dependent 'optic' constant in the Debye model. 1: model I with its uncertainty range. 2: model II. 3: model III. 4: model IV. 5: model V with 90% confidence intervals. 6: model VI with the standard confidence intervals. 7: Results obtained by E. Sharkov (1983) with processing evidence of various authors (see Table 8.1).

words, according to the data of Mason *et al.* (1974), one can state that the distinctions in $\varepsilon_\infty(t)$ and $\lambda_S(t)$ parameters in both the models mentioned are essentially lower than the 90% confidence intervals of each parameter value for a separately taken model. Therefore, the introduction of the C-C model (which is more complicated than the D model) for describing the dielectric properties of water (at least from the viewpoint of the $\varepsilon_\infty(t)$ and $\lambda_S(t)$ parameters) is completely unjustified (see Sharkov (1983) for more details). This circumstance is a major point, since it unambiguously indicates the prevalence of relaxators with a single (and strictly defined) relaxation time in the structure of freshwater.

A similar processing, performed in 1981 by Kaatze and Uhlendorf (1981) on the same basis material, but taking in some additional experimental data, allowed these authors to formulate the numerical Debye relaxation model (called here model VII conventionally), which is close to model VI with respect to $\varepsilon_\infty(t)$ and $\lambda_S(t)$ parameters. The distinctions between these models in the mean $\varepsilon_\infty(t)$ values are less than 0.2% ($t = 0$–60°C) and 1–0.2% for $\lambda_S(t)$ values. In the same paper, Kaatze and Uhlendorf proposed the following compact formula for $\varepsilon_\infty(t)$:

$$\lg \varepsilon_0(t) = 1.94404 - 0.00199t. \tag{8.44}$$

The working range of temperatures, over which, in this author's opinion, this approximation is valid, is as follows: $-4.1^\circ\text{C} \leq t \leq 60^\circ\text{C}$.

It is important to note that Kaatze and Uhlendorf (1981) (as well as, by the way, the authors of model VI (Mason *et al.*, 1974)) have neither found a regular

dependence for the optical constant $\varepsilon_\infty(t)$, nor presented it in analytical form. The reasons for this (strange at first sight) circumstance will be discussed below.

8.4.4 The analysis of the $\varepsilon_o(t)$ and $\lambda_S(t)$ parameters

Proceeding from the above considerations, our further study (following Sharkov, 1983) will be as follows: (1) to analyse thoroughly the temperature dependencies of $\varepsilon_o(t)$ and $\lambda_S(t)$ in the numerical models I–V as compared to model VI (in the relative ratio); (2) to compare the numerical calculations by models VI and the approximation (8.44) of model VII with the magnitudes of the $\varepsilon_\infty(t)$ and $\lambda_S(t)$ parameters obtained by Sharkov (1983) from experimental data processing (Table 8.1) under the assumption that the model D for fresh water is valid. The numerical values of parameters are given in the table along with the values of working wavelengths, the CP data of which were used in the graphical techniques of (8.20)–(8.21). The analysis of Figure 8.9 indicates that the approximating formulas for the static constant $\varepsilon_\infty(t)$ of models I–IV correspond well to each other and to models VI and VII: the distinctions in the approximation expressions do not exceed 0.5%.

The numerical values obtained by Sharkov (1983) from the CP experimental data processing by the technique of (8.20)–(8.21) (see Table 8.1), confirm to a fairly high accuracy (better than 0.4%) the validity of numerical approximation models (see Figure 8.9 (inset)). The analysis of the $\varepsilon_\infty(t)$ dependence indicates the predominantly linear decrease of static constant values with temperature with gradient $(\Delta\varepsilon_0/\Delta t) = -0.37$ per degree Celsius. Thus, in numerical calculations in the temperature range of 0–60°C any of the aforementioned approximations can be used to a degree of accuracy of the order of 0.5%.

It is of interest to note that attempts to find, by means of fine experiments (Szwarnowski, 1982), any features in the frequency characteristic of the complex dielectric constant in the decimetre and metre wavelength bands, which would differ from the Debye model, have failed. This fact testifies once again to the undoubted prevalence of solitary relaxators in the polarization properties of water, as well as to a vanishing contribution of water clusters, which seems rather strange by itself. As we shall show below, the real situation is significantly different even for weak electrolytes.

Of special interest (see Sharkov, 1983, 1996c; Liebe *et al.*, 1991; Lipton *et al.*, 1999) is the study of the dielectric properties of supercooled water (below 0°C) in connection with suppositions on the rearrangement of an like-ice structure of 'warm' water at a temperature lower than 0°C into some kind of ferroelectric structure (Angell, 1982), as well as in connection with the problems of remote sensing of convective cloudy systems. However, because of natural difficulties, detailed experimental data on measuring the CP of finite volumes of supercooled water are still absent. So, in 1976, Hasted and Shahidi (1976) presented the results of some fine laboratory experiments (at a frequency of 1652 Hz) on measuring the CP for supercooled water in the form of microdrop emulsion dispersed in an organic solution. The results of these experiments on measuring, in essence, the static constant $(-35 \leq t \leq -5.0°C)$ are shown in the inset in Figure 8.9 along with the fitting

formula (8.44). From comparison of these data it can be concluded, that the dielectric properties of supercooled water (at least from the viewpoint of parameter $\varepsilon_\infty(t)$) can be satisfactorily described within the framework of the relaxation model of 'warm' water (model VII). And, apparently, no sharp transformation of the relaxation mechanism in liquid water at negative temperatures does occur.

As far as the fitting dependencies of the relaxation wavelength are concerned, Figure 8.10 illustrates particular quantitative conformities in the approximations of various models in the range of $t = 0$–40°C. The best conformity is observed between models I and VI, namely, the differences in λ_S values do not exceed 1% ($t = 0$–50°C). For models III and VI the differences are of the order of 2–3%; the worst situation occurs for model II, where the distinctions exceed 5–10%. The numerical values of λ_S, obtained by Sharkov (1983) in experimental data processing (see Table 8.1), show that for the range of 20–25°C the approximation of model I (inset in Figure 8.10) is most suitable. Thus, for numerical calculations in the temperature range of 0 to -40°C the $\lambda_S(t)$ approximation of model I should be recommended. With increasing $t > 40^\circ$C all three models (I–III) sharply worsen in their conformity with model VI. The reasons for this are discussed below. Reliable experimental data on the temperature dependence of $\lambda_S(t)$ for supercooled water are absent. And we can only suppose that, if the exponential character of the $\lambda_S(t)$ dependence conserves also for $t = -40^\circ$C, then the relaxation wavelength can reach values of the order of 10 cm. Such a conclusion is substantiated by the results of our CP data processing for water at $t = -4.1^\circ$C (see the inset in Figure 8.10), as well as by the estimates of $\lambda_S(t)$ for supercooled water obtained earlier by the original technique using the experimental data from the double-frequency radiothermal system in sensing the supercooled drop clouds (Akvilonova and Kutuza, 1978). However, the analysis of the inset in Figure 8.10(b), where these results are reproduced (with appropriate re-calculation to fit them into the scale of the plots), indicates that final conclusions about the numerical approximation model can hardly be drawn because of considerable measurement errors.

8.4.5 Analysis of parameter $\varepsilon_\infty(t)$

Before proceeding to the analysis of optical constant values in the existing relaxation models, we shall consider the general contemporary situation concerning the availability of experimental data on frequency CP dependencies in the band ranging from short centimetre to submillimetre waves. It can easily be seen from the analysis of relations (8.16)–(8.17), that it is just this wavelength band where the features of spectral CP dependencies of water should make the main contribution to the formation of the values of parameter $\varepsilon_\infty(t)$. And their analysis will allow us to reveal the reasons for discrepancies in the empirical models in relation to the mentioned parameter.

Figure 8.11 presents the experimental (1970–1991) data on measuring the spectral dependence of a real part of CP in the wavelength band of 3–0.07 cm and in the temperature range of -4.1 to 80°C, as well as the fitting curves corresponding to these data. The analysis of the spectral dependencies presented indicates two

important circumstances. First, in the millimetre and submillimetre bands, experimental data are extremely limited over the temperature range. So, in the 0.07–0.5 cm band the data are available only in the range of 19–21°C. Second, even in this rather limited temperature range the conformity of compared experimental data over spectral dependencies is quite weak: approaching the submillimetre band the divergence between the ε_1 values exceeds 30–40%. The reasons for such serious nonconformities are related, most likely, to systematic errors in the experimental techniques used. So, Demyanov *et al.* (1974) have used the balance absorption method; Blue (1980) has measured the reflection coefficient; and Apletalin *et al.* (1970), Meriakri *et al.* (1980) and Volkov *et al.* (1980) have applied quasi-optical techniques. The experimental nonconformities mentioned should serve as a basis for in-depth study of the source of measurement errors, because the existing situation with the experimental CP data in the millimetre and submillimetre bands cannot be regarded as satisfactory. Similar conclusions were drawn later by Liebe *et al.* (1991) and Lipton *et al.* (1999). The experimental data in this region of electromagnetic waves are quite important for correct formation of the 'optical constant', since this band is some kind of transition between the modes of purely Debye and super-Debye absorptions in the submillimetre band (see Figure 8.3). It is still impossible to form a reasonable picture of spectral CP dependence in the millimetre and submillimetre bands within the temperature range required for remote sensing applications (from −40 to +90°C) (Sharkov, 1983, 1996c; Lipton *et al.*, 1999). However, taking into consideration the available data (Figure 8.11) and the character of spectral dependence of the Debye 'branch' in $\varepsilon_1(\lambda)$ as λ^{+1} (see relation (8.16)), we can state quite confidently that at $t \approx 0°C$ the boundary wavelength λ_B between the purely Debye and super-Debye bands tends to 0.3–0.4 cm; for 'supercooled' water ($t \leq -10°C$) $\lambda_B \approx 1$–2 cm, whereas for 'hot' water ($t > 60°C$) λ_B sharply 'runs' into the submillimetre region ($\lambda_B \approx 0.08$–0.06 cm, or in the frequency band of 12–17 cm^{-1}). The estimations of parameter $\varepsilon_\infty(t)$ carried out by different techniques bear a burden of the experimental nonconformities mentioned and of a limited (over the temperature range) volume of experimental data.

Figure 8.12, in which the plots of $\varepsilon_\infty(t)$ are constructed for existing models (the D model), illustrates their rather weak conformity with various models, not only in the quantitative, but even in the qualitative respect. So, the early (1952–1961) relaxation models (Saxton, 1952; Hasted, 1961; Van Loon and Finsy, 1957) were based on the idea that the optical constant does not depend (to a low degree of accuracy, of about 20%) on the temperature (model I), or on the data (Hasted and El Sabeh, 1953), which were interpreted later as a weak temperature growth (model IV). This attitude of the authors was justified, because they did not have at their disposal any reliable experimental data in the millimetre wavelength band at that time.

However, the subsequent (1961–1981) acquisition of experimental data on the CP of water (including those in the millimetre band) did not elucidate the situation in any way. So, in accordance with Ray's (1972) data, model II supposes a strong decrease of $\varepsilon_\infty(t)$ (Figure 8.12) down to 1 and below (at a temperature of 65°C), which is a doubtful physical result. Subsequent science publications did not confirm this fact either.

Rozenberg (1972), the author of model III, kept to the early models, supposing the optical constant $\varepsilon_\infty = 5.5$ to be constant within a wide temperature range, from -40 to $+75^\circ$C, without estimating the accuracy of this parameter. The author of model III, however, did not have at his disposal any appropriate experimental base to formulate such conclusions.

The digital models, formed by Mason *et al.* (1974) (model VI) and Kaatze and Uhlendorf (1981) (model VII), were constructed on the same experimental facts. Their analysis (Sharkov, 1983, 1996c) enables us to reveal a peculiarity which is traced as a considerable decrease of ε_∞ – from 6.0 down to 4.0 – with increasing temperature. On the other hand, in model VII the values of the parameter ε_∞ change drastically (up to 20%) as the temperature varies by 1°C only (see Figure 8.12: for $t = 20^\circ$C $\varepsilon_\infty = 5.5$, and for $t = 21^\circ$C $\varepsilon_\infty = 4.0$). Such 'kicks' in the optical constant values did not allow the authors of model VII to formulate the analytical form of the temperature dependence of $\varepsilon_\infty(t)$. One more interesting point follows from the analysis of Figure 8.12: the earliest relaxation model (model I by Saxton (1952)) includes, in essence, all modern approximation approaches for $\varepsilon_\infty(t)$ values.

Sharkov (1983) has shown that such an ('unstable') situation is due to the fact that the procedure of calculating the ε_∞ values has illegitimately included the experimental data obtained at wavelengths lying beyond the field of influence of the purely Debye absorption band. For example, for $t = 20^\circ$C the use of data at wavelengths shorter than 0.2 cm is incorrect. In this case, as mentioned above, the boundary wavelength between a purely Debye and super-Debye absorption bands very heavily depends on temperature. The analysis of processing of the experimental data obtained in 1980–1991, undertaken by Sharkov (1983) with account taken of the circumstance mentioned above, has shown (Figure 8.12) that the $\varepsilon_\infty(t)$ values, formed from relation (8.21) and from the data of various authors, lie within the limits of 5.0–5.9 in the wide range of temperatures ($t = 0$–50°C).

To finally solve the question of the temperature dependence of $\varepsilon_\infty(t)$, as well as of $\lambda_S(t)$ of the relaxation D model for freshwater, it is necessary to carry out successive experiments (by the unified technique) on measuring CP with regard to some kind of a 'choice rule' (Sharkov, 1983), namely: for 'cold water' ($t = 0$–20°C) in the wavelength band of 1–3 cm, for 'warm' water ($t = 20$–40°C) in the wavelength band of 0.6–1.5 cm and for 'hot' water ($t = 40$–90°C) in the wavelength band of 0.1–0.5 cm. Ignorance of the 'choice rule' formulated above, and the illegitimate inclusion into the processing procedure of the experimental data at wavelengths lying beyond the range of the purely Debye relaxation band for the temperature range under study (as was just done in constructing the models I and VI), will result in the aforementioned nonconformities in the $\varepsilon_\infty(t)$ parameter in the models. Sharkov (1983) has presented a demonstration example of the illegitimate construction of $\varepsilon_\infty(t)$ with a special 'capture' of the frequency region of super-Debye absorption. As a result, the range of 'kicks' in $\varepsilon_\infty(t)$ values was from 3.8 to 4.6 as the temperature varied by one degree only (from 21 to 22°C), which is a physically contradictory result.

The attempts to introduce the double-Debye model, undertaken by Liebe *et al.* (1991), slightly improved the situation, but, nevertheless, full clarity in the

relaxation model for the band of short millimetre and submillimetre waves was not achieved.

Thus, for the majority of remote sensing applications satisfactory approximation formulas for the static constant ($t = -40$ to $+90^{\circ}$C) and relaxation wavelength ($t = 0$–40°C) can be used from models I and VII. For supercooled and 'hot' water, however, additional purposeful investigations should be carried out, since a satisfactory temperature approximation of the relaxation wavelength value is absent. The approximation formulas for the 'optical' constant can be used only if account is taken of the essential ($\sim$20%) uncertainties in the parameter values. To finally solve the question of the temperature dependence of the 'optical' constant, a set of experiments should be carried out with allowance for the revealed 'rule of choice' of the temperature ranges and working wavelengths studied.

8.5 DIELECTRIC PROPERTIES OF SALT WATER

A cosmic feature of our planet lies in its riches of salt water. The World Ocean contains about 1413×10^{18} kg of aqueous solution of electrolyte of medium concentration. Salt water occupies about 71% of planet Earth's surface. The substances contained in such a huge amount of water can be subdivided into two categories. The first category includes dissolved substances such as salts, organic compounds and dissolved gases; the second category includes substances forming an independent phase, such as bubbles of gas and solid particles of both inorganic and organic origin. In addition, electrolytes and non-electrolytes are sometimes distinguished among dissolved substances. When dissolved in water, electrolytes form the particles which are able to transfer the electric charge (the ions) and, thereby, to decrease the electric resistance of a system. This phenomenon is not characteristic of non-electrolytes.

The substances dissolved in seawater are represented primarily by salts. The chemical composition of seawater is rather complicated in detail. Here it is sufficient to mention that a 'typical' specimen of seawater weighting 1 kg contains about 19 g of chlorine in the form of chloride ions, 11 g of sodium ions, 1.3 g of magnesium ions and 0.9 g of sulfur (mainly in the form of sulfate-ions). In other words, seawater represents an aqueous 0.5 M solution of NaCl and 0.05 M solution of $MgSO_4$. In addition, sea water contains small admixtures or traces of almost all the elements of Mendeleyev's table.

The well-known physical fact that the water possesses a considerable heat capacity suggests that the oceans represent an excellent thermostat for the entire climatic system of the Earth. This simple and, at the same time, fundamental fact involves some unusual consequences – it provides one of the necessary conditions (the 'greenhouse' effect) for the origin and development of biological life on Earth. In addition, the existence of moderate (and, moreover, comfortable for a human being) climatic conditions where there is a moderating influence from neighbouring seas has played an important part in the history and development of human civilization.

The oceans of the Earth represent an actively functioning system, which is regulated, first of all, by thermohaline processes. Therefore, the knowledge and monitoring of spatial-temporal fields of the ocean's surface salinity and of the surface field of temperature are most important problems of remote sensing (Miller, 2000; Miller and Payne, 2000; Miller *et al.*, 1998; Schmitt and Montgomery, 2000).

8.5.1 Electrolyte structure

The presence of electrolyte drastically changes the structure of water (Sinyukov, 1976; Horne, 1969; Dzens-Litovskii, 1967). The local violation of the water structure near an ion or, more correctly, the region of this violation, is called the hydrated atmosphere of an ion. It has a complicated composition and consists of an inner zone with an ordered structure and an outer zone with the reordered structure of water. Hydration can be quantitatively described by means of hydration numbers of ions or on the basis of the notion of the time a water molecule remains in an equilibrium state near an ion and in the pure water structure. The experimental investigation of hydration is fairly laborious; however, generally speaking, the greater the density of the charge of a cation, the stronger it is hydrated; cations are usually hydrated stronger than the corresponding anions.

Water structure theories based on the assumption of the existence of the destroyed structure of ice or ice-like crystalline structure in a liquid explain the strengthening or spliting effect of ions by the fact, how easily they can be disposed at emptinesses of a structure or at the place of a water molecule in the frame.

In accordance with the Frank–Wen model of liquid water, based on the idea of flickering clusters, the ion in the solution is supposed to be surrounded by two structured layers of water molecules – the two-zone model (Figure 8.13). The inner layer (A), which, apparently, can be identified with what is called a 'primary' hydration sphere, is more dense owing to electrostriction. And the water molecules inside this layer are less mobile and form strong bonds with an ion in its Coulomb field. By electrostriction is meant the appearance of mechanical spatial deformations in the dielectric structure under the effect of the electric field of an ion. Since in such a type of interaction the polarization of dielectrics in the electric field is proportional to the square of the electric field strength, the quadratic effects can appear in the ultimate polarization properties of a dielectric (see Prochorov, (1984) and also Chapter 2).

At a greater distance from an ion (region C in Figure 8.13(a)) the water molecules remain 'normal', though they can be very weakly polarized by the electric field being present everywhere. Of special interest is the intervening layer (B). In this space the Coulomb field of an ion is still strong enough to be capable of violating the 'normal' structure of liquid water. But, nevertheless it is still insufficiently great to be capable of causing rearrangement of water molecules and generating any new structure (as, for example, in the layer A). Therefore, layer B represents a region of comparative reordering. In any case, the ordering or

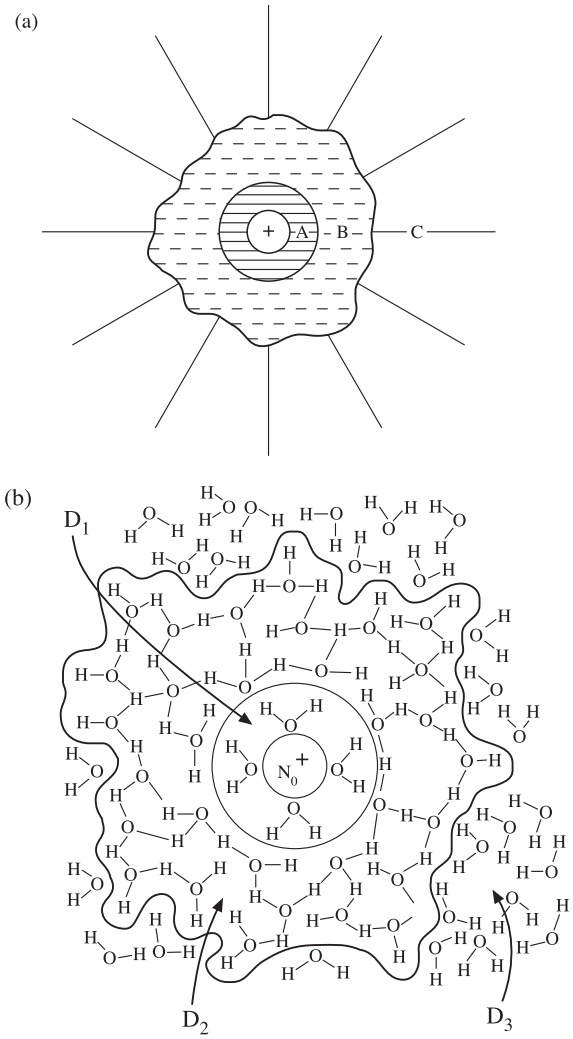

Figure 8.13. Schematic presentation of a hydro-rotation atmosphere of an ion in water solution. (a) Two-zone model. A: the 'inner' layer; B: the intervening layer (space); C: 'normal' water or the 'outer' layer (space). (b): Two-dimensional pattern of structure-ordered hydro-rotation atmosphere for ion Na^+. D_1: Electrostriction zone. D_2: Frank–Wen cluster zone. D_3: the intervening space ('free' water).

reordering effect of an ion depends on which one of indicated layers predominates. A very orderly zone is supposed (Sinyukov, 1976; Horne, 1969) to exist in the unchangeable state for all ions, whereas the specific properties of various types of ions are caused by changing a very disorderly zone B. Investigations of viscosity variation with the electrolyte concentration allow us to quantitatively evaluate the influence of various ions on water structure. The ions strengthening the water

structure, such as Na^+ and Mg^{2+}, increase the water viscosity (positive hydration), whereas the ions destroying the water structure, such as, for example, Cl^{-1}, K^+ and Cs^+, increase its fluidity (negative hydration). One should keep in mind that, depending on the temperature of solution, the degree of an ion's influence on the water structure can drastically change – so, at 27°C the hydration process for a sodium ion changes from positive to negative. Similar features exist for other ions and cations as well. Subsequent investigations have shown that these features are most likely to be associated with the structure features of an ordered zone owing to the fact that the inner, very orderly zone is, in its turn, separated into two subzones (Figure 8.13(b)). The zone closest to an ion consists of a very orderly pattern of water molecules which experience strong electrostriction; and adjacent to it is the zone that is determined by the size of the Frank–Wen cluster zone with weaker electrostriction effects. The inner electrostriction zone can be identified with the so-called primary hydration shell. This is apparently confirmed by the fact that in the case of the Na^+ ion it contains four water rigidly structured molecules, whereas in the general very orderly zone (zone A) of the hydration atmosphere of a sodium ion the number of water molecules varies (depending on temperature) from 52 to 21 (Figure 8.13(b)) (Horne, 1969).

As the concentration of salts increases up to 1.5–2 mol/l, the boundaries of zone B come into contact, and the free water zones in the electrolyte virtually disappear (the full solvation regime). As the concentration further increases, the solution assumes a structure resembling a composition of a melt of salts with conservation of the crystalline structure elements (Sinyukov, 1976).

As we have noted above, the water molecule as a whole can experience two types of motion – translational and rotational. The water molecule is characterized by the high value of electric dipole moment; therefore, in the external electric field this molecule tends to be turned and to assume the position corresponding to the external field direction. The time of relaxation of a rotational process can be determined by measuring the frequency dependence of the full dielectric constant in the alternate electric field, and such results (see section 8.4) are quite indicative. At a particular temperature only one value of relaxation time is observed, and this indicates, that the reorientation of particles of only one type takes place. Experiments on water viscosity, as well as dielectric investigations have shown that the only reoriented particles in a liquid water are the monomers, rather than any polymeric forms $(H_2O)_n$. Apparently, the polymeric (cluster) water complexes do not possess pronounced electric dipole moments and cannot essentially distort the general Debye polarization pattern of liquid (fresh) water (Figure 8.3). This result is, without doubt, of momentous significance. However, its psychological effect was so great that for more than 40 years the validity of the purely Debye model for electrolytes has been stated with variations (with a negative sign) of only numerical values for the static constant and relaxation wavelength. Such a rather 'naive' point of view has been put forward, without any proof being adduced, for a long time, not only by specialists in the physico-chemistry of water solutions (Hasted *et al.*, 1948; Lane and Saxton, 1952; Horne, 1969), but by radio-engineers and radio-physicists as well (Krasiuk and Rosenberg, 1970; Akindinov *et al.*, 1976). And only in 1984 has Sharkov

(1984) critically analysed in detail the previous experimental data and his own data and shown the necessity of this point of view being largely reconsidered.

So, in spite of the progress made in the study of the thermodynamic and the physicochemical properties of solutions of strong electrolytes, there is no quantitative theory of electrodynamic properties of such water systems which would allow us to determine the dielectric parameters by calculation. In papers by Hasted *et al.* (1948) and Lane and Saxton (1952), on the basis of experiments carried out within a rather limited frequency band, it was stated that the dielectric characteristics of strong solutions of electrolytes (and the aqueous solution of NaCl in particular) are described by the purely Debye relaxation model only. And the first estimations of parameters of this model were given (in tabular form) in the same papers as a function of temperature and salinity of a solution. This presentation has been widely publicized and was reflected in its final form in Stogryn's (1971) empirical model. And, furthermore, this presentation has been actively propagandized by the authors of a series of subsequent papers (Hasted and El Sabeh, 1953; Hasted and Roderick, 1958; Yastremskii, 1961; Ermakov *et al.*, 1975; Klugman, 1980). But these authors' own experimental data obviously contradicted the statement that the dielectric properties of strong electrolytes are described by the purely Debye relaxation model. Detailed comparison of the experimental data on the dielectric parameters of electrolyte solutions obtained in the centimetre and millimetre bands, with corresponding calculations by Stogryn's model, allowed Sharkov (1984) to state that the viewpoint on attributing strong electrolyte solutions to the purely Debye type should be accepted as being invalid. Because this circumstance is important for microwave sensing applications, the next section will be devoted to a more attentive study of this problem (following Sharkov (1984)).

8.5.2 The experimental data processing technique

The Debye type of a polar liquid is known to be a particular case of the more general relaxation model, the so-called Cole–Cole (C-C) model. According to this model (equation (8.34)), the complex dielectric permittivity (CP) is described by the following empirical relation:

$$\dot{\varepsilon}(\lambda, S, t) = \varepsilon_\infty(S, t) + \frac{\varepsilon_0(S, t) - \varepsilon_\infty(S, t)}{1 + \left[\mathrm{j}\dfrac{\lambda_S(S, t)}{\lambda}\right]^{1-\alpha(S,t)}}, \tag{8.45}$$

where $\varepsilon(\lambda, S, t) = \varepsilon_1(\lambda, S, t) + \mathrm{j}\varepsilon_{2C}(\lambda, S, t)$; ε_0 and ε_∞ are the static and 'optical' constants of a model, $\alpha(S, t)$ is the parameter of distribution of relaxation times, $\lambda_S(t)$ is the relaxation wavelength, λ is the working wavelength, S is the salinity (in parts ‰), t is the temperature; $\varepsilon_{2C}(\lambda, S, t)$ is the corrected value of the imaginary part of CP (in accordance with (8.8)):

$$\varepsilon_{2C}(\lambda, S, t) = \varepsilon_2(\lambda, S, t) - 60\sigma(S, t)\lambda, \tag{8.46}$$

i.e. $\varepsilon_2(\lambda, S, t)$ minus the correction for the ionic conductivity component. In the

limiting case $\alpha(S,t) \to 0$ the C-C model transfers into the purely Debye relaxation model. The assigning of an investigated electrolyte (the aqueous solution of NaCl) to the corresponding relaxation type and the estimation of the model's parameters (in the general case, α, λ_S, ε_0 and ε_∞) were accomplished by constructing the C-C diagrams from the experimental data. These diagrams represent a set of curves which approximate the experimental data points in the Cartesian coordinate system (Figure 8.6(b)). Quantities ε_0 and ε_∞ were found as the abscissa values when fitting curves intersect the abscissa axis, and quantities α and λ_S were estimated by relations

$$\lambda_S = \lambda \left[\frac{V(\lambda,S)}{U(\lambda,S)}\right]^{1/(1-\alpha(S))}, \tag{8.47}$$

$$\alpha = \frac{2}{\pi}\Psi, \tag{8.48}$$

where V and U are the distances from the experimental point of a fitting semicircle up to points ε_0 and ε_∞, respectively, Ψ is the angle (in radians), formed by the abscissa axis and the line connecting the centre of a circle with point ε_∞. To determine unambiguously the relaxation model type by the technique considered, the accuracy of the initial experimental data on ε_0 and ε_{2C} should be not worse than 5–7%.

8.5.3 Spectral dependences of strong electrolytes

The measurements of the dielectric parameters of highly absorbing strong solutions of electrolytes to the indicated accuracy represent a fairly complicated experimental problem. At present, a limited amount of successive experimental data on measuring the CP of a solution of NaCl is available. These data are predominantly concentrated within a narrow wavelength band of 3.5–2.5 cm and are obtained at temperature of 25°C. And only separate data points are available in the other frequency and temperature ranges (see the reference book by Akhadov (1977)).

For this reason, to obtain the general picture it seems expedient to thoroughly and critically analyse the available experimental data in the centimetre and millimetre bands (Sharkov, 1984). As far as the decimetre and metre bands are concerned, the uncertainty in the experimental data on dielectric parameters is very great (up to qualitative distinctions in the same dependencies). For example, according to the data by Smirnov and Sharkov (1979), the value of $\varepsilon_1(\lambda,S,t)$ in the decimetre band decreases with increasing concentration of aqueous solution of NaCl. According to other data (Klugman, 1980), this value increases; and according to the data of Christensen *et al.* (1966) and by Smirnov and Sharkov (1979), $\varepsilon_{2C}(\lambda,S,t)$ assumes even negative values in the decimetre band for $S \geq 100‰$. It is still impossible to obtain a rather unambiguous picture in the decimetre and metre bands. In this connection, we shall limit further consideration to the analysis of the experimental data (on electrolytes) obtained in the range 3.6–0.4 cm.

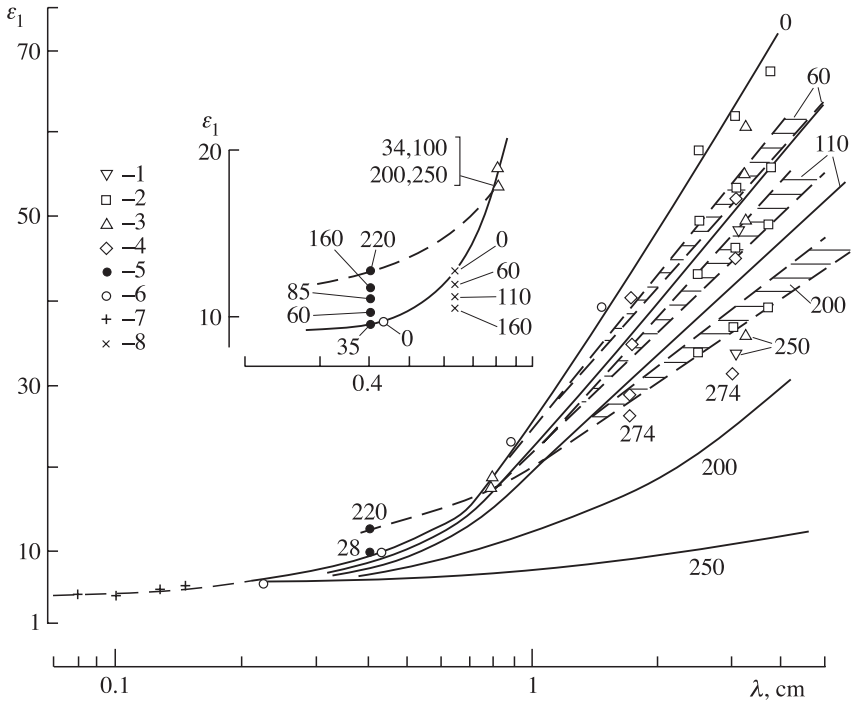

Figure 8.14. Spectra of the real part of the permittivity of water solution NaCl in the range 0.4–3.5 cm at 25°C. Symbols and dotted lines display experimental data. Shaded areas present spread of data. Solid lines are calculations of spectra of $\varepsilon_1(\lambda)$ for water solution NaCl in accord with the Stogryn model. Figures next to experimental data and curves present values of salinity (in parts ‰). Open triangles (at 0.8 cm) are data by Onishenko and Sharkov (1982). 1, data by Harris and O'Konski (1957). 2, Barthel *et al.* (1970). 3, Yastremskii (1961). 4, Christensen *et al.* (1966). 5, Ermakov *et al.* (1975) (at 20°C). 6, Van Loon and Finsy (1975). 7, Apletalin *et al.* (1970). 8, points calculated by E. Sharkov using empirical Lane and Saxton model (1952) at 25°C.

The joint analysis of the data, obtained by Onishenko and Sharkov (1982), and of the results in the 4-mm band (Ermakov *et al.*, 1975), points to the necessity of essential correction of the widespread point of view, that the CP (and, hence, the emissive characteristics) are not sensitive to salinity variations in the millimetre band (see, for example, Wilheit, 1979; Wilheit and Chang, 1980; Ulaby *et al.*, 1981, 1982, 1986; Miller, 2000). The results, obtained by Onishenko and Sharkov (1982), are presented in Figures 8.14 and 8.15. Together with the data from papers by Ermakov *et al.* (1975), Harris and O'Konski (1957), Barthel *et al.* (1970), Yastremskii (1961) and Christensen *et al.* (1966), these results form a set of frequency dependencies, in the band 0.4–3.5 cm, of the real and imaginary parts of the CP of aqueous solutions of NaCl for various degrees of concentrations (the salinity was determined in parts ‰). On the same figures are plotted the frequency dependencies, in the band 0.08–3.5 cm, of distilled water's CP according to the data

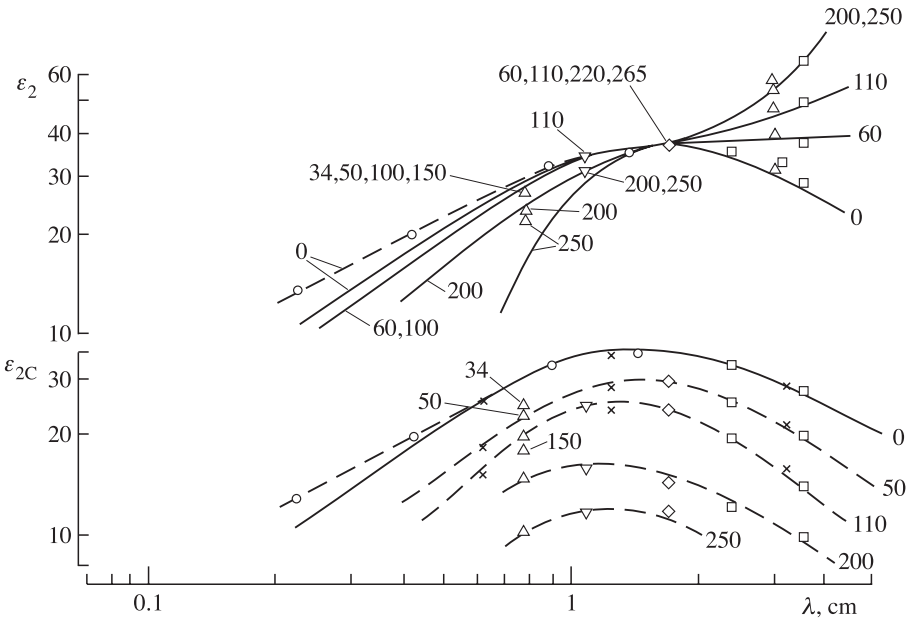

Figure 8.15. Experimental and calculated spectra of imaginary full ε_2 and corrected ε_{2C} parts of the permittivity of water solution NaCl. Dotted lines are curve-fitting of experimental data. Legends as for Figure 8.14.

taken from papers by Grant and Shack (1967), Apletalin *et al.* (1970) and Van Loon and Finsy (1975).

The analysis of frequency dependencies of $\varepsilon_1(\lambda)$, presented in Figure 8.14, gives rise to the following important conclusion. In the band of 0.8 cm there exists the critical wavelength λ_{CR}, at which the converging (from the long-wave extremity) branches of a set of frequency dependencies are 'retracted' and then diverge as the wavelength decreases (see Figure 8.14 (inset)). Thus, the analysis of these data indicates the existence of two characteristic regions in the frequency dependence of $\varepsilon_1(\lambda)$: for $\lambda > \lambda_{CR}$ the concentration dependence gradient $k_1 = (1/\varepsilon_1)(\partial\varepsilon_1/\partial S)$ is negative and equals $k_1 = -0.25\%$ per 1‰ of change of salinity (with increasing salinity up to 200‰). At the same time, for $\lambda < \lambda_{CR}$ coefficient k_1 changes its sign – it becomes positive and equals about 0.15% (per 1‰) at the wavelength of 0.4 cm.

Figure 8.15 presents the sets of frequency dependencies of an imaginary part of CP according to the data by Onishenko and Sharkov (1982) and bringing in the data of papers by Ermakov *et al.* (1975), Harris and O'Konski (1957), Barthel *et al.* (1970), Yastremskii (1961), Christensen *et al.* (1966) and Van Loon and Finsy (1975), as well as the so-called 'corrected' $\varepsilon_{2C}(\lambda, S, t)$, i.e. with subtraction of the correction for the 'through' (ionic) component of conductivity.

Here it is interesting to note, that in the $\varepsilon_2(\lambda)$ dependencies some critical wavelength ($\lambda_{CR} \sim 1.7$ cm) is also observed, at which the sensitivity of $\varepsilon_2(\lambda)$) to salinity is absent, i.e. $k_2 = (1/\varepsilon_2)(\partial\varepsilon_2/\partial S) \approx 0$. In this case, unlike the dependence

of a real part of CP, the opposite situation arises: for $\lambda > \lambda_{CR}$ and $k_2 < 0$ for $\lambda < \lambda_{CR}$. In considering the $\varepsilon_{2C}(\lambda, S, t)$ dependence attention should be given to the following important circumstance. As seen from Figure 8.15, in general, the character of the frequency dependence of $\varepsilon_{2C}(\lambda, S, t)$ remains similar to $\varepsilon_2(\lambda)$ for the freshwater (i.e. to the form of the Debye relaxation maximum). However, the maximum value of $\varepsilon_{2C}(S)$ sharply drops with increasing mineralization: it decreases almost three times as S increases up to 250‰. In this case the relaxation wavelength shifts to the side of shorter wavelengths: whereas for freshwater $\lambda_S \approx 1.75$ cm, for salinity of 250‰ the value of λ_S equals 1.2 cm. A sharp decrease of relaxation losses can be, apparently, explained by formation of a quasi-crystalline structure in the electrolyte and by orientational stabilization of a considerable part of polar molecules of water.

Let us now compare the experimental data obtained with calculations of CP values carried out using the empirical Stogryn model (shown by solid curves in Figures 8.14 and 8.15). Analysis of the figures indicates that, whereas in mineralizations of solutions up to 60‰ (in the band of 1.5–3.5 cm) the indicated model can describe the frequency dependencies accurately enough (to ~10–15%), for $S > 100$‰ and $\lambda < 1$ cm this model fails to give even a qualitatively correct description of the modern experimental data. Note that the earlier (1951–1952) experiments (Lane and Saxton, 1952), on the results of which Stogryn based his empirical model of CP of electrolytes, contained an obvious systematic error in measuring ε_1 in the 6-mm band. So, according to the data of the paper by Lane and Saxton (1952), ε_1 decreases with increasing mineralization of a solution, whereas the real situation is just the opposite (see Figure 8.14 (inset)). It was this circumstance which gave Lane and Saxton reason to suppose, that the dielectric characteristics of strong electrolytes were described by the relaxation Debye model, and to present the first estimates of the model's parameters (in tabular form) depending on the temperature and salinity of the solution. This presentation has been widely publicized (as we have already mentioned above) and was formulated in a completed form in Stogryn's empirical model (Stogryn, 1971). However, the comparison of the data, calculated by the model of Lane and Saxton (1952) (for $t = 25^{\circ}$C and $\lambda = 0.62$ cm), with the results of modern experiments (Figure 8.14 (inset)) reveals the systematic error indicated (Onishenko and Sharkov, 1982). Furthermore, we note that Stogryn has compared the calculations by his model with the experiments, in which the mineralization values were limited to 28‰ only. Though at the time, when he had formed his model, there were already publications (Harris and O'Konski, 1957; Barthel *et al.*, 1970; Yastremskii, 1961; Christensen *et al.*, 1966) on investigations of electrolytes with salinity of up to 275‰.

Thus, the critical analysis of available experimental data and those obtained by Onishenko and Sharkov (1982) revealed a fairly complicated character of frequency dependencies of CP of strong electrolytes in the centimetre and millimetre bands. The widespread empirical model of Stogryn does not describe satisfactorily the mentioned dependencies either from the quantitative or from the qualitative side. A new empirical model must be constructed which would more adequately describe the experimental frequency and concentration dependencies of CP.

8.5.4 The C-C diagrams for strong electrolytes

The C-C diagrams presented in Figure 8.16 are constructed (Sharkov, 1984) for 10, 20 and 25°C using the experimental data, obtained in the wavelength band from 3.6 to 0.8 cm, and for freshwater in the band of 17.2–0.4 cm. It is impossible to construct the C-C diagrams for a wider temperature range (i.e. for $t < 10$°C and $t > 25$°C) because of the absence of successive experimental data at several frequencies in the millimetre and centimetre bands.

The analysis of constructed C-C diagrams for the investigated electrolyte indicates that, in spite of the fact that the used experiments have been performed in different years and by different techniques, nevertheless, the general picture is revealed unambiguously enough: the C-C diagrams of the strong NaCl solution represent not full semicircles (as for polar Debye-type liquids), but only partial arcs, whose centre is essentially displaced from the abscissa axis, this effect being most strongly prominent in cooling the electrolyte (in our case for $t < 10$°C) (Figure 8.16(a)–(c)).

This circumstance enables us to draw a major conclusion, that the dielectric parameters of strong electrolytes are described by the relaxation Cole–Cole model ($a \neq 0$), rather than by the purely Debye relaxation model ($a = 0$), as had long been thought. This circumstance entails a series of consequences and, in particular, quite different (as compared to purely Debye ones) dependencies of the C-C model parameters of electrolyte solutions on temperature and concentration (see below). And this circumstance, in its turn, drastically changes the physicochemical concepts of the structure of electrolytes (Sinyukov, 1976; Horne, 1969).

Now we shall analyse the validity of the experimental data of papers by Hasted *et al.* (1948), Hasted and ElSabeh (1953) and Lane and Saxton (1952), because it was the results of these papers, which underlay the Debye model concept for electrolytes and have been used till now in constructing and modifying the physicochemical models of electrolyte solutions. The validity of the experimental data from papers by Hasted *et al.* (1948), Hasted and ElSabeh (1953) is questionable because of certain circumstances. First, the value $\varepsilon_1(S)$ of the real part of CP, obtained (in the centimetre wavelength band) for $S = 60$‰, is greater than for $S = 28$‰, which obviously contradicts both the accepted general picture of concentration dependencies $\varepsilon_1(S)$, and the other experiments presented later in the same wavelength band. Besides, if we analyse the data by Hasted *et al.* (1948), Hasted and ElSabeh (1953) by the considered technique for obtaining the C-C model parameters, then the ε_∞ value becomes either negative (for 10°C and $S = 34$ and 60‰) or zero (for 20°C and $S = 60$‰). In this case the value of parameter ε_0 for the NaCl solution numerically corresponds to the ε_0 value for freshwater. Similar data processing results clearly indicate serious systematic errors in the original measurements carried out by Hasted *et al.* (1948) and Hasted and ElSabeh (1953).

As far as the paper by Lane and Saxton (1952) is concerned, then, as was shown in paper by Onishenko and Sharkov (1982) (see above), the experimental data on the dielectric properties of a strong electrolyte, obtained in that paper in the millimetre wavelength band, also contain serious systematic errors which have resulted in

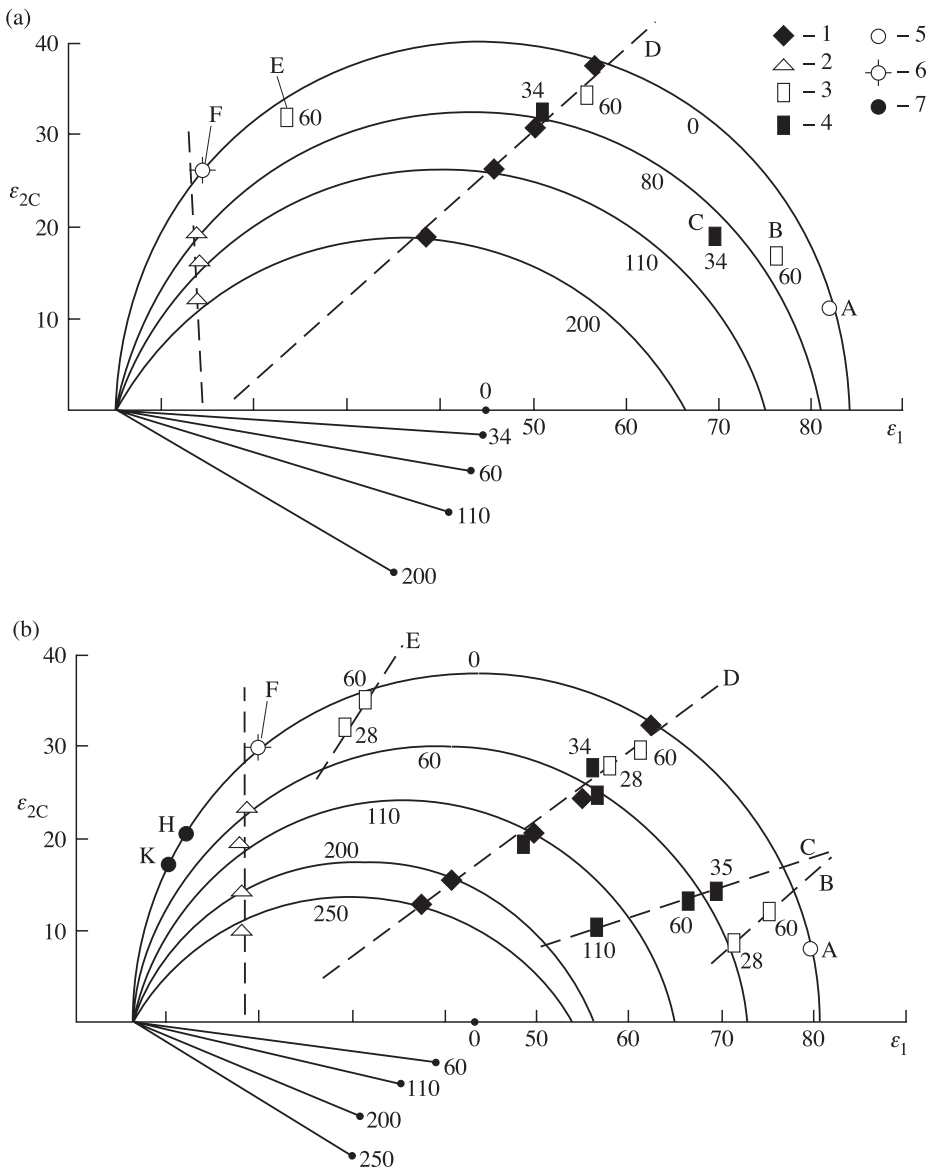

Figure 8.16. Cole–Cole diagrams for the water solution NaCl at 10°C (a), 20°C (b) and 30°C (c). Diagrams by E. Sharkov (1984) using the following data: 1, Yastremskii (1961); 2, Onishenko and Sharkov (1982); 3, Hasted and ElSabeh (1953); 4, Hasted *et al.* (1948); 5, Grant *et al.* (1957); 6, Grant and Shack (1967); 7, Demyanov *et al.* (1974); 8, Barthel *et al.* (1970); 9, Christensen *et al.* (1966); 10, Hasted and Roderick (1958); 11, Pottel and Lossen (1967). Figures next to experimental data and curves show values of salinity (in parts ‰). Letters display operating wavelengths for (a) and (b) diagrams: A = 17.24 cm; B = 9.22; C = 10; D = 3.2; E = 1.26; F = 0.8; H = 0.5; K = 0.4. For (c) diagram: A = 11.49 cm; B = 10; C = 5.66; D = 3.6; E = 3; F = 2.5; G = 1.76; H = 0.8.

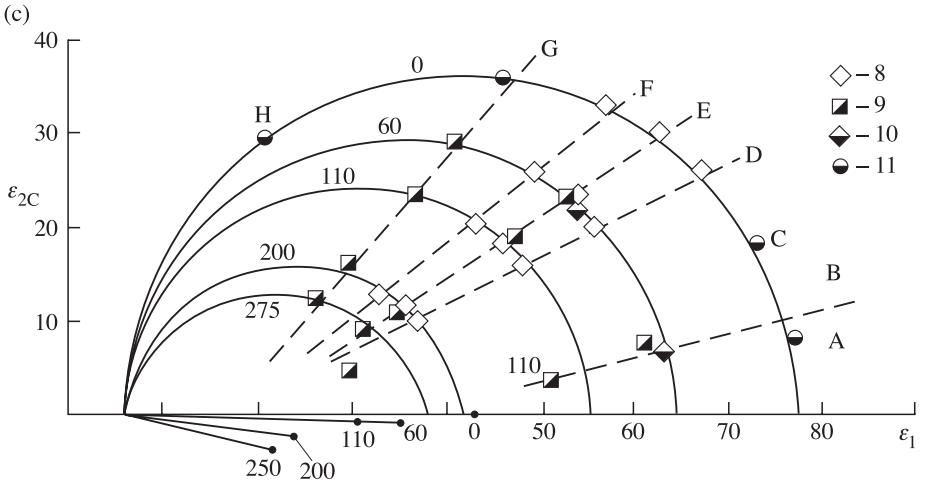

Figure 8.16 (c)

qualitative contradictions with the modern data. That is to say, according to the data of Lane and Saxton (1952), the $\varepsilon_1(S)$ value at the wavelength of 0.62 cm decreases with increasing electrolyte concentration, whereas in reality the $\varepsilon_1(S)$ value should rise. We can easily be convinced of the latter conclusion by considering the corresponding C-C diagrams (see Figure 8.16(a) and (b)). For the indicated reasons the data of these papers have not been used in the analysis presented below, though they have been plotted on C-C diagrams for illustration (see Figure 8.16(a) and (b)).

8.5.5 The C-C model parameters for strong electrolytes

The concentration dependencies of the relaxation times distribution parameter are virtually linear (Figure 8.17(a)) – the lower the solution temperature, the greater the deviation in dielectric properties of electrolyte from the Debye model. A more thorough study indicates an important feature of the dependencies considered; namely, at any values of solution salinity a pretty sharp (virtually jump-wise) decrease of the $\alpha(S)$ value is observed in the narrow temperature range (22–25°C). At 25°C the deviation of the considered model from the Debye one is insignificant (especially for low salinities of solution). This fact is enough to just explain why the results of processing performed by Sharkov (1984) almost fully correspond to the results of the processing of the early data (Barthel *et al.*, 1970) by the Debye model, undertaken in the paper by Ermakov *et al.* (1975) (see Figure 8.17(b) and (c)). Generally speaking, this circumstance just explains why many researchers adhere to the purely Debye model of electrolytes, since the main scope of experiments was accomplished in the range of 'room' temperatures.

The analysis of obtained concentration $\varepsilon_0(S)$ dependencies (Figure 8.17(b)) indicates that, though the qualitative character of these curves in relation to similar dependencies of the Debye model was conserved (i.e. $\varepsilon_0(S)$ decreases with

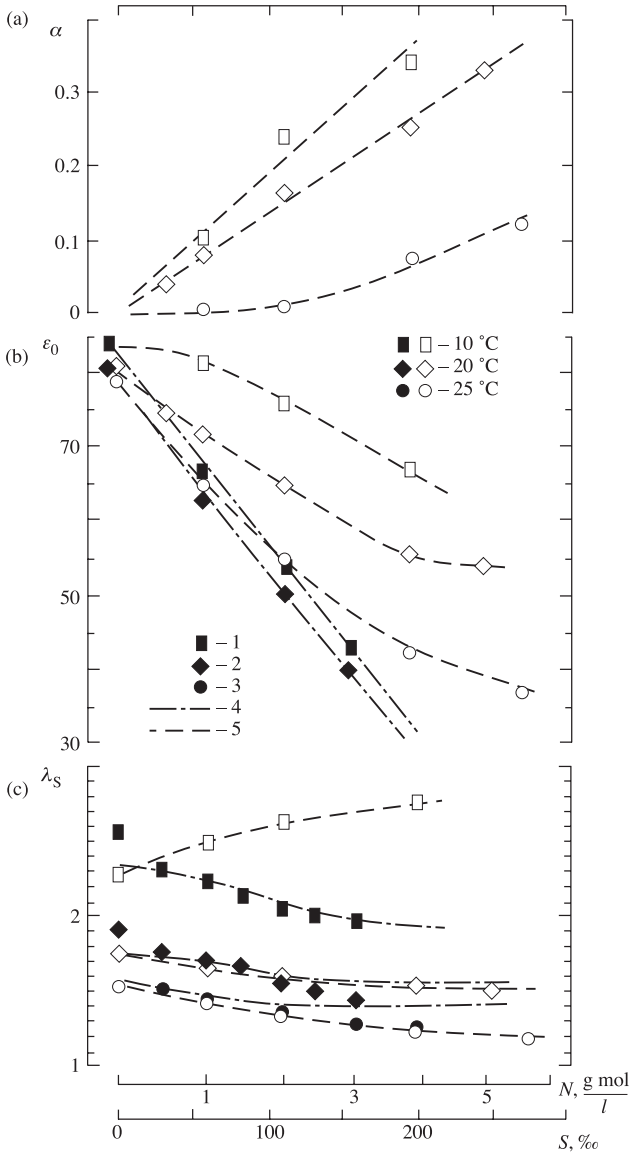

Figure 8.17. Relation of C-C and D model parameters to salinity of water solution NaCl. (a) distribution parameter; (b) static constant; (c) relaxation wavelength. *S* is salinity (in parts per thousand). *N* is molar concentration (in g mol/l). Open symbols display processing results obtained by Sharkov (1984) using data by Yastremskii (1961), Ermakov *et al.* (1975), Onishenko and Sharkov (1982), Harris and O'Konski (1957), Barthel *et al.* (1970), Christensen *et al.* (1966), Demyanov *et al.* (1974), Grant *et al.* (1957), Grant and Shack (1967); Pottel and Lossen (1967). Solid symbols: 1, 2 and 3, results obtained by Ermakov *et al.* (1975) using D model; 4 and 5, calculations using Stogryn (1971) model and Sharkov (1984) model.

increasing concentration of a solution), nevertheless the $k_0 = (1/\varepsilon_0)(\partial\varepsilon_0/\partial S)$ gradient considerably decreased. Note that this gradient is one of the basic parameters featuring in physicochemical models of electrolyte solutions. Whereas in the Debye model the value of this gradient was 0.23–0.3 (per one ‰) and virtually did not depend on temperature (see Figure 8.17(b)) in Stogryn's approximation model, processing with regard to features of the C-C model revealed a strong temperature dependence – from 0.1 (at 10°C) up to 0.18–0.2 (at 25°C), the main drop being a fall, as in the case of $\alpha(S, t)$), to the temperature range of 22–25°C.

The magnitudes of $\varepsilon_0(S)$ also underwent considerable variations – their values were found to be essentially higher than the purely Debye $\varepsilon_0(S)$ values – by 30–40% for $S = 60 \geq 100$‰. Note also a certain physical incorrectness of Stogryn's approximation of $\varepsilon_0(S)$ (or $\varepsilon_0(N)$), obtained in accordance with the Debye model concept: at solution salinity greater than 250‰ ($N \geq 5.1$) the ε_0 values become negative (at 20°C), which is invalid physically. If, however, we proceed from the C-C model, then, as can easily be seen from the analysis of Figure 8.17(b), the essentially nonlinear character of the concentration dependence of $\varepsilon_0(N)$ is observed (even at $t = 25$°C), and the static constant does not assume values lower than 35 (for solution salinity up to 250‰). For cooled water ($t = 10$°C) the $\varepsilon_0(S)$ dependence is much weaker, and for weak and medium electrolytes ($S \leq 50$‰) the values of static constant virtually do not differ from ε_0 of fresh water. At the same time, the distribution parameter reaches the value of 0.1, which noticeably differs from the Debye model data.

The results of diagram processing by the C-C model technique, presented in Figure 8.17 for determining the character of the relaxation wavelength variation with solution salinity, reveal the qualitative distinction from the data known in the literature (the Debye model) (Stogryn, 1971; Yastremskii, 1961). Here we should mention, first of all, that at 10°C the λ_S value increases (in the Debye model it decreases) with increasing electrolyte solution concentration, whereas at 20°C the qualitative character of dependencies coincides with the Debye model, though some quantitative distinctions take place (see the curves for 20 and 25°C). A virtual coincidence of Sharkov's (1984) results with those calculated by Ermakov *et al.* (1975) in accordance with the Debye model concept is not surprising (Figure 8.17(c)), because the relaxation process in electrolyte solutions at these temperatures (according to Sharkov's (1984) results) approaches the purely Debye type with $a \to 0$. (This is very noticeable on the C-C diagrams in Figure 8.16(c) as well.) A pretty sharp variation of model parameters near 25°C can be associated most likely with the change in character of the hydration processes (from negative to positive) for chlorine ions at 27°C (Sinyukov, 1976).

The analysis of presented data indicates that the dependencies of the optical constant on temperature and salinity are weakly prominent for the studied variations of temperature (10–25°C) and salinity (0–250‰) and are expressed by the relation

$$\varepsilon_\infty = 5.8 \pm 0.2, \tag{8.49}$$

not revealing any quantitative regularities inside these boundaries. The indicated relation has more likely a qualitative character, since there are no systematic data

Table 8.2. Calculated values of A_i and B_i coefficients in approximations $\varepsilon_0(S,t)$; $\lambda_S(S,t)$ and $\alpha(S,t)$

	$t = 10°C$		$t = 20°C$		$t = 25°C$	
	A	B	A	B	A	B
ε_0	-3.15×10^{-6}	-3.92×10^{-4}	1.60×10^{-6}	-1.79×10^{-3}	3.11×10^{-6}	-2.99×10^{-3}
λ_S	-2.26×10^{-6}	1.54×10^{-3}	1.52×10^{-6}	-1.02×10^{-3}	6.21×10^{-7}	-1.02×10^{-3}
α	0	1.82×10^{-3}	0	1.22×10^{-3}	1.62×10^{-6}	0

on the dielectric properties of strong electrolytes in the short-millimetre wavelength band at the boundary of transition into the super-Debye absorption band.

In virtue of the practical importance of semi-empirical models of the dielectric parameters of electrolytes (for example, for the theory and practice of microwave remote sensing), we shall present below the results of least-squares approximation (Sharkov, 1984) of the Cole–Cole model parameters $\varepsilon_0(S,t)$, $\alpha(S,t)$ and $\lambda_S(S,t)$, obtained after processing the corresponding diagrams, as the following quadratic forms:

$$\begin{aligned} \varepsilon_0(S,t) &= \varepsilon_0(0,t)[1 + F_1(S,t)], \\ \lambda_S(S,t) &= \lambda_S(0,t)[1 + F_2(S,t)], \\ \alpha(S,t) &= F_3(S,t), \\ F_i(S,t) &= B_i(t)S + A_i(t)S^2, \end{aligned} \tag{8.50}$$

where $i = 1, 2, 3$, and $\varepsilon_0(0,t)$ and $\lambda_S(0,t)$ correspond almost precisely (to an error lower than 1%) to the Debye model approximations for the freshwater (Stogryn, 1971). Because the number of temperature points was limited (10, 20 and 25°C), in determination of the parameters the corresponding analytical approximations $A_i(t)$ and $B_i(t)$ have not been found, but are presented in the form of Table 8.2.

In conclusion to this section we note that the results of analysis (Sharkov, 1984) gave rise to the new semi-empirical relaxation model for the dielectric properties of a strong monoelectrolyte of aqueous solution of NaCl. However, at present it is not possible to give a full answer to the question on concentration dependencies of the Cole–Cole model parameters for a monoelectrolyte within a wide range of temperatures. This requires the reliable and, mainly, sequential experiments to be performed by a unified technique in the wavelength band from 0.2 to 5–6 cm and in the wide range of temperatures – from 80–90°C to negative ones (a supercooled electrolyte solution).

8.5.6 Dielectric properties of polyelectrolytes

As we have already noted, the thorough study of the dielectric properties of mixed electrolytes is rather complicated because of the diversity of the physicochemical

features of components of natural electrolytes. Nevertheless, the existing (and, of course, not complete) data indicate that the main contribution to the polarization properties of solutions is made by the strong NaCl electrolyte, which is virtually fully dissociated in an aqueous solution. Below are presented the experimental data on measuring the dielectric parameters of a mixed solution of salts which is close in composition to seawater (Smirnov and Sharkov, 1979).

Table 8.3 presents the results of an investigation of the dielectric characteristics in the microwave bands ($\lambda = 10$, 18, 75 and 150 cm) of composite solutions of sodium chloride, magnesium chloride and magnesium sulfate (the partial concentrations of components are indicated in Table 8.3). The same table gives the possible radiothermal contrasts of radio-emission of corresponding media (see equation (7.47)). It follows from the analysis of the data of Table 8.3 that the admixtures of magnesium salts very weakly influence, in general, the real part of the dielectric constant of a mixture (it remains constant within the limits of the experimental error) and essentially increase the attenuation in an electrolyte. Owing to this fact, the basically negative contrast in radiothermal characteristics of composite solutions with respect to a monosolution is possible (from +0.2 to −4.0 K).

The highly sensitive radiothermal complexes, now existing in experimental practice, will probably, make it possible to remotely determine the physicochemical features of composite natural salt solutions from the spectral characteristics of their radio-emission.

8.6 SPECTRAL AND TEMPERATURE CHARACTERISTICS OF THE EMISSIVE PROPERTIES OF WATER BASINS

Using the models of dielectric properties of water and electrolytes developed above, we shall analyse theoretically the emissive properties of smooth surfaces of the aforementioned media with allowance for atmosphere illumination based on relation (7.20):

$$T_{\mathrm{B}}(\lambda, S, \theta, t) = \kappa(\lambda, S, \theta, t)T_0 + [1 - \kappa(\lambda, S, \theta, t)]T_I(\lambda, \theta), \tag{8.51}$$

where $\kappa(\lambda, S, \theta, t)$ is the emissivity of a smooth water surface, determined by Fresnel's coefficients $R(\lambda, S, \theta, t)$ from relation (7.17), which is a direct consequence of Kirchhoff's law. Here T_0 is the thermodynamic temperature of the studied surface and $T_I(\lambda, \theta)$ is the brightness temperature of the sky and atmosphere.

The analysis of Figure 8.18, where the frequency dependencies $\kappa(\lambda)$ are presented within a wide wavelength band, indicates that the studied dependence contains two wavelength bands which essentially differ in temperature and salinity effect on $\kappa(\lambda)$. The frequency boundary lies (conventionally) in the 5–7 cm band. Below this wavelength value the emissivity very weakly depends on salinity, in contrast to the thermodynamic temperature dependence, where a strong negative gradient is observed. In the decimetre and metre bands the salinity has a strong effect on $\kappa(\lambda)$ (mainly through increasing the losses in the aqueous medium), the salinity effect being increased with the working wavelength. Besides, the temperature

Table 8.3. Dielectric characteristics of mixed electrolyte solutions

Type of solution mixture and component concentrations (‰)	$\lambda = 10$ cm, $t = 18°$C			$\lambda = 18$ cm, $t = 10°$C			$\lambda = 75$ cm, $t = 18°$C			$\lambda = 150$ cm, $t = 18°$C		
	ε_1	ε_2	ΔT_B, K	ε_1	ε_2	ΔT_B, K	ε_1	ε_2	ΔT_B, K	ε_1	ε_2	ΔT_B, K
NaCl(20)	77.7	39.8	0	81.1	44.8	0	80.3	80.4	0	80.5	168	0
NaCl(20)+$MgCl_2$(5,4)	76.4	40.6	+0.26	80.7	48.3	−0.95	80.1	86.2	−1.58	80.3	172	−0.45
NaCl(20)+$MgCl_2$(7,8) +$MgSO_4$(5)	76.1	44.7	−1.0	80.2	51.6	−1.85	79.7	94.5	−3.92	80.6	187	−2.47

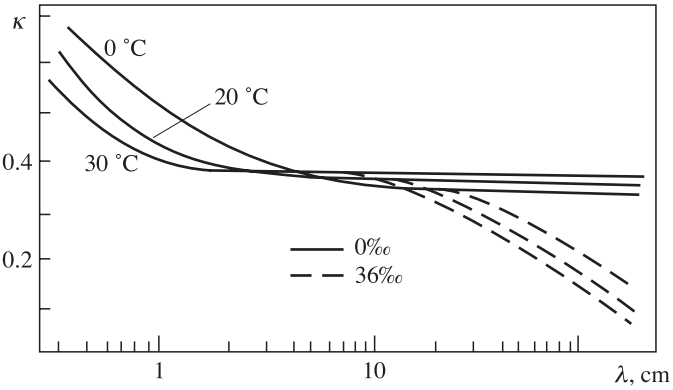

Figure 8.18. Spectra of smooth water surface emissivity at temperatures 0, 20 and 30°C for fresh and saltwater.

dependence has a positive gradient for freshwater and a negative gradient for salt (sea) water. The detailed numerical data on temperature and salinity dependencies of emissivity for the wavelengths ranging from 1 mm to 1 m are presented in papers by Hyatt (1970), Rabinovich and Melentev (1970), Lepley and Adams (1971) and Raizer *et al.* (1974). These tabulated values should be used with caution, because all these calculations were based, in essence, on the early models (Saxton and Lane, 1952) of dielectric properties of water and aqueous solutions of electrolytes (see sections 8.5 and 8.6).

The presence of sky illumination $T_I(\lambda, \theta)$ qualitatively changes the observational situation (Raizer *et al.*, 1975a): strong (up to 1000 K) metre-band cosmic radiation (of the Sun and the galaxy) essentially narrows down the information region of salinity and temperature dependence $T_B(\lambda, \theta, S, t)$ from the side of metre-band waves (Figure 8.19) and, in general, strongly transforms the spectral dependencies of brightness temperature with respect to the spectral dependencies of emissivity (Figure 8.18).

The temperature and salinity effect on the radio-emission of a water surface is most prominent in the 50–70 cm band, the temperature gradient $(\Delta T_B/\Delta t)$ (i.e. the quantity, which just determines the remote sensing efficiency) being qualitatively different for salt and freshwater. Figure 8.20 shows the thermodynamic temperature dependencies of $T_B(S, t)$ for fresh and seawater (for salinity of 20‰ and 37‰) at the wavelengths of 18 and 75 cm. All brightness temperature variations are nearly linear – for freshwater the value of the $\Delta T_B/\Delta t$ gradient equals about 0.5 K at 1°C for centimetre and decimetre bands. For seawater the positive gradient decreases and assumes negative values in the metre band (−0.3 K/1°C for the wavelength of 75 cm). Figure 8.21 presents the salinity dependencies of brightness temperature at the same wavelengths with account taken of illumination. Variation (increase) of a solution's salinity results in a lowering the radiobrightness temperature at these wavelengths. However, at higher temperatures ($t = 40$°C) a prominent nonlinearity of the salinity dependence of T_B is noticeable, which is related physically to a sharp growth of

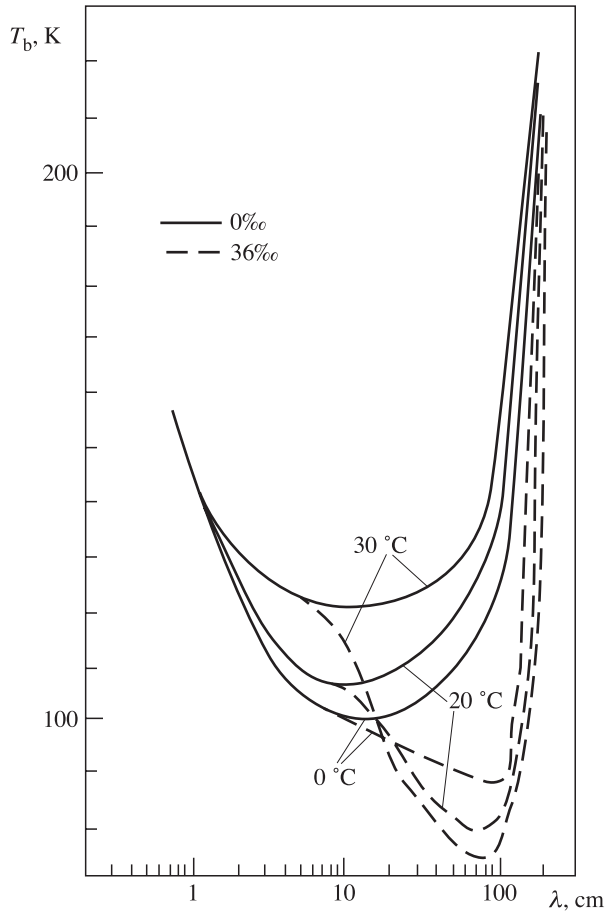

Figure 8.19. Spectra of radiobrightness temperature of a smooth water surface at temperatures 0, 20 and 30°C for fresh and salt water.

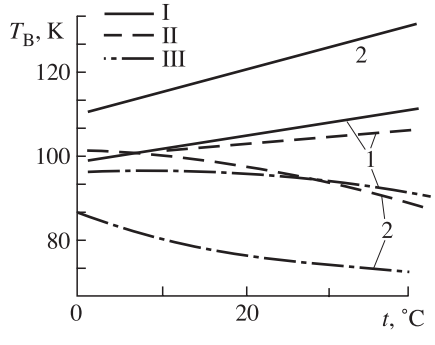

Figure 8.20. Temperature-dependent radiobrightness of a smooth water surface at wavelengths 18 cm (1) and 75 cm (2). I: fresh water. II: salinity is 20‰. III: 36‰.

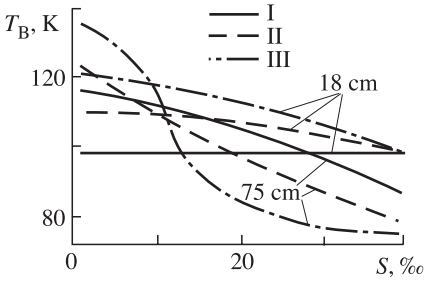

Figure 8.21. Salinity-dependent radiobrightness of a smooth water surface at wavelengths 18 and 75 cm. I: at temperature 0°C . II: 20°C. III: 30°C.

dielectric losses at low concentrations of salts (5–15‰). As the temperature decreases, the nonlinearity of the $T_B(S)$ dependence noticeably becomes smoother. So, whereas for the wavelength of 75 cm and at 30°C the gradient for weak salinities can reach 4–5 K (at 1‰), for 18 cm it decreases down to 0.5. At $t = 0$°C the salinity dependence of brightness temperature in the decimetre band completely disappears (Figure 8.21). Thus, investigations of salinity in the polar regions of the ocean using this wavelength band (18–21 cm) are rather problematic. Brightness contrast calculations were performed (Smirnov and Sharkov, 1979) on evidence derived from experiemental dielectric data (see Table 8.4).

It is of interest to note that, according to the data of Smirnov and Sharkov (1979), the influence of the other (apart from sodium chloride) salts in mixed solutions provide a negative contrast (in relation to a monosolution), but of rather small magnitudes (from 0.2 to 3.9 K) (see Table 8.3).

The experimental data, obtained in the course of aircraft work on studying surface salinity fields (Droppleman *et al.*, 1970; Chukhrai and Shutko, 1978; Blume and Kendall, 1982; Blume *et al.*, 1977), are, generally, in satisfactory agreement with the developed model.

As an effective example, we shall consider the results of aircraft investigations of the sea surface salinity (SSS) field of the coastal zone of the Atlantic Ocean near Chesapeake Bay (Miller, 2000). These investigations have been carried out by means of the microwave passive instrument at the wavelength of 21.4 cm. The fluctuation sensitivity threshold of the instrument, normalized with respect to the salinity value by using the contrast value calculated from the aforementioned model, was found to be some tenths of a part ‰ for the three-dimensional pixel of 1×1 km (see section 5.6). Plate 2 (see the colour section) shows the spatial fields of sea surface salinity of the coastal zone of the Atlantic Ocean before (Plate 2(a)) and after (Plate 2(b)) tropical cyclone 'Fran' passed through the southern states of the USA (on September 8–10, 1996). This powerful cyclone caused strong rainfall in the basin of rivers feeding the Chesapeake Bay. A strong freshwater pulse through the river drainage basins into the coastal zone of the Atlantic Ocean was formed, and it was recorded on the radiothermal microwave maps (Plate 2). It would not be possible to obtain a similar result using contact means (from on board a ship) in the spatial–temporal scales investigated.

Table 8.4. Dielectric characteristics of strong electrolyte NaCl

Normality, mol/l	Salinity, ‰	$\lambda = 10$ cm, $t = 18°$C			$\lambda = 18$ cm, $t = 10°$C			$\lambda = 75$ cm, $t = 18°$C			$\lambda = 150$ cm, $t = 18°$C		
		ε_1	ε_2	ΔT_B, K	ε_1	ε_2	ΔT_B, K	ε_1	ε_2	ΔT_B, K	ε_1	ε_2	ΔT_B, K
0	0	79.4 (78.33)	10.2 (13.52)	0	81.7 (82.48)	6.8 (10.21)	0	82.3 (80.79)	4.1 (1.86)	0	82.1 (80.82)	3.7 (0.93)	0
0.20	12	78.4	27.3	3.1	82.3	34.7	5.3	80.4	56.3	9.4	82.3	116	23.2
0.31	17.9	76.2	34.9	4.2	82.9	42.2	5.3	79.7	73.7	14.4	80.4	160	30.9
0.63	36.0	76.4	47.2	8.0	83.1	57.8	11.4	80.2	108	23.3	79.9	203	36.5
1.83	100.1	72.0	65.8	13.6	77.6	79.2	17.1	79.4	139	30.2	77.8	231	39.2
3.92	200.7	68.1	78.6	18.3	71.8	97.6	22.1	72.7	165	35.4	74.1	258	41.9
5.08	250	64.9	82.3	19.0	72.2	104	23.5	70.2	178	37.5	70.9	267	42.8

Note. Figures in brackets are theoretical values of water dielectric constant on the D model basis.

8.6.1 Requirements for SSS observations

Salinity is a significant variable for upper ocean dynamics at very high latitudes (near-freezing temperatures and ice formation lead to a salinity-dominated stratification), in the western Pacific warm pool (very high precipitation and evaporation), and in subtropical high-salinity regions. The warm pool also represents a region, where the surface freshwater flux induces a shallow salt stratification and a 'barrier layer', that isolates the surface from the main thermocline, with important consequences for surface layer heating. Salinity also has a strong influence (the halosteric effect) on the calculation of surface layer heat storage from the observed sea level. The application of remotely sensed SSS to the study of these different ocean dynamics phenomena implies different requirements for space, time and even salinity resolution, due to the different scales involved and the contrast in surface water characteristics. Typical values required to resolve some of the specific phenomena are (Kerr *et al.*, 2000c,d):

- Barrier layer effects on the tropical Pacific heat flux: 0.2 practical salinity unit (1 psu = 1‰), 100×100 km, 30 days.
- Halosteric adjustment of heat storage from the sea level: 0.2 psu, 200×200 km, 7 days.
- N. Atlantic thermohaline circulation: 0.1 psu, 100×100 km, 30 days.
- Surface freshwater flux balance: 0.1 psu, 300×300 km, 30 days.

The North Atlantic thermohaline circulation and convection in the subpolar seas has the most demanding requirements, and it is the most technically challenging, because of the lower brightness/SSS ratio at low water temperatures. A compromise for all these different requirements would be met by considering the optimized requirements as a general goal for the SMOS mission (Schmitt and Montgomery, 2000; Kerr *et al.*, 2000c,d; Martin-Niera *et al.*, 2000) (see also Chapter 14).

Here we note that the first successful remote aircraft experiments, performed in Russia and USA at the end of 1970s and at beginning of the 1980s (Chukhrai and Shutko, 1978; Blume and Kendall, 1982; Blume *et al.*, 1977), gave rise to unjustifiable hopes for the rapid implementation of space experiments to study salinity fields by means of antenna systems having huge apertures (Blume *et al.*, 1978) for ensuring the necessary spatial resolution. Though these projects have failed, expert oceanologists nevertheless believe that the study of the spatial–temporal variability of the surface salinity field of the World Ocean with the spatial resolutions available soon will be one of the problems given priority in the future development of remote sensing (Lagerloef *et al.*, 1995; Miller *et al.*, 1998; Schmitt and Montgomery, 2000; Miller, 2000; Miller and Payne, 2000).

At present, great efforts are being directed towards scientific–technological development of radio-interferometric technology, which is sometimes called passive aperture synthesis, for ensuring acceptable spatial resolution (Milman, 1988; Camps *et al.*, 1997, 1998; Camps and Swift, 2000; Kerr *et al.*, 2000b, 2000c, 2000d; Wigneron *et al.*, 2000; Martin-Neiza and Goutoule, 1997). Parallel to this approach, designers are working on versions of antennas with large-scale apertures,

but with a lightweight structure (inflatable antennas), as well as deployable mesh surfaces and other structural versions of antennas (Njoku *et al.*, 1999, 2000b; Wilson *et al.*, 2000).

8.7 EMISSIVE PROPERTIES OF ICE SURFACES

The ice surfaces of congealing seas at middle and high latitudes, as well as glacial ice surfaces (Antarctica, Greenland, glaciers in mountains) are quite important objects, which essentially influence the hydrological and meteorological characteristics of the Earth's surface–atmosphere system. In this case the phase transitions of water and ice are accompanied by releasing and absorbing huge masses of heat, by changes in the optical regime and salinity, by the generation of strong electrical fields. The ice surface of seas, oceans and land is a fine regulator in the thermal and dynamical interaction of the ocean and atmosphere. Its inhomogeneities in width and huge spatial size mean that high-speed and reliable means are required to determine and diagnose age gradations, cohesion, the size of ice fields and their thickness. As durable investigations of Earth's ice surfaces by various remote sensing techniques have shown, microwave methods provide significantly different information on the structure and physicochemical composition of ice systems as compared to the data provided by the methods in the optical and IR wavelength bands. This is due to the fact that the phase transition of liquid water into the solid state is characterized by radical changes in dielectric properties (see section 8.2).

If, however, the ice surface is qualified with regard to its place in the system of dielectrics (and, accordingly, with regard to emissive characteristics), one can distinguish at least three types of ice systems – glacial ice, freshwater ice and sea ice. All these types of ice surfaces are substances which significantly differ in the electrodynamical respect. In addition, we note that their role in thermal and dynamical interaction in the ocean–atmosphere system is significantly different as well.

Since **glacial ice** (Antarctica, Greenland, glaciers in mountains) is generated through a very complicated morphological formation from precipitated snow, rather than from a liquid phase, the strong influence of the internal geometrical structure on dielectric and emissive properties of glacial ice fields over great spatial scales is obvious. As we have noted above (section 8.2), the dielectric properties of glacial ice specimens are very close to freshwater ice characteristics – the real part of the dielectric constant is virtually constant in the microwave band with very small variations in temperature and structure. In other words, the so-called dielectric anisotropy takes place here (Matsuoka *et al.*, 1996, 1997). The imaginary part, however, was found to be strongly influenced by weak mineralization, by the presence of organic substance and admixtures of gas bubble type, and by thermodynamic temperature. However, since the magnitude of this part is small, its value and variations have virtually no effect on emissive characteristics. Using equation (7.47) one can easily obtain the emissivity value for glacial ice – it will be equal to 0.93. And, thus, the radiothermal contrast between the ice surface and water surface

can constitute considerable values namely, 100–150 K. Note that the indicated radiothermal contrast is greatest among the natural surfaces of the Earth.

However, the first investigations of the thermal radiation of glacial ice in Antarctica, carried out by Russian researchers from the 'Kosmos-243' satellite in 1968, brought about an unexpected surprise. A serious decrease of emissive properties of resonance type was recorded in the centimetre band in the inner regions of Antarctica (Basharinov *et al.*, 1971) and then in Greenland. This result was confirmed later by the American investigations from the 'Nimbus-5' satellite in 1972 (see Plate 3). The effect was so unexpected and obscure, that it was called 'Antarctica's puzzle'. The essence of the problem lies in the fact that in formally restoring the dielectric properties of Antarctica's inner regions by the known formulas (7.47) a physically contradictory result is obtained – the continental regions of Antarctica would represent the lakes of freshwater in this case.

This 'puzzle' was soon (in 1973) resolved by the efforts of Russian scientists (Gurvich *et al.*, 1973). The frequency-selective variation of thermal radiation of Antarctica's inner regions was found to be caused by the effect of volume dissipation of a substance's thermal radiation on mesoscale geometrical features of the structure of a glacier in its formation from the snow mass. Certainly, the use of the homogeneous dielectric model to interpret emissive characteristics is not admissible in the given case.

The microwave investigations have clearly indicated a complicated internal structure of the glacial ice surfaces of Antarctica and Greenland in mesoscales. Neither contact measurements, nor optical observations could reveal these features at all.

A more interesting point is that the exchange between the atmosphere and the Antarctic ice sheet takes place largely through sublimation processes, i.e. through the direct transition from the solid state to a gaseous one (avoiding the melting process). Thereby, some peculiar areas in the Antarctic ice sheet are formed, which can serve in many respects as the Earthly analogues of the northern ice cap of Mars (Siegert and Fisher, 2002).

Drifting sea ice is a rather peculiar physical body. Unlike glacial ice, it represents, first of all, a multicomponent system, which includes solid, liquid and gaseous phases. The solid phase represents an ice-crystalline consolidated skeleton, the liquid phase is a 'pickle' formed from the seawater, and the gaseous phase represents air bubbles of a quite diversified, dispersed structure. Under natural conditions sea ice almost always represents a three-phase system. This essential fact determines its physico-mechanical properties: the ice as a solid body always exhibits viscoelastic properties, and as a dielectric it shows essential electrical spatial–temporal inhomogeneity; and, accordingly, it includes a spectrum of relaxation mechanisms (see section 8.2). The above considerations and the severity of the hydrometeorological conditions of formation and existence of ice make the direct (contact) investigation of electrophysical properties of sea ice a really complicated experimental and technological problem. Nevertheless, even the first microwave radiothermal investigations with highly sensitive instruments (Bespalova *et al.*, 1976b) have demonstrated a

highly efficient recognition of various types of sea ice and its spatial and temporal characteristics.

As we have already noted, it is difficult to form a detailed picture of the dielectric properties of sea ices, since they strongly depend on the mineral composition of sea water in a particular basin, as well as on the temperature and meteorological history of solid phase formation. For this reason, contemporary researchers follow an opposite path in a certain sense – they carry out remote microwave investigations of various types of sea ice and then restore the electrophysical characteristics of drifting sea ice in accordance with some particular model (see, for instance, Hewison and English (1999)). On the basis of the results of these authors, we shall consider some types of sea ice and the spectral features of their emissive properties.

Grease ice is a matt, brownish ice undulating as surface waves, but it also includes flat, shiny ice rind. This category is thinner than 10 mm, and the emissivities show a strong dependence on thickness, ranging from those of open water to thick new ice (Figure 8.22 and Table 8.5).

Nilas includes light, dark, and rafted nilas, which could not be resolved radiometrically. This is a flat, new ice with no air or brine pockets and, hence, it exhibits no significant surface or volume scattering. The emissivity is dependent on the ice thickness, saturating when it is greater than about 30 mm. The upper line (Figure 8.22 for the nilas diagram) represents a best fit calculated for only the thicker samples of Baltic nilas. This shows high emissivity across the spectrum, as expected. The limited amount of Arctic nilas observed generally has a lower emissivity than that found in the Baltic owing to the difference in salinity. The lower curve in this diagram is a fit to only the Arctic samples, which may be thinner than the ice used to calculate the Baltic nilas line.

Bare new ice is a thicker, homogeneous, flat, dark ice formed within the last few days, undisturbed by pressure ridging or snowfall. It is characterized by flat emissivity spectra. This ice excludes Arctic samples.

Snow-covered new ice is as above, but includes a thin surface (a few centimetres) of fresh, dry snow. This category also includes a **pancake** ice (close-packed, regular, circular floes of less than 10 m diameter) and **icecakes** (similar, with larger diameter). Lower frequencies see a higher effective emissivity, as they penetrate the snow to the slightly warmer underlying surface. **Compact consolidated ice**, when the snow surface was wetter, is included in this category because of its spectral characteristics.

Broken ice covers a variety of forms, from pure slush found in fine-grained **Shuga**, **brash ice** to larger, crushed ice floes making up close and very close pack ice. This grouping shows a large range of spectra owing to the irregularity of the samples' ice fields.

Compact consolidated ice comprises large ice floes that have frozen together, often with ridging and variable amounts of dry snow surface. This is the most extensive ice type observed in the Baltic, and is typically 30–50 cm thick. The spectrum (Figure 8.22) shows lower emissivity at higher frequencies, characteristic of the volume-scattering mechanism of small brine and air pockets within the thicker, older ice pack and its snow cover.

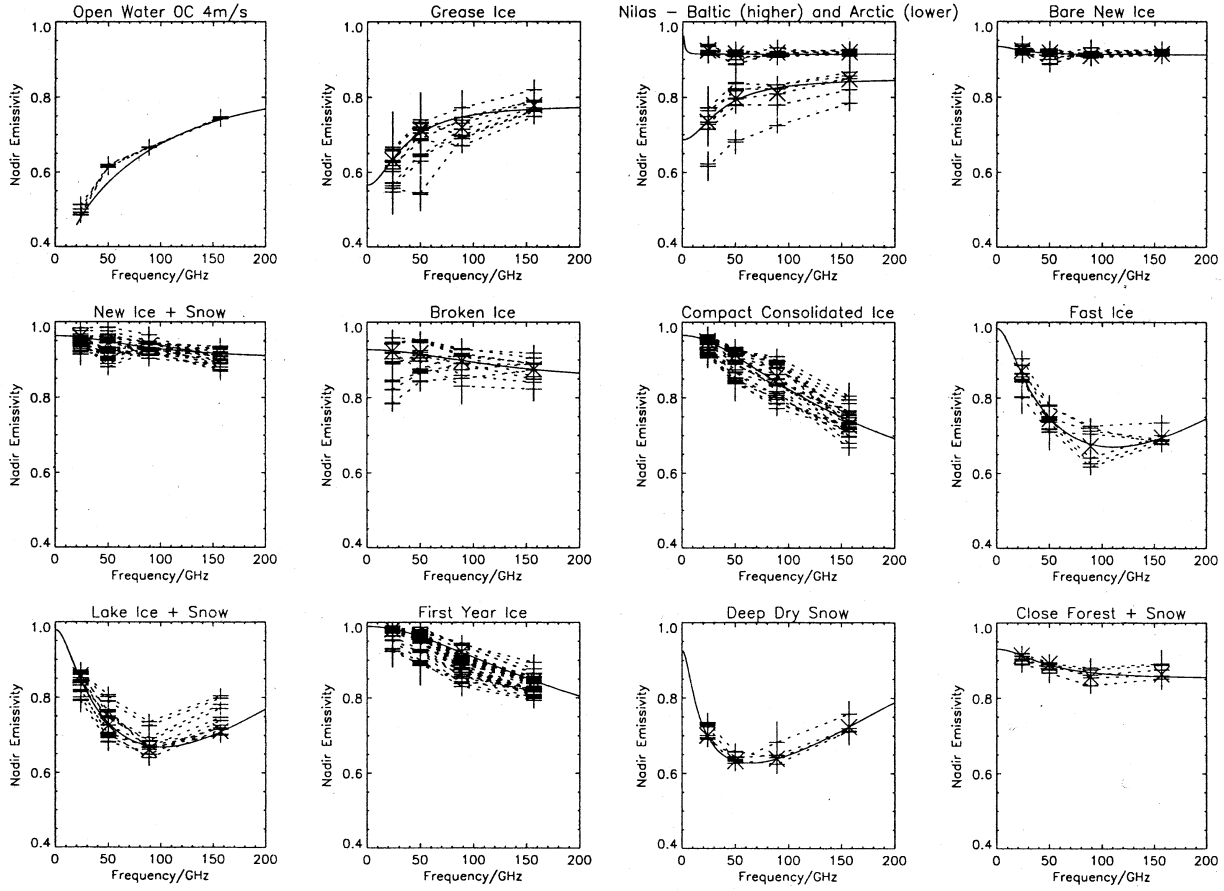

Figure 8.22. Nadir emissivity spectra of natural media. All samples within each surface category are shown, linked with dashed lines, and error bars represent the standard error of mean. The average dependences are shown as continuous lines (Hewison and English, 1999).

Table 8.5. Average emissivity of surface categories

	Nadir emissivity			
Category	(24)	(50)	(89)	(157)
Water, 0°C	0.504	0.617	0.660	0.743
Grease ice	0.632	0.714	0.720	0.779
Baltic nilas	0.924	0.916	0.918	0.919
Bare new ice	0.923	0.918	0.910	0.915
New ice + snow	0.961	0.944	0.937	0.915
Broken ice	0.923	0.918	0.897	0.875
Compact pack ice	0.950	0.913	0.857	0.726
Fast ice	0.872	0.744	0.672	0.969
Lake ice + snow	0.858	0.726	0.662	0.711
First year ice	0.981	0.964	0.922	0.844
Deep dry snow	0.700	0.633	0.640	0.724
Close forest + snow	0.923	0.891	0.857	0.864
Fresh wet snow	0.957	0.962	0.964	0.955

Note. Figures in brackets are working frequencies in GHz.

Fast ice is the landlocked ice found along the northern shore of the Baltic. It is typically 60 cm thick, and has a flat surface as it cannot be affected by pressure ridging, and occasionally has a thin (a few centimetres) surface of snow. This is the oldest of the Baltic ice types (although still 'first year'), and the volume scattering is evident – even at 24 GHz. Some samples did show spectra intermediate between that of fast ice and other types. A trend is evident for an increase in emissivity above 100 GHz, which suggests increasing absorption, although scattering is still a dominant mechanism.

Despite the snow cover, **lake ice** areas showed very similar emissivity spectra to fast ice, which has a similar structure. This provides evidence that the brine pockets do not dominate the volume-scattering process.

Attention should be paid to the considerable scattering (or, as authors Hewison and English (1999) say, the errors) in separate realizations of spectral characteristics. This is associated with a strong spatial–temporal variability of sea ice fields and with their complicated hierarchical structure. This phenomenon was noticed long ago, beginning with the first works on the remote study of sea ices (Bespalova *et al.*, 1976b). But until now these hierarchical spatial features of sea ice fields have not been investigated fully enough, which greatly complicates the procedures of image recognition of remote microwave observations from spacecraft (Comiso and Kwok, 1996; Parkinson *et al.*, 1999; Belchansky and Alpatsky, 2000; Comiso, 2000).

The analysis of emissive properties of sea ices, however, results in the conclusion that the identification (within a limited band) of various types of ice from microwave spectra is not satisfactory. It is necessary both to essentially extend the range of working frequencies (up to decimetres), and to use the polarization properties, as

well as the features of spatial patterns of objects both in the radiothermal and in the scatterometric mode of observation (Matzler and Wiesmann, 1999; Pulliainen *et al.*, 1993, 1999; Pulliainen and Hallikainen, 2001; Wiesmann and Matzler, 1999; Wiesmann *et al.*, 2000).

We shall pay attention also to the fact that the use of simple relaxation models (of the Debye model type) for interpreting complex electrophysical systems, such as various types of sea ice, can lead to paradoxical conclusions. So, Hewison and English (1999), when interpreting the frequency properties of lake ice covered with snow, obtained the value of a static constant of dielectric permittivity (for the Debye model, section 8.3) for such a system, which is essentially lower (1.78) than the optical constant value (67.1). This indicates that the range of use of the models of homogeneous dielectrics with simple relaxation mechanisms for real natural media is fairly limited, and in many cases the application of simple relaxation models (of the Debye type) is not productive.

8.8 RADIATION PROPERTIES OF THE TERRESTRIAL SURFACES

Apart from the huge water and ice areas, a considerable part of the Earth's surface are the continents, which, in their turn, have a great type of diverse surfaces. In this section we shall consider the dielectric and radiation properties of the terrestrial surfaces in the homogeneous, isothermal, half-space approximation (the primitive models) as a fundamental model for forming more complicated electrodynamic models, which are better suited to the real terrestrial surfaces.

8.8.1 Primitive models

Under indicated conditions (homogeneous and isothermal) the radiation characteristics of the emitting half-space are determined by the dielectric properties of a medium and by the physical temperature (see equations (7.20), (7.44)). In order to imagine more clearly the qualitative distinctions in radiation properties of the terrestrial media, we shall consider the dependence of the emissivity of some terrestrial media on dielectric properties and, accordingly, the microwave contrasts received by remote sensing devices.

Figure 8.23 presents the diagram of dielectric properties of some (natural and artificial) media and their emissivity. The 'coldest', in the microwave sense, of the earth media is the water surface and, especially, the sea surface in the decimetre and metre bands. From the artificial media the 'coldest' are the metal surfaces, since the real and imaginary parts of the dielectric constant tend (formally) to infinity. As usual, the coefficient of reflection (in power) in the centimetre band equals less than 0.05–0.01.

Rock and sandy surfaces, in contrast to aqueous media, are 'hot' media with emissivity values of about 0.9–0.95 in a very wide wavelength band – from a few millimetres up to kilometres. Glacial ice, as well as the surface media on the Moon,

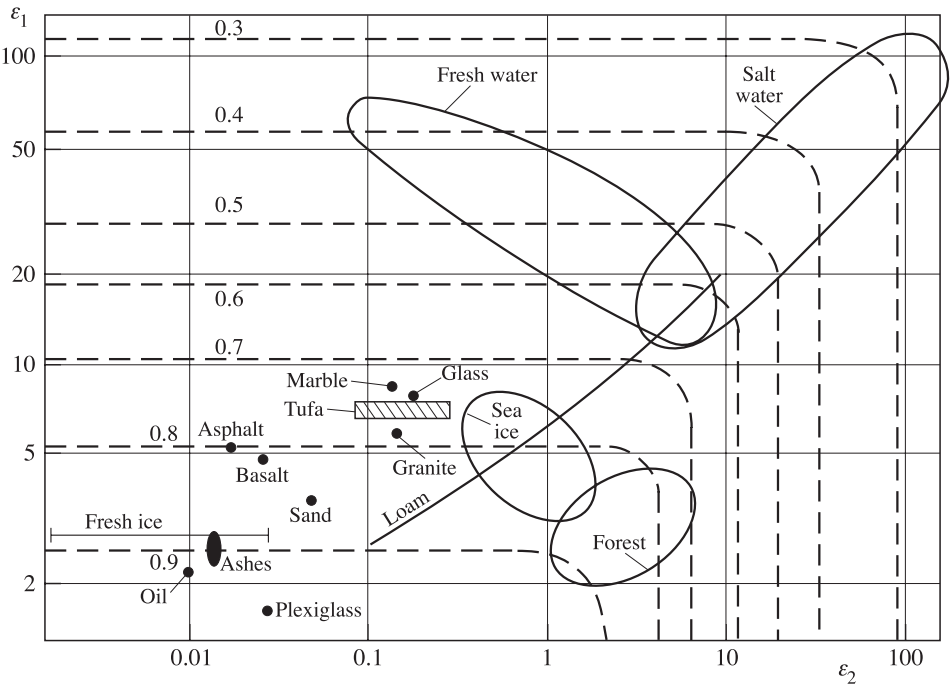

Figure 8.23. Emissivity curves for vertical incidence and for different permittivities of various terrestrial media. Dashed lines show levels of constant emissivity.

Mars, Venus and Mercury can also be attributed to the same group of 'hot' natural media.

As we have already noted (section 8.2), in some cases very rigid chemical bonds can be obtained in artificial polymeric systems by means of special processing. The consequence of this is a low mobility of the basic polymer chain and a limited possibility for motion of separate groups and links. Thus, the dipole-group polarization is insignificant and the dielectric permittivity of polymers is minimal; also minimal are the dielectric losses and losses for pure conductivity. A similar situation arises in some widely used building materials (such as glass, asphalt, cement, concrete and modern synthetic building materials). The emissivity of such materials, as well as of rocks, reaches the values of 0.95–0.99 (Figure 8.23) in a very wide wavelength band.

The intermediate ('warm') class of emitting terrestrial surfaces represents substances which contain water (both fresh and salt) in various physicochemical forms. First of all, one should mention here the soils of both naturally occurring type, and of the agricultural landscape. Among these surfaces can also be included vegetation, which contains in its basis a great amount of saline aqueous solutions. However, one should bear in mind in this regard, that the radiation properties of vegetation *in vivo* are largely determined by its geometrical characteristics, rather than by dielectric

properties as such. This circumstance is clearly seen for large tracts of forest and for a grassland (Figure 8.23), whose emissivity is close to black-body radiation.

Let us now consider these basic classes of Earth more closely.

8.8.2 Rocks

The detailed studies of the dielectric properties of the terrestrial rocks in the microwave band, carried out at the end of the 1950s and in the 1970s, were based on the need to solve radio-astronomical problems in studying the surface layers of the Moon, and later of Mars, based on the belief that there is a certain identity of rocks constituting the upper surfaces of the Moon, Mars and Earth (Troitskii, 1954, 1967; Krotikov, 1962; Parkhomenko, 1965; Alekseev *et al.*, 1967; Tikhonova and Troitskii, 1970; Krupenio, 1974).

Since prominent electronic polarization is observed in rocks (see section 8.2), the absence of frequency dependence of dielectric properties within a wide range of frequencies, from the submillimetre up to the kilometre band, is obvious. This has been confirmed by direct experiments, generally speaking (Krotikov, 1962; Parkhomenko, 1965). In these investigations the dependencies on the chemical composition and density of the terrestrial rocks studied (such as quartz, granite, pumice, tuff, volcanic ashes, basalt) were found. Beginning with wavelengths of about several kilometres ($\sim 10^4$ Hz), the low-frequency polarization mechanisms and, in particular, intersurface polarization come into effect. Because these wavelengths are not used directly in remote sensing, we shall return to discussing the microwave band. Detailed study in this band has shown that some invariant can be formed between the real part of a dielectric constant, the tangent of dielectric loss angle ($\mathrm{tg}\delta$) and the density of the substance investigated. Such invariants from the density were found experimentally for the terrestrial rocks in 1962 (Krotikov, 1962) and were called Krotikov's relations:

$$\frac{\sqrt{\varepsilon_1} - 1}{\rho} = a = \text{const}; \frac{\mathrm{tg}\delta}{\rho} = b = \text{const}. \tag{8.52}$$

Subsequent laboratory experiments (Tikhonova and Troitskii, 1970) made it possible to reveal the values of constants in Krotikov's relations depending on the rock structure (holocrystalline and decrystallized) and on the content of silicon oxide, SiO_2, that determines the history of the given rock formation. It was shown to an acceptable accuracy that Krotikov's constants depend on the SiO_2 percentage (x) as follows:

$$\frac{\sqrt{\varepsilon_1} - 1}{\rho} = a = \frac{40}{x}; \frac{\mathrm{tg}\delta}{\rho} = b = \frac{A}{x^3}. \tag{8.53}$$

Thus, having obtained from microwave observations the a and b values, it is possible to restore the SiO_2 content from the a value and then the type of crystalline structure from the b value. Then, from the type of rock and SiO_2 content, one can restore the relationship between the other oxides as well. Using this particular remote technique, the basic parameters of lunar soil were determined before the landing of the Apollo mission spacecraft. These parameters included, in particular, the dielectric constant

($\varepsilon_1 = 2$–2.5), the density (0.75–1 g/cm^3), the type of rocks (the SiO_2 content is 57%), the homogeneity of rocks over the lunar surface (lands and seas) and the absence of considerable dust cover. The indicated relationships are used now in microwave studies of radiation of regolith covers of Mercury (Shchuko and Kartashov, 1999).

8.8.3 Soils

Soil moisture represents one of the basic components of the power budget at the land–atmosphere boundary mainly through its influence on the latent energy exchange. From the point of view of scientific and agricultural–technological problems, it is important to obtain the data on soil moisture stored at various soil horizons. They include: the surface soil moisture, which is determined by the water content in the liquid state in the upper 5 cm of soil and the stored water at horizons up to 20 cm and at horizons up to 1 m. The stored water can be present both in vegetation, in the root system of plants and in the form of unbound and bound water, snow and ice in the soil bulk. For apparent hydrological and meteorological reasons the surface soil moisture rather poorly correlates with the stored water. Therefore, one of the basic problems of agricultural technology and the hydrogeology of land consists in detecting the moisture profile and in clear separation of these types of soil moisture. The cost of direct observation of soil moisture is very high and its performance is very labour-consuming; therefore, remote aerospace monitoring of soil moisture fields is the only reasonable alternative (Schultz, 1988; Vinnikov *et al.*, 1999; Schultz and Engman, 2000).

A series of techniques for remote sensing of soil moisture have recently been proposed (Schultz and Engman, 2000). They can be implemented under the strict constraint of the absence of cloud cover, and also preliminary data on the observed territory (such as the soil character, the type of surfaces) should be available. These techniques include the method of moisture determination from the data of measurements of reflected solar radiation in the near-infrared band (1.0–1.5 μm), which is based on that fact that the reflectivity greatly decreases with increasing moisture. Much more sensitive to moisture variation is the degree of polarization of light reflected by soil in the visible range – which has stimulated the development of the polarization method. An increase in the heat capacity of soil with growing moisture produces the contrast of surface temperatures and, hence, of thermal radiation from wet and dry areas of soil – which serves as a physical basis for the method of moisture determination from the data of measurements of infrared thermal radiation. A principal feature of these methods is the very insignificant depth of the skin-layer (1–10 μm), from which the information is obtained (see section 1.6), and, as a result, difficulties arise in the interpretation of results. The principal disadvantages of the methods considered are the non-feasibility of the method in the presence of cloudiness and the necessity of taking account of the influence of the thickness of the atmosphere.

Most promising, for the purposes of global monitoring of soil moisture, are passive and active microwave methods (Sharkov and Etkin, 1976; Njoku and

Kong, 1977; Schmugge and O'Neill, 1986; Ulaby *et al.*, 1981, 1982, 1986; Reutov and Shutko, 1990a,b; Promes *et al.*, 1988; Njoku and Li, 1999; Shutko, 1982, 1986; Singh *et al.*, 2000; Rao *et al.*, 1999; Schultz and Engman, 2000; Kerr *et al.*, 2000a; Paloscia *et al.*, 1999, 2000a; Paape *et al.*, 2000; Stoffregen *et al.*, 2002; Yechieli and Wood, 2002). The physical basis for the possibility of soil moisture determination by means of passive techniques is the fact that, as the moisture increases, the dielectric permittivity of soil grows, and, therefore, its emissivity and radiobrightness temperature decrease. Note here that the reflectivity recorded by microwave active instruments (scatterometers and ground-penetrating radars), is not bound up with the influence of the thermodynamic temperature and thermophysical properties of a medium (unlike passive microwave techniques). Therefore, active and passive microwave techniques can provide various scientific information of measurements.

The fact of radiobrightness temperature decreasing with increasing ground moisture was clearly traced for the first time when the data of the measurements of microwave radiation, obtained from the 'Kosmos-243' satellite (1968) at wavelengths of 0.8–8.5 cm, was processed. In papers by Basharinov *et al.* (1969, 1971) it was noted that a lowering of the radiobrightness at the areas of continents in the latitude belt of 30–50° was observed at the places of moistening of terrestrial surfaces, where the emissivity of soils was equal to 0.7–0.8. The vast amount of statistical material obtained as a result of processing the data of microwave radiation measurements from the 'Kosmos-243' satellite, revealed the virtually linear character of radiobrightness temperature decreasing with growing moisture at the wavelengths of 3.4 and 8.5 cm in measurements over agricultural landscape. The subsequent series of ground and aircraft measurements confirmed the fact that the radiation properties of various types of surfaces depend on moisture. Since then complicated models have been developed, which take into account temperature and moisture profiles, the type of soil and the contribution of moist and rough vegetation (Kondratyev *et al.*, 1970, 1973; Popov *et al.*, 1974; Shulgina, 1975; Schmugge and O'Neill, 1986; Liou *et al.*, 1999; Burke and Simmonds, 2001). Let us now discuss in more detail the possibilities of soil moisture determination by means of the passive microwave sensing technique.

The radiobrightness temperature of soil, measured in the direction of the normal, is determined as follows ($S(\theta) = 1$ in equations (7.101)–(7.102)):

$$T_{\mathrm{B}} = \kappa(m) \int_0^{\infty} \gamma(z, m) T(z) \exp\left\{ - \int_0^{z} \gamma(z', m)\, \mathrm{d}z' \right\} \mathrm{d}z, \tag{8.54}$$

where $\kappa(z, m)$ is the soil emissivity, $\gamma(z, m)$ is the absorption coefficient, $T(z)$ is the temperature profile in soil and m, z are the moisture and the vertical coordinate, respectively. The integral expression in (8.54) is sometimes called the effective temperature. Note that this expression is valid for smooth (with respect to used wavelength) profiles of thermal and electrical parameters of a medium (see section 7.7 for more details).

The emissivity of soil depends both on its properties (its physicochemical structure, electrical parameters, the features of its distribution in depth), and on the interface surface characteristics (smoothness or roughness, the presence of vegetation). For bare soil or for a surface whose radius of roughness is much greater than the wavelength the emissivity factor $\kappa(z, m)$ can be determined in terms of Fresnel's mirror reflection coefficient, if the emitting layer of soil is homogeneous in depth:

$$\kappa(m) = 1 - |R(m)|^2. \tag{8.55}$$

Special investigations of the reflection coefficients of soil, which is linearly inhomogeneous in depth, have shown (Shulgina, 1975) that for real soils the influence of inhomogeneity on the reflection coefficient is insignificant and that these coefficients can be calculated, to a first approximation, by Fresnel's formulas. (Only at great wavelengths, of the order of 60 cm, and for soils having a dry surface is the influence of inhomogeneity essential.) However, even in the case of a smooth surface, the radiobrightness temperature of soil represents a fairly complex functional of temperature and moisture (8.54). Since in the general case the remote sensing task should consist in studying both the moisture content characteristics and the temperature regime of the soil, it is worth considering the influence of soil moisture (as a function of emissivity) and the influence of the temperature profile separately.

Suppose we have an isothermal medium (i.e. $T(z) = T_0$) with a constant (in depth) value of moisture. From (8.54) it can easily be seen that the radiobrightness temperature of a medium will be equal to

$$T_B = \kappa(m) T_0. \tag{8.56}$$

On the basis of detailed experimental data from studying two different types of ground (sandy and clayey) in a wide band of wavelengths (from 0.8 to 226 cm), Popov *et al.* (1974) have calculated the emissivity of these types of ground in the mentioned band of waves, which virtually covered the whole band now used in remote sensing practice. Figure 8.24 presents the dependencies of emissivities of clay (a) and sand (b) on the volume moisture for several wavelengths calculated by formula (8.55). The contribution of an imaginary part of the dielectric constant of a medium to the medium's emissivity equals the relative value of up to 30% for moisture of about 20%. Therefore, this contribution cannot be neglected (as it has been in some papers). It can be seen from the analysis of the plots in Figure 8.24, that both for low ($m < 5\%$) and high ($m < 15\%$) moistures the $\kappa(m)$ dependence essentially deviates from the linear. It should be noted that the linear model is also often (and worthlessly) used in the empirical models. The linearity of these dependencies (and, in the case of the isothermal model, the linearity of moisture dependencies of the radiobrightness temperature) can take place only within a limited range of moistures (from 5% up to 15% approximately), this interval being essentially dependent on the working wavelength range and on the type of ground. For high moisture variations the plots of Figure 8.24 should be used as calibration curves. A sharp nonlinearity for low moisture values is associated, physically, with a complicated mechanism of water interaction with soil's skeleton

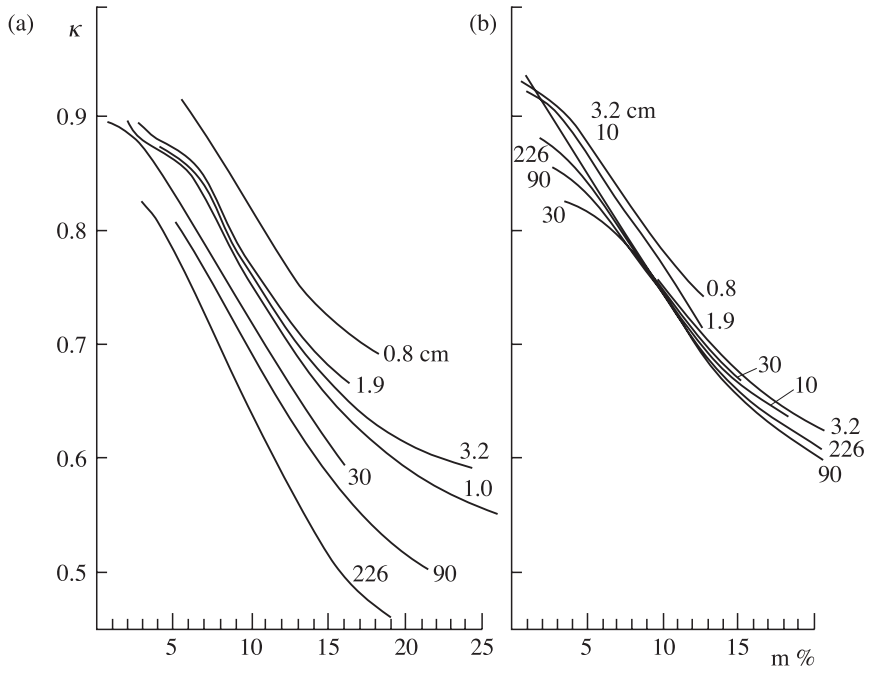

Figure 8.24. Nadir field moisture-dependent emissivity of bare soils: clay (a) and sand (b) surfaces at various wavelengths (cm) (figures next to curves).

and pores, which results in changing the dielectric properties of water and in giving rise to the so-called strongly bound water (Boyarskii *et al.*, 2001; Xu and Sun, 2002; Park, 2001).

From the practical point of view, it is important to know the 'sensitivity' of the radiobrightness temperature to moisture variations ($\Delta T_B/\Delta m$). The estimates of this value disregarding the sky illumination at the rectilinear section of the plot (at $T_0 = 300$ K) give for a clayey ground at the wavelength of 226 cm the value of 8.6 K/%; at the wavelength of 90 cm, 7.5 K/%; at 30 cm, 7.2 K/%; at 3 cm, 7 K/%. For sandy ground the $\Delta T_B/\Delta m$ value is virtually constant throughout the considered wavelength band and equals about 6.1 K/%. For moisture higher than 15% at all wavelengths a sharply nonlinear saturation section begins, where the aqueous solution makes, physically begins, the main contribution to the microwave emission.

Now we shall analyse the sky illumination effect on the radiobrightness temperature of moist ground (see equation (7.20)). The noise temperature of the sky at zenith does not exceed 10 K in the range from 3 up to 30 cm, and as the wavelength further increases, it sharply grows up to 500 K for $\lambda = 300$ cm (Esepkina *et al.*, 1973). With increasing the observation angle θ (as you approach the horizon) the noise temperature of sky grows according to the law $T_I = T_{IZ}/\cos\theta$, where T_{IZ} is the noise temperature at zenith.

From formulas (7.20) it can easily be seen that the presence of sky illumination decreases quantity $\Delta T_B/\Delta m$. This effect, which is not so essential at wavelengths of 3 to 30 cm at the wavelength $\lambda = 226$ cm at the thermodynamic temperature of ground $T_0 = 300$ K, leads to virtually full independence of the radiobrightness temperature on the moisture and on the type of ground, since in this case expressions (7.20) give $T_B = T_0$. Radiobrightness temperature variation, corresponding to 1% moisture variation, will be equal, taking account of sky illumination, for clay (sand) at the wavelength of 90 cm to 6.4 (4.2) K/% and at the wavelength of 30 cm to 7.1 (6.0) K/%, at the wavelength of 3 cm to 6.7 (6.0) K/%. As would be expected, the radiobrightness temperature sensitivity to moisture variation is at a maximum in the wavelength band from 3 up to 30 cm, in which the noise temperature of sky is minimum.

It is interesting to note that the presence of moisture has an essential effect on polarization characteristics of radiation of a medium (section 7.4). The basic characteristic in this case is the polarization factor determined by the relation

$$p(\theta) = \frac{T_{BV}(\theta) - T_{BH}(\theta)}{T_{BV}(\theta) + T_{BH}(\theta)}, \tag{8.57}$$

where T_{BV} and T_{BH} are radiobrightness temperatures of vertically and horizontally polarized components of radiation. Since the effective temperature does not depend on the type of polarization, the expression for the polarization factor is simplified:

$$p(\theta) = \frac{\kappa_V(\theta) - \kappa_H(\theta)}{\kappa_V(\theta) + \kappa_H(\theta)}. \tag{8.58}$$

The calculations by formula (8.58) indicate that the moisture dependence of polarization factor (Figure 8.25) is nearly linear with the slop of about 1% per 1% of moisture for clay, and 0.6–1.0% per 1% of moisture for sand up to moisture values of 15–20%, after which the tendency to saturation begins to reveal itself. If the radiometric system makes it possible to distinguish the 1% variation of the polarization factor (here by the per cent is meant the unit of measurement of polarization factor, rather than the relative per cents), then for $\theta = 45^\circ$ about 10 gradations of moisture from 0 to 20% can be distinguished confidently.

Let us estimate now the sky illumination effect on polarization measurements. Substituting expression (7.20) with corresponding indices into (8.57) and taking into account (8.55), we obtain

$$p(\theta) = \frac{\kappa_V(\theta) - \kappa_H(\theta)}{\kappa_V(\theta) + \kappa_H(\theta) + \dfrac{2T_I(\theta)}{T_0 - T_I(\theta)}}. \tag{8.59}$$

The solid line in Figure 8.26 presents the dependencies of polarization factor p on the observation angle (a) and on the wavelength (b) for clay of 10% moisture ($T_0 = 300$ K) calculated by formula (8.59). The dashed line indicates the same dependencies disregarding the sky illumination. As can be seen from Figure 8.26(a), the

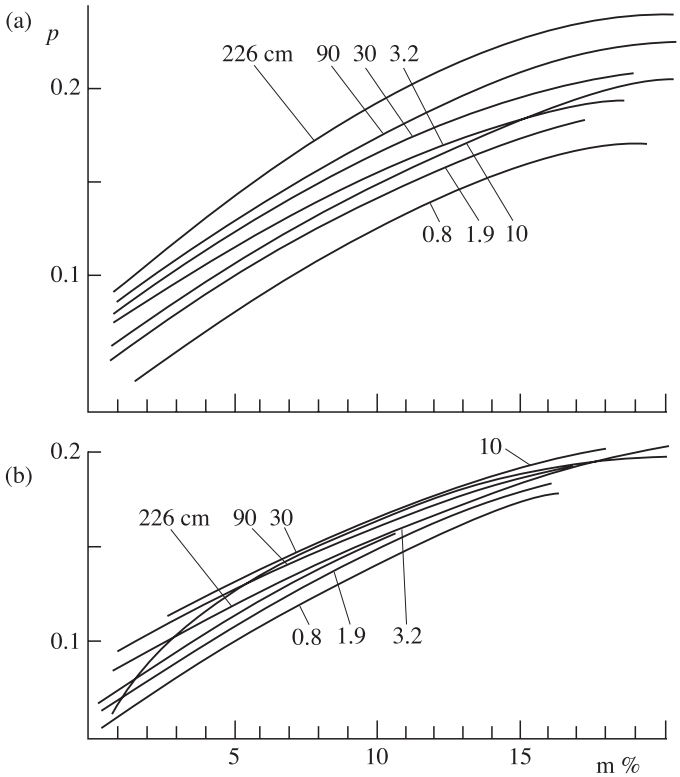

Figure 8.25. Field moisture-dependent polarization coefficient of bare clay (a) and sand (b) soils at various wavelengths (cm) (figures next to curves). The observation angle is 45°.

difference between polarization factor values with allowance for sky illumination and the same values disregarding sky illumination reaches a considerable value (more than 30% for $\lambda = 0.8\,\text{cm}$, $\theta = 80^\circ$). At great observation angles ($\theta = 80^\circ$) the maximum appears in the dependence, and then a sharp drop takes place. For each observation angle (Figure 8.26(b)) there exists some critical wavelength, at which the polarization factor drops to zero.

It is clear from the physical considerations that the main contribution to the microwave emission of a semi-infinite medium is made by the layer of some particular depth, because the radiation of all underlying layers decays in overlying ones. This estimation can be performed quite easily, assuming a variable upper limit in the integral expression for the effective temperature (8.54). Then the expression for the effective temperature will be as follows:

$$T_{\text{B}} = T_0(1 - \exp(-\gamma z)). \tag{8.60}$$

It can easily be seen from this expression, that the main contribution (about 90%) to the thermal radiation of a semi-infinite medium is made by the layer of finite depth

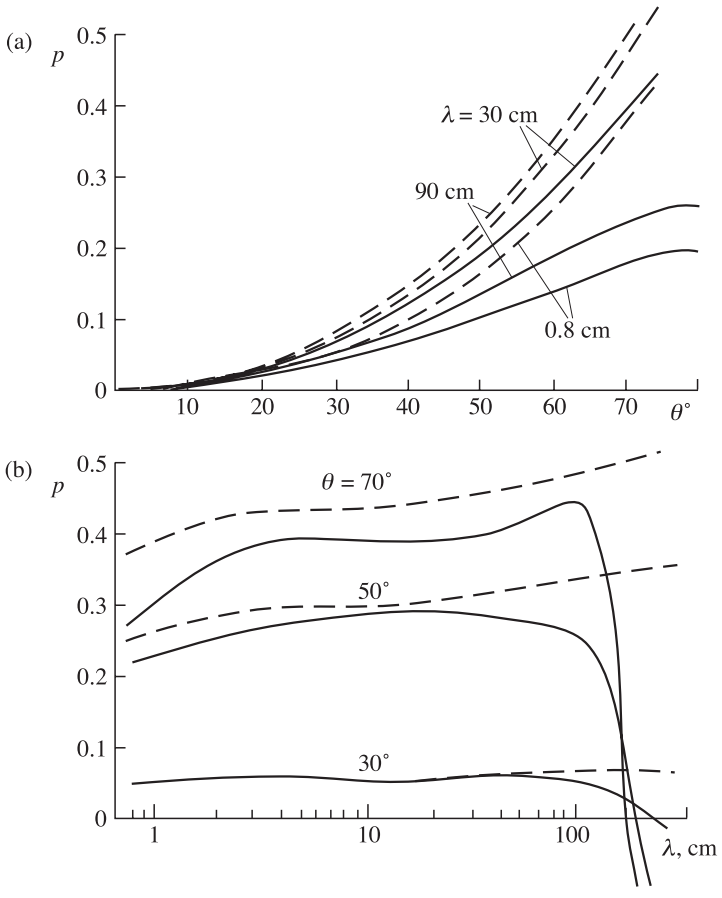

Figure 8.26. Polarization features of radio-emission for clay soil surface with moisture 10% ($T_0 = 300\,\mathrm{K}$) taking into consideration 'sky' radio-emission (continuous lines) and not taking it into consideration (dashed lines): (a) the relationship of polarization coefficient versus observation angle; (b) the relationship of polarization coefficient versus work wavelengths.

l_{ef}, which is equal to

$$l_{\mathrm{ef}} = \frac{2.3}{\gamma}\,(\mathrm{m}). \tag{8.61}$$

The calculated values of quantity l_{ef}/λ for moisture of 10% for sand (clay) in the band of 20 cm were 4.5 (1) and in the band of 75 cm were 5.3 (0.53).

Now we shall consider the effect of the temperature regime of soil on its emissive properties. The analysis of the data on the temperature regime of soil, carried out by Kondratyev *et al.* (1970), has shown that the temperature profiles are well approximated by the relation:

$$T(z) = \{[T'(0) + \alpha(T_0 - T_2)z]z + T_0 - T_2\}\exp(-\alpha z) + T_2, \tag{8.62}$$

where T_0 is the temperature at $z = 0$; $T'(0)$ is the temperature gradient near the surface; T_2 is the asymptotic value of temperature for $z \to \infty$; and α is the empirical parameter. According to the data of some investigations, in summer at any time of day $T = T_2$ even at the depth of about 40 cm (Liou *et al.*, 1999).

Generally speaking, temperature profile approximation by expression (8.62) is possible for any profile characterized by monotonous transition to T_2 or possessing a maximum or minimum (i.e. where the diurnal or seasonal 'wave' of the thermal regime in the soil bulk is investigated).

As a first approximation, we shall consider the case of $\gamma = \text{const}$. This case is accomplished in the region of wavelengths, for which the absorption coefficient is sufficiently high that, at the distance of effective depth of radiation penetration into soil ($0 < z < l_{\text{ef}}$), the moisture and, along with it, the absorption coefficient has no time to be changed noticeably.

Making integration (8.54) with allowance for (8.62), we obtain

$$T_{\text{B}} = \kappa(m)\left[\frac{T'(\theta)}{\gamma(1+\alpha/\gamma)^2} + \frac{\alpha}{\gamma}\frac{T_0 - T_2}{(1+\alpha/\gamma)^2} + T_2\right]. \tag{8.63}$$

Let us now show how, by measuring the radiobrightness temperature at several wavelengths (in other words, implementing microwave spectroscopy), one can determine the moisture and the temperature profile parameters. Consider the range of wavelengths, for which $(\alpha/\gamma) < 1$. In this case equation (8.63) takes a more simple form

$$T_{\text{B}j} = \kappa_j(m)\left[T_0 + \frac{T'(0)}{\gamma_j(m)}\left(1 - 2\frac{\alpha}{\gamma_j(m)}\right)\right]. \tag{8.64}$$

Thus, in the wavelength range under consideration, the radiobrightness temperature is determined by the values of temperature and its gradient at the surface, but does not depend on the asymptotic value of temperature. Since the emissivity is a complicated function of moisture, for determining it, as well as for finding three other unknown quantities – m, α and $T'(0)$ (T_0 can be considered to be specified) – it is necessary to have the measurement data for radiobrightness temperature at four wavelengths ($j = 1, 2, 3, 4$), at which the absorption coeficients satisfy the inequality $(\alpha/\gamma) < 1$. Though this system of equations is nonlinear, nevertheless it can be resolved, for example, by the method proposed by Kondratyev *et al.* (1970). That is to say, from the four measured values of radiobrightness temperature in the range of wavelengths for which $(\alpha/\gamma) < 1$, provided that T_0 is specified (quantity T_0 can be obtained from the data of measurements in the thermal infrared band) and from the moisture dependence of absorption coefficients at these wavelengths, it is possible to determine the soil moisture and the temperature gradient near the surface, the surface emissivity and the exponential factor of the temperature profile which characterizes the thermal ground regime.

The case of $(\alpha/\gamma) < 1$, considered above, occurs at strong absorption of electromagnetic waves in a medium. The second extreme case of great wavelengths, for which $(\alpha/\gamma) \gg 1$, enables one to determine the asymptotic value of the temperature

profile T_2 from the equality

$$T_{\mathrm{B}} = \kappa(m) T_2. \tag{8.65}$$

This is the case of weak absorption, and, naturally, the main contribution to the radiobrightness temperature is made by the layers at temperature T_2. The inequality $(\alpha/\gamma) \gg 1$ is met for decimetre-band wavelengths. For example, for the wavelength of 60 cm, as the moisture changes from 3% to 12%, the (α/γ) ratio changes from 60 to 15, approximately.

The further development of this approach has lead Kondratyev and Shulgina (1971) to the idea of using the periodic scanning at a fixed observation angle in order to eliminate the given surface temperature in measurements (see equation (8.63)) and to limit the study by quantities depending on temperature profile parameters we are interested in. So, in the range of wavelengths for which $(\alpha/\gamma) < 1$, equation (8.64) for fixed observation angle θ takes the form

$$T_{\mathrm{B}j} = \kappa_j(m, \theta) \left[T_0 + \frac{T'(0) \cos\theta}{\gamma_j(m)} \left(1 - 2 \frac{\alpha \cos\theta}{\gamma_j(m)} \right) \right]. \tag{8.66}$$

As a result of periodic scanning over the observation angle $\theta = \theta_0 + \theta_1 + \theta_1 \cos \Omega t$, the received signal (8.66) also is a periodic function of time, but in this case the amplitude of the first Fourier harmonic no longer depends on T_0. This makes it possible to use, as a method of measuring the useful signal, its separation at frequency Ω (for example, by the synchronous detection method; see Chapter 3) and the determination of temperature profile parameters and characteristics of soils from the amplitude of the first harmonic. If we make use of the circumstance that within a rather wide range of observation angles $(0 < \theta \leq \pi/4)$ the emissivity only weakly depends on the observation angle (see, for instance, Hewison and English, 1999), then we can perform integration and obtain the following expression for the amplitude of the first harmonic of a received signal

$$T_{\mathrm{B}j}^{(1)} = -2\kappa_j(m) \frac{T'(0)}{\gamma_j(m)} \left[\sin\theta_0 J_1(\theta_1) - \frac{\alpha}{\gamma_j(m)} \sin 2\theta_0 J_1(2\theta_1) \right], \tag{8.67}$$

where $J_1(x)$ is the Bessel function (Gradshteyn and Ryzhik, 2000). In this case the constant component can be presented in the form

$$T_{\mathrm{B}j}^{(0)} = \kappa_j(m) T_0, \tag{8.68}$$

because the corrections, caused by the fixed observation angle and scanning amplitude, will be small (2–3%). The proposed differential technique is reduced to measuring the ratio of the first harmonics (8.67) at various wavelengths and to subsequent determination of moisture and thermal profile characteristics. The advantage of such an approach consists in the fact that the ratios of harmonics can be measured to a greater accuracy than harmonics themselves.

Thus, the proposed method makes it possible, in the homogeneous half-space approximation, to determine by means of the microwave spectroscopy method (at

observation to the nadir or in the mode of periodic scanning over the observation angle) the basic characteristics of the state of a surface layer of soil: the moisture and temperature profile parameters.

However, in many practical cases the one-frequency modes of measurement in the decimetre band (the channel of the 21 cm wavelength) have been successfully used. In these cases fairly simple semi-empirical two-layer models were applied at data interpretation for remote determination of soil water content (in the layer of 0–2 cm) and effective temperature (at the depth of 11 cm) (Burke and Simmonds, 2001; Liou *et al.*, 1999; Ruf and Zhang, 2001).

Even the first microwave investigations of mesoscale and macroscale fields of moisture have indicated a very important feature of constructing these fields, namely, a complicated multiscale hierarchic structure. The detailed analysis of these problems is beyond the scope of this book, and we recommend the reader to address the specialized literature on this subject (Schugge *et al.*, 1988; Sadeghi *et al.*, 1988; Engman, 1997; Vinnikov *et al.*, 1999; Crow and Wood, 1999).

8.8.4 Tilled soil

Humus, one of the most important components of tilled soil, has a basic effect on the structure and physical properties of soil. The presence of humus in soils, even in small quantities, can drastically change their structural-functional hydrophysical and mechanical properties, the changes being due both to aggregation of the mineral part of elementary soil particles (called the skeleton), and to modification of its surface. Humus is a very complicated set of various compounds, the most basic of which are humic and fulvic acids. The molecules of humic acids have a loose, spongy structure with a great number of inner pores and, owing to this circumstance, they noticeably change the water-retaining ability of soils.

From the optical sensing viewpoint, humic substances colour the soil in darkish tones, and this circumstance makes it possible to distinguish soils with varying humus contents in the optical band. The spectral reflectivity of soil depends not only on the quantity of humus in it, but also on the spectral reflective properties of the soil-forming rock. For this reason the relative error of determination of humus content can be quite high. Furthermore, in the optical band the information is obtained from a very thin surface film (see section 1.6), which is subject to various external effects. Especially high error occurs in cases where the humus content is low (1–2%): it reaches 200–300% (Bobrov and Galeyev, 2001). The remote measurements of microwave properties of soils with considerable humus content are of undoubted practical interest. Detailed investigations of the dielectric and emissive properties of humus-containing soils have not been carried out yet; therefore, it is important to evaluate the first in-the-field experiments in this field. Bobrov and Galeyev (2001) have shown that radiothermal contrasts exhibit themselves not in the static state, but in the dynamic action mode (of intensive irrigation) and subsequent drying of soil. Experimental investigations of the dynamics of the radiobrightness temperature of soils with various humus contents were carried out at frequencies of 6.25 and 8.0 GHz. And it was shown here, after

fairly intensive irrigation of the surface of test sites because of the various changes of soil structure and differences that arise in the drying rate, that a radiobrightness contrast (up to 60 K) appears, which is retained for 2–3 days. In this case the ratio of diurnal variations of emissivity for two sites with various humus contents depends on the initial moistening. Noticeable structure-changing effects, which influence the brightness contrast value, have been noticed after short-term freezing of the soil surface. All this testifies to the fact that the entire system is fairly complicated and, apparently, it is sharply nonlinear from the viewpoint of both temporal dynamics and spectral emissive characteristics.

8.8.5 Vegetation

Vegetation on the Earth's surface represents a complicated and diverse system from the viewpoint of its electrodynamic properties. This is, first of all, due to a complicated hierarchic geometrical construction – a root system, a trunk, a system of branches and then a system of leaves and fruits. The dielectric properties of each of these subsystems, in their turn, depend in a complicated manner on the dielectric properties of electrolytes which supply a plant with nutrients from a soil and then with photosynthetic products (see, for instance, McDonald *et al.* (1999)). From the remote sensing point of view, the observational strategy and electromagnetic models will depend, first of all, on the required generalization of an image. If the question is about macroscales and mesoscales (as, for example, in the case of investigations of the Amazon rainforest area, the Sahel zone in Africa or a vast prairie grassland (Birrer *et al.*, 1982; Calvet *et al.*, 1995, 1996; Sharkov, 1998; Liou *et al.*, 1999; Prigent *et al.*, 1997, 2000, 2001), then in such a case it is possible to use the electromagnetic models of continuous homogeneous medium (of the film-on-the-substrate type) (see section 7.5) or the cloud model over the smooth boundary within the radiative transfer theory framework (see Chapter 9). Since vegetation possesses a certain attenuation frequency response, it represents some kind of frequency filter which 'blocks' remote investigations of the soil beneath vegetation. For example, Liou *et al.* (1999) have shown that, whereas in the decimetre band (21 cm) it is possible to obtain information under the dense grass cover of the US prairie, then the microwave devices of the SSM/I complex set (see Chapter 14) at frequencies of 9, 37 and 85 GHz are no longer sensitive to the soil moisture (under the grass cover), though these channels are sensitive to moisture in bare soil. Here one should have in mind that between the state (the degree of ripeness and the vegetation growth stage) of vegetation (which is determined from the optical sensing data by means of the NDVI technique), soil moisture state and thermal regime there are no direct correlation links (Chen *et al.*, 1997; Sharkov, 1998). This is due to the fact that the soil–plant system represents a sharply nonlinear system in the spatial-temporal dimension, and the vegetation growth stages and the degree of ripeness (the colour NDVI index) reflect the state of moisture with a considerable time delay, however, at quite certain spatial-temporal averaging. So, Choudhury (1987) has shown that the polarization difference (i.e. the difference of vertically and horizontally polarized brightness temperature, observed at 37 GHz frequency of SMMR on

board the 'Nimbus-7'), in monthly averaging correlates, to a high degree of confidence, with the NDVI index fields for arid and semi-arid regions of India, Africa and Australia. In other words, the polarization difference in the microwave sensing can serve as a fine indicator of the primary surface productivity in arid zones.

If we consider the scales of several (groups) or a single plant, then the electrodynamic model should take into account the hierarchic (fractal) construction of separate subsystems of plants, each of which has both its intrinsic hierarchic system of construction and its intrinsic dielectric properties (Ramson *et al.*, 1997; Ferrazzoli and Guerriero, 1996; Ferrazzoli *et al.*, 2000; McDonald *et al.*, 1999).

Of importance also are investigations of the biological evolution of a vegetation system's elements. A rather unusual and, at the same time, quite indicative example in this respect can serve for the comparison of optical and microwave brightness images of vegetation objects – a leaf each from an oak and a birch tree (Plate 4). The microwave images of the leaves were obtained at the 600 GHz frequency and are presented in 'false' colours (Rehm and Brand, 1999). Whereas the optical image gives a picture of surface distribution of the chlorophyll components of a leaf, the microwave image provides information on the temperature regime and spatial distribution of electrolyte solutions inside the leaf bulk. Obtaining such complex information by the other methods is rather problematic.